INFLUENCE OF REINFORCED COLUMN DETAILS ON BUILDING COLLAPSE ENVELOPE

A THESIS SUBMITTED TO
THE GRADUATE SCHOOL OF NATURAL AND APPLIED SCIENCES
OF
MIDDLE EAST TECHNICAL UNIVERSITY

BY

GÜNCEL VARA

IN PARTIAL FULFILLMENT OF THE REQUIREMENTS
FOR
THE DEGREE OF MASTER OF SCIENCE
IN
CIVIL ENGINEERING

JUNE 2022

Approval of the thesis:

INFLUENCE OF REINFORCED COLUMN DETAILS ON BUILDING COLLAPSE ENVELOPE

submitted by **GÜNCEL VARA** in partial fulfillment of the requirements for the degree of **Master of Science** i**n Civil Engineering, Middle East Technical University** by,

Prof. Dr. Halil Kalıpçılar
Dean, Graduate School of **Natural and Applied Sciences** _____

Prof. Dr. Erdem Canbay
Head of the Department, **Civil Engineering** _____

Prof. Dr. Barış Binici
Supervisor, **Civil Engineering Dept., METU** _____

Examining Committee Members:

Prof. Dr. Ahmet Yakut
Civil Engineering Dept., METU _____

Prof. Dr. Barış Binici
Civil Engineering Dept., METU _____

Prof. Dr. Kağan Tuncay
Civil Engineering Dept., METU _____

Prof. Dr. Erdem Canbay
Civil Engineering Dept., METU _____

Assoc. Prof. Dr. Alper Aldemir
Civil Engineering Dept., Hacettepe University _____

Date: 20.06.2022

I hereby declare that all information in this document has been obtained and presented in accordance with academic rules and ethical conduct. I also declare that, as required by these rules and conduct, I have fully cited and referenced all material and results that are not original to this work.

Name, Last name : Güncel Vara

Signature :

ABSTRACT

INFLUENCE OF REINFORCED COLUMN DETAILS ON BUILDING COLLAPSE ENVELOPE

Vara, Güncel
Master of Science, Civil Engineering
Supervisor: Prof. Dr. Barış Binici

June 2022, 126 pages

Building collapse envelopes are simple yet reliable data representations used for depicting load-carrying and deformation capacities of reinforced concrete buildings and the relationship of these two types of performance-related quantities. These envelopes exhibit variations when structural parameters of the buildings they represent are tweaked. This study is intended to investigate the influence of reinforced concrete column details on building collapse envelopes. Numerical models of two five-story residential buildings light-to-moderately damaged and under the risk of progressive collapse after an earthquake event are created, and variants of these models are prepared by changing compressive concrete strength, floor number, stirrup spacing and longitudinal steel reinforcement ratio values. Results obtained by the analyses of these models are employed to construct corresponding building collapse envelopes. These envelopes are compared among themselves to examine the impacts of introduced parameter changes. Comparisons revealed that the four groups of parameters tested with the analyses of variants introduce consistent impacts to building collapse envelopes and these impacts could be further investigated for improving available reinforced concrete column design and assessment procedures.

Keywords: Reinforced Concrete, Columns, Building Collapse Envelope, Progressive Collapse

ÖZ

BETONARME KOLON DETAYLARININ BİNA GÖÇME ZARFI ÜZERİNDEKİ ETKİSİ

Vara, Güncel
Yüksek Lisans, İnşaat Mühendisliği
Tez Yöneticisi: Prof. Dr. Barış Binici

Haziran 2022, 126 sayfa

Bina göçme zarfları, betonarme binaların yük taşıma ve deformasyon kapasitelerini ve performans ilintili bu iki tür değer arasındaki ilişkiyi ortaya koymak için kullanılan, basit ancak güvenilir veri temsilleri olarak tanımlanabilir. Bu zarflar, temsil ettikleri binaların yapısal parametrelerinde ayarlamalar yapıldığında değişiklikler sergilemektedir. Bu araştırmayla, betonarme kolon özelliklerinin bina göçme zarfları üzerindeki etkisinin araştırılması amaçlanmaktadır. Belirli bir deprem olayının gerçekleşmesinin ardından orta düzeyde hasar görmüş ve progresif göçme riski altında bulunan iki ayrı beş katlı konut tipi binanın sayısal modelleri oluşturulmuş ve beton basınç dayanımı, kat sayısı, etriye aralığı ve boyuna donatı çeliği oranı değerleri değiştirilerek bu modellerin varyantları oluşturulmuştur. Bu modellerin analizlerinden elde edilen sonuçlar, karşılık gelen bina göçme zarflarının kurulması için kullanılmıştır. Elde edilen zarflar, gerçekleştirilen parameter değişikliklerinin etkilerini incelemek amacıyla kendi aralarında karşılaştırılmıştır. Karşılaştırma sonuçları, varyantların analizleri aracılığıyla test edilen dört parameter grubunun, bina göçme zarfları üzerinde, mevcut betonarme kolon tasarım ve değerlendirme prosedürlerini iyileştirmek için yararlanılabilecek tutarlı etkilere sebep olduğunu ortaya koymuştur.

Anahtar Kelimeler: Betonarme, Kolonlar, Bina Göçme Zarfı, Progresif Göçme

To my family and friends…

ACKNOWLEDGMENTS

I would like to convey my deepest gratitude to my supervisor Prof. Dr. Barış Binici firstly for taking me in as a graduate student during possibly one of the darkest times of my academic and personal life, and for putting up with my whims and fancies during my graduate studies. This work in its current form would not be, if it was not for his patience, mentorship and dedication.

I would also like to extend my special thanks to Beyazıt Bestami Aydın and Batu Türksönmez for their invaluable assistance in times of dire straits. These two distinguished people have provided much-needed guidance whenever I was in a river of troubles related to this body of work.

I am also grateful to all my family members and friends for being there for me, either in person or as an image in my mind.

TABLE OF CONTENTS

ABSTRACT v

ÖZ vii

ACKNOWLEDGMENTS ix

TABLE OF CONTENTS x

LIST OF TABLES xiii

LIST OF FIGURES xv

LIST OF ABBREVIATIONS xxiv

LIST OF SYMBOLS xxvi

CHAPTERS

1 INTRODUCTION 1

1.1 General 1

1.2 Literature Review on the Concept of Progressive Collapse 3

1.3 Objective and Scope 12

1.4 Organization of the Thesis 13

2 TEST BUILDINGS 15

2.1 Introduction 15

2.1.1 Building I 16

2.1.2 Building II 18

2.2 Live Column Removal Tests 20

2.3 Assessment of the Buildings According to the Principles for the Identification of Risky Structures (RYTEIE) 22

2.3.1 Building Assessment Procedure According to RYTEIE 23

2.3.2 Assessment Procedures for Building I 30
2.3.3 Assessment Procedures for Building II 33
2.4 Assessment of the Buildings According to the Turkish Building Earthquake Code (TBEC) 36
2.4.1 Building Assessment Procedure According to TBEC 37
2.4.2 Assessment Procedures for Building I 48
2.4.3 Assessment Procedures for Building II 51
2.5 Discussion 53
3 BUILDING COLLAPSE ENVELOPES 55
3.1 Introduction 55
3.2 Verification Studies 56
3.2.1 Verification Model I: Cantilever Beam 57
3.2.2 Verification Model II: Portal Frame 59
3.2.3 Verification Model III: Five-Story Residential Building 63
3.3 Pushover Analyses of Test Buildings with Column Removal Procedure 71
3.3.1 OpenSees® Software 71
3.3.1.1 Structural Elements 72
3.3.1.2 Materials 74
3.3.2 Building Model Variants 75
3.3.3 Numerical Models 76
3.4 Results 79
3.4.1 Vertical Pushover Analyses 79
3.4.2 Building Collapse Envelopes 80
3.4.2.1 Envelopes for the Models of Building I 81

3.4.2.1.1 Envelopes for Concrete Strength Variants 83
3.4.2.1.2 Envelopes for Floor Number Variants..... 88
3.4.2.1.3 Envelopes for Longitudinal Reinforcing Steel Ratio Variants 91
3.4.2.1.4 Envelopes for Stirrup Spacing Variants 95
3.4.2.2 Envelopes for the Models of Building II..... 99
3.4.2.2.1 Envelopes for Concrete Strength Variants 101
3.4.2.2.2 Envelopes for Floor Number Variants..... 105
3.4.2.2.3 Envelopes for Longitudinal Reinforcing Steel Ratio Variants 109
3.4.2.2.4 Envelopes for Stirrup Spacing Variants 113
4 DISCUSSIONS AND CONCLUSIONS..... 117
4.1 Discussion of Results 117
4.2 Conclusions 119
4.3 Future Directions 119
REFERENCES 121

LIST OF TABLES

TABLES

Table 2.1 Structural member details for Building I 17

Table 2.2 Structural member details for Building II 19

Table 2.3 Earthquake ground motion levels to be used according to building intended purpose of use (RYTEIE) 23

Table 2.4 Local soil classess according to RYTEIE 24

Table 2.5 Local soil impact coefficients for the short period range according to RYTEIE 24

Table 2.6 Local soil impact coefficients for the period of 1.0 seconds according to RYTEIE 25

Table 2.7 Chapters of RYTEIE to be referred to according to the type of load-carrying system 26

Table 2.8 Information Level Coefficients for buildings according to RYTEIE 27

Table 2.9 Column classification table according to RYTEIE 28

Table 2.10 m_{limit} and $(\delta/h)_{limit}$ values for columns according to RYTEIE 29

Table 2.11 Floor shear force ratio limit values depending on the average of infill wall and column axial compression stresses according to RYTEIE 29

Table 2.12 Risk identification procedure results for Building I according to RYTEIE 32

Table 2.13 Risk identification procedure results for Building II according to RYTEIE 35

Table 2.14 Information Level Coefficients for Buildings 38

Table 2.15 Local soil impact coefficients for the short period range according to RYTEIE 40

Table 2.16 Local soil impact coefficients for the period of 1.0 seconds according to RYTEIE 40

Table 2.17 Building Use Classes and Building Importance Coefficients 42

Table 2.18 Earthquake Design Classes (EDCs) 42

Table 2.19 Building Height Ranges Defined According To Building Height Classes and Earthquake Design Classes 43

Table 2.20 Performance Targets and Assessment/Design Approaches to be Applied for Built Cast-In-Place Reinforced Concrete, Precast Reinforced Concrete and Steel Buildings (Except High Buildings - BHC ≥ 2) 44

Table 2.21 Live load mass participation coefficients 45

Table 2.22 Performance assessment procedure results for Building I according to TBEC 50

Table 2.23 Performance assessment procedure results for Building II according to TBEC 52

Table 3.1 Details of the AS-2HT specimen 57

Table 3.2 Mechanical properties of the materials of the portal frame 60

Table 3.3 Details of model variants in comparison to original building models 75

Table 3.4 Vertical pushover analysis results for Building I 79

Table 3.5 Vertical pushover analysis results for Building II 80

LIST OF FIGURES

FIGURES

Figure 1.1 Representations of the most common failure propagation types encountered in frame structures. Red circles and blue arrows represent plastic hinges and failure propagation direction, respectively (Kiakojouri et al., 2020). 6

Figure 1.2 Representations of collapse-resisting mechanisms by which loads of failed members are redistributed among adjacent intact members: (a) beam mechanism; (b) arch action; (c) catenary action; (d) Vierendeel action; (e) non-structural member contribution (Kiakojouri et al., 2020). 7

Figure 1.3 Illustration of the applications of (a) pushdown analysis; and (b) pulldown analysis (Liu, 2014) 10

Figure 2.1 Typical Floor Plan of Building I..... 16

Figure 2.2 Typical Floor Plan of Building II 18

Figure 2.3 Column removal order followed in the live column removal test for Building I 20

Figure 2.4 A view of Building I during live column removal tests at the removal step of the last column initiating total collapse 21

Figure 2.5 Column removal order followed in the live column removal test for Building II 21

Figure 2.6 A view of Building II during live column removal tests after the removal step of the last column with the building partially collapsed due to roof displacement induced by heavy machinery 22

Figure 2.7 Horizontal Elastic Acceleration Spectrum according to RYTEIE 26

Figure 2.8 Horizontal Elastic Acceleration Spectrum for Building I according to RYTEIE 31

Figure 2.9 Bar chart representing the number of column-type members under risk on each floor of Building I 32

Figure 2.10 Horizontal Elastic Acceleration Spectrum for Building II according to RYTEIE 34

Figure 2.11 Bar chart representing the number of column-type members under risk on each floor of Building II 35

Figure 2.12 Section damage zones defined by TBEC (2018) 39

Figure 2.13 Horizontal Elastic Acceleration Spectrum according to TBEC 41

Figure 3.1 General layout of the AS-2HT test specimen 57

Figure 3.2 Shear Force versus Tip Deflection Behavior of Specimen AS-2HT 58

Figure 3.3 Comparison of shear Force versus tip deflection behavior represented by experimental data and OpenSees analysis outputs 59

Figure 3.4 General layout of the portal frame 60

Figure 3.5 Details of the portal frame 61

Figure 3.6 Base Shear versus Lateral Displacement response of the Portal Frame according to experiment results 62

Figure 3.7 Comparison of shear force versus lateral displacement response of the portal frame represented by experimental data and OpenSees analysis outputs 63

Figure 3.8 DCR values for the first-story columns in the verification of live column removal test (Initial state with no column removal) 64

Figure 3.9 DCR values for the first-story columns in the verification of live column removal test (Step 1) 65

Figure 3.10 DCR values for the first-story columns in the verification of live column removal test (Step 2) 65

Figure 3.11 DCR values for the first-story columns in the verification of live column removal test (Step 3) 66

Figure 3.12 DCR values for the first-story columns in the verification of live column removal test (Step 4) 66

Figure 3.13 DCR values for the first-story columns in the verification of live column removal test (Step 5) 67

Figure 3.14 DCR values for the first-story columns in the verification of live column removal test (Step 6) 67

Figure 3.15 DCR values for the first-story columns in the verification of live column removal test (Step 7) 68

Figure 3.16 DCR values for the first-story columns in the verification of live column removal test (Step 8) 68

Figure 3.17 DCR values for the first-story columns in the verification of live column removal test (Step 9) 69

Figure 3.18 DCR values for the first-story columns in the verification of live column removal test (Step 10) 69

Figure 3.19 DCR values for the first-story columns in the verification of live column removal test (Step 11) 70

Figure 3.20 General layout of the beamWithHinges element type..... 73

Figure 3.21 Rectangular fiber layout (left) and fiber section of a rectangular column with multiple material types 74

Figure 3.22 Stress-strain relationships of Concrete01 (left) and Steel01 (right) material models in OpenSees 74

Figure 3.23 Building collapse envelope for the original model of Building I 81

Figure 3.24 Pushover curves for the original model of Building I for data points used in corresponding envelope 82

Figure 3.25 Building collapse envelope for the modified model of Building I with f_c=10 MPa 83

Figure 3.26 Building collapse envelope for the modified model of Building I with f_c=20 MPa 84

Figure 3.27 Pushover curves for the modified model of Building I with f_c = 10 MPa for data points used in corresponding envelope 84

Figure 3.28 Pushover curves for the modified model of Building I with f_c = 20 MPa for data points used in corresponding envelope 85

Figure 3.29 Building collapse envelopes of the concrete strength variants of Building I for the average of DCR values of 30% of first-floor columns with highest DCR values under the application of gravity loads only 86

Figure 3.30 Building collapse envelopes of the concrete strength variants of Building I for the average of DCR values of all first-floor columns recorded under the application of gravity loads only 86

Figure 3.31 Building collapse envelope for the modified model of Building I with 8 stories 88

Figure 3.32 Building collapse envelope for the modified model of Building I with 10 stories 88

Figure 3.33 Pushover curves for the modified model of Building I with 8 stories for data points used in corresponding envelope 89

Figure 3.34 Pushover curves for the modified model of Building I with 10 stories for data points used in corresponding envelope 89

Figure 3.35 Building collapse envelopes of the floor number variants of Building I for the average of DCR values of 30% of first-floor columns with highest DCR values under the application of gravity loads only 90

Figure 3.36 Building collapse envelopes of the floor number variants of Building I for the average of DCR values of all first-floor columns recorded under the application of gravity loads only..... 90

Figure 3.37 Building collapse envelope for the modified model of Building I with d=16 mm for longitudinal reinforcing steel bars 92

Figure 3.38 Building collapse envelope for the modified model of Building I with d=22 mm for longitudinal reinforcing steel bars 92

Figure 3.39 Pushover curves for the modified model of Building I with d=16 mm for data points used in corresponding envelope 93

Figure 3.40 Pushover curves for the modified model of Building I with d=22 mm for data points used in corresponding envelope 93

Figure 3.41 Building collapse envelopes of the longitudinal rebar ratio variants of Building I for the average of DCR values of 30% of first-floor columns with highest DCR values under the application of gravity loads only 94

Figure 3.42 Building collapse envelopes of the longitudinal rebar ratio variants of Building I for the average of DCR values of all first-floor columns recorded under the application of gravity loads only 94

Figure 3.43 Building collapse envelope for the modified model of Building I with s=100 mm 96

Figure 3.44 Building collapse envelope for the modified model of Building I with s=200 mm 96

Figure 3.45 Pushover curves for the modified model of Building I with s=100 mm for data points used in corresponding envelope 97

Figure 3.46 Pushover curves for the modified model of Building I with s=200 mm for data points used in corresponding envelope 97

Figure 3.47 Building collapse envelopes of the stirrup spacing variants of Building I for the average of DCR values of 30% of first-floor columns with highest DCR values under the application of gravity loads only 98

Figure 3.48 Building collapse envelopes of the stirrup spacing variants of Building I for the average of DCR values of all first-floor columns recorded under the application of gravity loads only 98

Figure 3.49 Building collapse envelope for the original model of Building II 100

Figure 3.50 Pushover curves for the original model of Building II for data points used in corresponding envelope 100

Figure 3.51 Building collapse envelope for the modified model of Building II with fc=10 MPa 101

Figure 3.52 Building collapse envelope for the modified model of Building II with fc=20 MPa 102

Figure 3.53 Pushover curves for the modified model of Building II with fc=10 MPa for data points used in corresponding envelope 102

Figure 3.54 Pushover curves for the modified model of Building II with fc=20 MPa for data points used in corresponding envelope 103

Figure 3.55 Building collapse envelopes of the concrete strength variants of Building II for the average of DCR values of 30% of first-floor columns with highest DCR values under the application of gravity loads only 103

Figure 3.56 Building collapse envelopes of the concrete strength variants of Building II for the average of DCR values of all first-floor columns recorded under the application of gravity loads only 104

Figure 3.57 Building collapse envelope for the modified model of Building II with 8 stories 105

Figure 3.58 Building collapse envelope for the modified model of Building II with 10 stories 106

Figure 3.59 Pushover curves for the modified model of Building II with 8 stories for data points used in corresponding envelope 106

Figure 3.60 Pushover curves for the modified model of Building II with 10 stories for data points used in corresponding envelope 107

Figure 3.61 Building collapse envelopes of the floor number variants of Building II for the average of DCR values of 30% of first-floor columns with highest DCR values under the application of gravity loads only 107

Figure 3.62 Building collapse envelopes of the floor number variants of Building II for the average of DCR values of all first-floor columns recorded under the application of gravity loads only 108

Figure 3.63 Building collapse envelope for the modified model of Building II with d=14 mm for longitudinal reinforcing steel bars 109

Figure 3.64 Building collapse envelope for the modified model of Building II with d=18 mm for longitudinal reinforcing steel bars 110

Figure 3.65 Pushover curves for the modified model of Building II with d=14 mm for data points used in corresponding envelope 110

Figure 3.66 Pushover curves for the modified model of Building II with d=18 mm for data points used in corresponding envelope 111

Figure 3.67 Building collapse envelopes of the longitudinal rebar ratio variants of Building II for the average of DCR values of 30% of first-floor columns with highest DCR values under the application of gravity loads only 111

Figure 3.68 Building collapse envelopes of the longitudinal rebar ratio variants of Building II for the average of DCR values of all first-floor columns recorded under the application of gravity loads only 112

Figure 3.69 Building collapse envelope for the modified model of Building II with s=100 mm 113

Figure 3.70 Building collapse envelope for the modified model of Building II with s=200 mm 114

Figure 3.71 Pushover curves for the modified model of Building II with s=100 mm for data points used in corresponding envelope 114

Figure 3.72 Pushover curves for the modified model of Building II with s=200 mm for data points used in corresponding envelope 115

Figure 3.73 Building collapse envelopes of the stirrup spacing variants of Building II for the average of DCR values of 30% of first-floor columns with highest DCR values under the application of gravity loads only 115

Figure 3.74 Building collapse envelopes of the stirrup spacing variants of Building II for the average of DCR values of all first-floor columns recorded under the application of gravity loads only..... 116

LIST OF ABBREVIATIONS

ABBREVIATIONS

AEM : Applied Element Method

AFAD : Disaster and Emergency Management Presidency

ALP : Alternate Load Path

ASCE : American Society of Civil Engineers

BHC : Building Height Class

BUC : Building Use Class

CD : Controlled Damage

CEM : Cohesive Element Method

CP : Collapse Prevention

DCR : Demand-to-capacity Ratio

DEM : Discrete Element Method

EDC : Earthquake Design Class

FEM : Finite Element Method

GSA : General Services Administration

LD : Limited Damage

LSP : Linear Static Procedure

LVDT : Linear Variable Differential Transformer

METU : Middle East Technical University

NDP : Non-linear Dynamic Procedure

NIST : National Institute of Standards and Technology

NSP : Non-linear Static Procedure

OpenSees : The Open System for Earthquake Engineering Simulation

PBD : Performance-Based Design and Assessment Approach

PD : Pre-failure Damage

PEER : Pacific Earthquake Engineering Center

RYTEIE : The Principles for the Identification of Risky Structures

TBEC/TBDY : Turkish Building Earthquake Code

TNT : Trinitrotoluene

UFC : Unified Facilities Criteria

US : United States

USA : United States of America

UU : Uninterrupted Use

WTC : World Trade Center

LIST OF SYMBOLS

SYMBOLS

A_c : Gross column cross-section area [m^2]

A_g : Gross cross-sectional area [m^2]

A_{os} : Area of transverse steel (circular cross-section) [m^2]

A_{sh} : Sum of the projections of the area values of all stirrup leg and tie cross-sections in the columns or shear wall end zones, along the height corresponding to transverse steel spacing [m^2]

A_{st} : Longitudinal reinforcement steel area [m^2]

A_{sw} : Area of transverse reinforcement in the direction of loading spaced at s [m^2]

b : Section width [m]

b_k : Cross-sectional dimension of the core of column or shear wall end region for each of the horizontal directions perpendicular to each other (distance between the outermost transverse reinforcement axes) [m]

$(c_u)_{30}$: Average undrained shear strength in the first 30 meters [kPa]

$c_{u,i}$: Undrained shear strength of the ith sub-layer [kPa]

D : Distance between hoop/confining reinforcement axes [m]

DD-1 : Earthquake ground motion level with an exceedance probability of 2% in 50 years (return period of 2475 years)

DD-2 : Earthquake ground motion level with an exceedance probability of 10% in 50 years (return period of 475 years)

DD-3 : Earthquake ground motion level with an exceedance probability of 50% in 50 years (return period of 72 years)

d' : Clear cover [m]

d_b : Longitudinal reinforcement diameter (average in tension) [m]

E : Earthquake impact

F_1 : Local soil impact coefficient for the period of 1.0 second

F_S : Local soil impact coefficient for short period range

f_c : Concrete compressive strength [MPa]

f_c' : Concrete compressive strength [MPa]

f_{ce} : Average (expected) concrete compressive strength [MPa]

f_{ck} : Concrete compressive strength [MPa]

f_{cm} : Current concrete compressive strength [MPa]

f_{su} : Ultimate strength of reinforcement steel [MPa]

f_y : Steel yield strength [MPa]

f_{yh} : Yield strength of transverse reinforcement steel [MPa]

f_{yk} : Reinforcing steel yield strength [MPa]

f_{yl} : Yield strength of longitudinal reinforcement steel [MPa]

f_{ywe} : Average (expected) yield strength of transverse reinforcement [MPa]

f_{ywm} : Current transverse reinforcement yield strength [MPa]

G : Dead load impact

H_N : Building total height [m]

H_T : Total height of building including basement floors [m]

h : Section height [m]

h_i : Thickness of the ith sub-layer [m]

L_p : Plastic hinge length [m]

L_s : Shear span [m]

m_{limit} : Limit value for impact / capacity ratio

N : Applied axial load [kN]

$(N_{60})_{30}$: Average number of standard penetration blows in the first 30 meters

$N_{60,i}$: Number of standard penetration blows for the ith sub-layer

n : Live load reduction factor

n_s : Total number of floors including basement floors

P : Applied axial load [kN]

P_0 : Section axial load capacity [kN]

Q : Live load impact

S_1 : Map spectral acceleration coefficient for the period of 1.0 second

$S_{ae}(T)$: Horizontal elastic spectral acceleration value [g]

S_{D1} : Spectral acceleration coefficient for the period of 1.0 second

S_{DS} : Short period spectral acceleration coefficient

S_S : Short period map spectral acceleration coefficient

s : Stirrup spacing [mm]

T_A : Corner period of horizontal elastic acceleration spectrum [sec]

T_B : Corner period of horizontal elastic acceleration spectrum [sec]

T_L : Period of transition to constant displacement in horizontal elastic spectrum [sec]

V_e : Shear force calculated under the impacts of vertical loads and earthquake impacts [kN]

V_r : Shear strength of column, beam or shear wall section [kN]

$(V_S)_{30}$: Average shear-wave velocity in the first 30 meters [m/sec]

$V_{S,i}$: Shear-wave velocity of the ith sub-layer [m/sec]

α_{se} : Confining steel effectiveness coefficient

δ : Member floor displacement [mm]

δ/h : Effective interstory drift ratio, vectoral

$(\delta/h)_{limit}$: Limit value for effective interstory drift ratio

$\varepsilon_c^{(CD)}$: Confined concrete unit shortening limit allowed for controlled damage performance level

$\varepsilon_c^{(CP)}$: Confined concrete unit shortening limit allowed for collapse prevention performance level

$\varepsilon_c^{(LD)}$: Confined concrete unit shortening limit allowed for limited damage performance level

$\varepsilon_s^{(CD)}$: Reinforcement steel unit deformation limit allowed for controlled damage performance level

$\varepsilon_s^{(CP)}$: Reinforcement steel unit deformation limit allowed for collapse prevention performance level

$\varepsilon_s^{(LD)}$: Reinforcement steel unit deformation limit allowed for limited damage performance level

ε_{su} : Reinforcing steel unit elongation corresponding to ultimate strength

$\theta_p^{(CD)}$: Plastic rotation limit allowed for controlled damage performance level [rad]

$\theta_p^{(CP)}$: Plastic rotation limit allowed for collapse prevention performance level [rad]

$\theta_p^{(LD)}$: Plastic rotation limit allowed for limited damage performance level [rad]

ρ_s : Volumetric ratio of transverse reinforcement steel

ρ_{sh} : Volumetric ratio of transverse steel along the considered direction

$\rho_{sh,min}$: Smaller of the volumetric transverse steel ratios in both horizontal directions

ρ_l : Volumetric ratio of longitudinal reinforcement steel

φ_u : Curvature prior to collapse

φ_y : Yield curvature

ω_{we} : Mechanical reinforcement ratio of effective confining reinforcement

CHAPTER 1

INTRODUCTION

1.1 General

Reinforced concrete frame structures, composed mainly of beams and columns, provide a structural system for resisting large applied moments. These systems mostly work on the principle of load transmission from the superstructure to the soil by the "strong column-weak beam" concept, and, according to this concept, beams are generally designed to be ductile in order to be capable of deforming to certain extents, while the columns are expected to have limited amounts of deformation, since vertical loads are carried and transmitted mostly by these members. Such systems are thus susceptible to structural damage and even collapse in cases of column losses. Columns might be destroyed because of large structural demands due to extreme events of nature, such as earthquakes, as well as by human-induced causes such as explosions or random column removals to open up spaces to utilize for various uses. It is, therefore, of great importance that such structures be designed by considering possible column removal/loss scenarios. Efforts towards this end require improving column design procedures and exploring load redistribution capabilities of structures in cases of progressive collapse.

Examining the ultimate failure states of structures is a useful method to compare structural demands and capacities, and building collapse envelopes are handy assessment tools serving to this purpose. These envelopes are constructed by analyzing the structural performance of a given building at its ultimate limit states. With each point on these envelopes corresponding to a different structural setting resulting in failure, it is possible to juxtapose these with structural demand data representations to obtain a sound comprehension of structural performance in various cases. Therefore, parameters affecting structural performance could be

tweaked in order to produce such cases with the purpose of putting forth plausible structural choices to deal with likely column removal/loss progressions.

A thorough understanding of such progressions requires, perhaps, a meticulous inquiry into the originating causes of them, a robust and valid set of criteria to detect their point of initiation. By this way, the effects of changes in reinforced column details on building collapse envelopes would be revealed, and remedies and precautions for progressive collapse events initiated by column removals or failures can be proposed.

This study is intended to investigate the influence of reinforced concrete column details on building collapse envelopes through experimental and numerical efforts to examine the structural performance of two different residential buildings located in the Elazığ Province of Turkey, which were lightly or moderately damaged after an earthquake event in January 2020. Live column removal tests were conducted on these buildings to observe their load redistribution capabilities and progressive collapse patterns in events of column removals or failures. These buildings are then assessed for their structural performance according to relevant building codes in motion in Turkey to determine their structural risk status. Numerical models of the original buildings in addition to variants of these models with altered reinforced concrete column members are created in OpenSees software environment, and a series of analyses are conducted to obtain their building collapse envelopes. Structural demand curves for each of these models under different earthquake settings are determined via single-mode modal analyses and compared with the constructed collapse envelopes to determine their performance in order to reveal the effects of different preferences for reinforced concrete column design on building collapse envelopes.

1.2 Literature Review on the Concept of Progressive Collapse

All types of buildings are under a perpetual risk of experiencing extreme events within their service life. These events might either be natural, such as earthquakes, hurricanes and tsunamis, or human-induced, such as fires, vehicular collisions or even terrorist attacks (Adam et al., 2018). Regardless of their origin, such events might result in localized damage to the buildings, especially in cases where abnormal structural demands created by their presence are left out of the conventional structural design workflow. Then, these localized impacts might mark the onset of total collapse, This type of structural failure initiated by a local damage which cannot be mitigated by the structural system, and resulting in a damage state that is not proportional to this local damage is called progressive collapse (Ellingwood, 2006).

The first recorded instance of progressive collapse could be found at the turn of the twentieth century, which is the collapse of St. Mark's Campanile in Venice in 1902 (Bazant & Verdure, 2007) due to stress redistribution spanning centuries and caused by creep and shrinkage (Ferretti & Bazant, 2006). The underlying factor resulting in this event was not unveiled back in the day; therefore, progressive collapse as a novel structural phenomenon could not be discussed in the structural engineering scene until the collapse of Ronan Point Tower in London in 1968. Following a gas explosion in a kitchen on the 18th floor of the building, an exterior bearing panel was destroyed, resulting in the loss of support of the floors above, and the debris formed subsequently crushed the floors below (Gurley, 2008). The British building codes were revised after this event (Russell et al., 2019)., and this motion brought about some changes in the building codes in the US (Pearson & Delatte, 2005).

It was not until the terrorist attack on the Alfred P. Murrah Federal Building in Oklahoma, USA back in 1995 that progressive collapse concept warranted drastic changes in the building codes and structural design guidelines in motion throughout the world. Upon the explosion of a truck loaded up with approximately 1,800 kg of TNT-type explosives and parked near the northern side of the building, one of the exterior columns was instantly removed, and the associated air blast destroyed two

adjacent columns in addition to some of the floor slabs. A large transfer girder at the third floor of the building failed to redistribute the imposed loads after the explosion and resulted in the progressive collapse of nearly 70% of the building with casualties (Mlakar et al., 1998). The fact that the building was collapsed because of a risk that could not be counted among the structural ones incorporated into structural design procedures sparked an interest in how to mitigate such risks, especially for high-importance structures.

The terrorist attack on the World Trade Center towers in New York, USA, notoriously known as the 9/11 incident, marks another milestone in the history of research on progressive collapse. Many principal structural components such as core and perimeter columns and floors were destroyed by the impact of aircrafts flown into the towers, and the fires initiated by the inflammation of jet fuel in the planes caused heat-induced damage on structural steel members within the course of minutes, resulting ultimately in rapid loss of capacity and subsequent progressive collapse (NIST, 2005). The scale and toll of this attack raised questions about the precautions to be taken in buildings against the type of encountered structural failure. The aftermath of this event had seen a surge of revisions and additions to the existing building codes such as ASCE 7-16 (2017), GSA (2013) and Eurocode 1 (2006), and the creation of new building codes such as UFC 4-023-03 (2009) and the International Building Code (2009). Relevant bodies of some other countries, such as Australia, Canada, China, New Zealand and the United Kingdom followed suit to adapt their codes to the novel structural necessities introduced by this event (Adam et al., 2018). In addition, the Department of Defense and the National Institute of Standards and Technology in the USA commenced meticulous and extensive research to advance the guidelines related to progressive collapse, and these efforts sparked the interest of scientists all over the world, creating a collective undertaking to expand the literature on progressive collapse ever since.

There are several types of progressive collapse progression that could be observed in structures (Figure 1.1), and these types are distinguished in the work of Starossek

(2007) by the fashion in which the failure of load-carrying members propagate through a structure after the initiation of a localized damage.

- Pancake-type collapse is initiated by the collapse of vertical load-carrying members, and followed by the vertical rigid body motion of components such as slabs. Potential energy stored in normally static members is converted to kinetic energy upon their separation from the structural body, and these components exert impact on the other parts of the structure. Other vertical load-carrying elements are destroyed due to such impacts, resulting in a collapse progression in the vertical direction. Collapse of the World Trade Center (WTC) towers in the US is a textbook example of pancake-type collapse.
- Zipper-type collapse is often initiated by the failure of one or a few structural elements, followed by the redistribution of forces to the intact parts of the structure. Rapidness of the initial failure results in impulsive loading, which, in turn, stimulates a dynamic response in the structure. This type of response induces static and dynamic effects, introducing a force concentration in and subsequent failure of members similar to the initially failing ones in terms of form and function. The ultimate result of this order of events is a collapse progression in a direction that is nearly orthogonal to those of principal forces in the failed elements. This type of failure is demonstrated in the collapse of Tacoma Narrows Bridge in the US in 1940.
- Domino-type collapse is often signalled by the initial overturning of a member, followed by the fall of it around a bottom edge under rigid-body motion. The accompanied transformation of potential energy to kinetic energy comes to a halt with the sudden stop of motion by means of the activation of other elements. Adjacent elements are overturned by the horizontal loading induced by the decelerated member, and the collapse proceeds in horizontal direction.
- Section-type collapse takes place in beams under bending or members under axial tension, when the member is cut and the internal forces are redistributed

to the intact parts of its cross-section. This collapse type is similar to zipper-type collapse, in the respect that the collapse propagates from the point of failure to the intact parts.

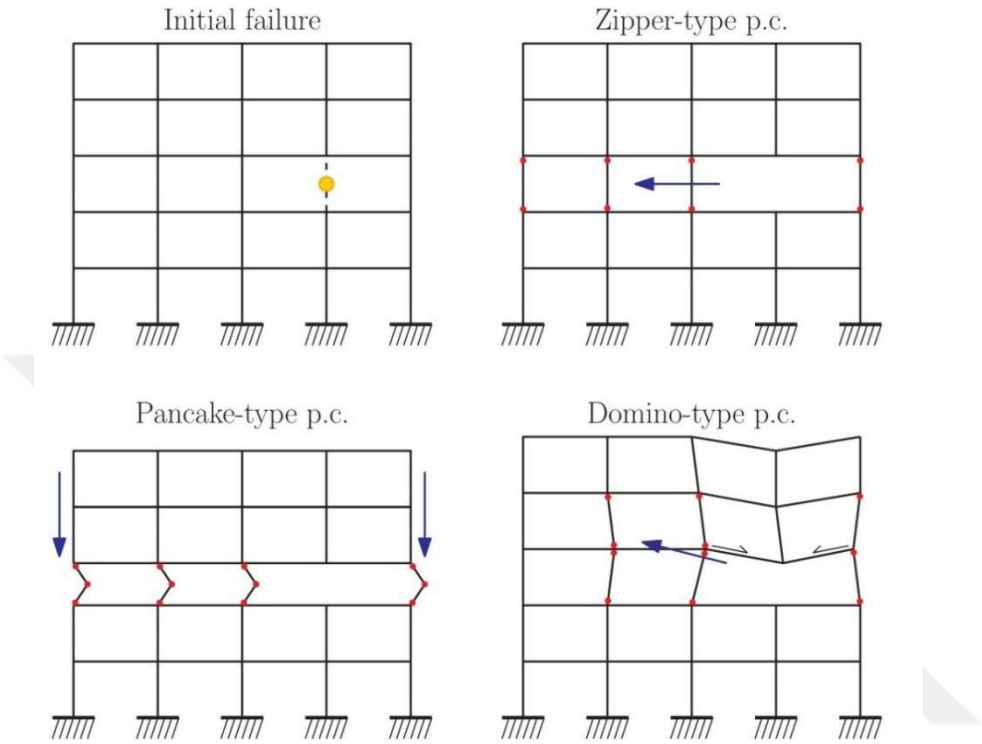

Figure 1.1 Representations of the most common failure propagation types encountered in frame structures. Red circles and blue arrows represent plastic hinges and failure propagation direction, respectively (Kiakojouri et al., 2020).

- Instability-type collapse occurs following an initial failure of elements placed for stabilizing members under compression, which results in the instability of these members. Removal of stabilizing members renders the members vulnerable to sudden failure in the presence of small perturbations, thus marking the onset of failure progression. In this type of collapse, complete destruction may occur immediately without following a sequence of member failures leading to total collapse, especially in cases where the initial failure occurs by the destabilization of a key structural member.
- Mixed-type collapses are also possible where two or more of the collapse types described above take place in tandem.

All these definitions above demonstrate that the most serious initiating event for any type of progressive collapse is usually the failure of a vertical load-carrying member. Many researchers investigated the ways buildings behave in the presence of such member losses to observe their capability to divert the onset of a possible progressive collapse event (Izzuddin & Elghazouli, 2004; Qian et al., 2015; Qiao et al., 2018). In such cases, structures may avoid progressive collapse by redistributing the load of the failed member among adjacent elements to create alternative load paths through several resisting mechanisms (Figure 1.2), namely beam arch effect, beam bending mechanism, catenary action, non-structural member contribution and catenary action (Adam et al., 2018).

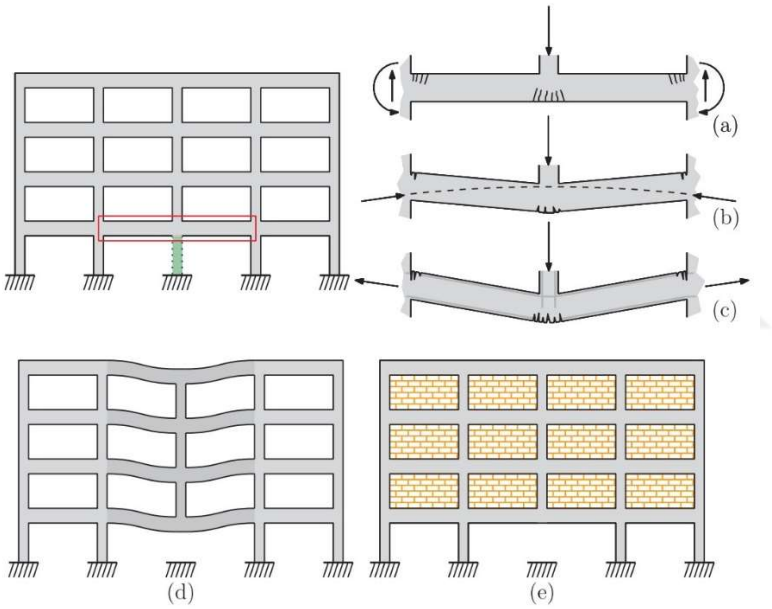

Figure 1.2 Representations of collapse-resisting mechanisms by which loads of failed members are redistributed among adjacent intact members: (a) beam mechanism; (b) arch action; (c) catenary action; (d) Vierendeel action; (e) non-structural member contribution (Kiakojouri et al., 2020).

Resorting solely to resisting mechanisms to weather progressive collapse events may not prove useful for certain cases, since the prediction of the occurrence probability and impact of extreme impacts inducing collapse onset is a challenging task. This assessment justifies that taking progressive collapse risks into account in structural design procedures by setting a set of widely applicable rules is not practical or

possible, and reviews of design codes verify this view (Adam et al., 2018; Byfield et al., 2014; Ellingwood et al., 2007; Cormie et al., 2009). Nevertheless, many researchers managed to propose viable design methods against progressive collapse, some of which are critically considered by prominent international building codes and guidelines. These methods are grouped under the titles of (1) tying force method; (2) alternate load path method; and (3) key element design method

Tying force (i.e. tie force) method is intended for providing the bare minimums of continuity, ductility and tying in structures under low risk of progressive collapse through simplifying a statically indeterminate structure by creating a locally determinate version of the same structure (Li et al., 2011). Tying is usually established by vertical and horizontal ties attained by specifying a minimum tie force requirement. Many national and international building codes recognize tying force method as a valid design method, given that the method generally capable of demonstrating an acceptable contribution to robustness (Arup, 2011; Byfield & Paramasivam, 2007; Li et al., 2011).

Alternate load path (ALP) method involves analyses of the structure of interest for progressive collapse probability following the removal of a load-carrying member (column or wall) with the aim of reaching a state where the redistribution of additional loads transferred from locally damaged areas does not cause a range of damage exceeding specified limits (McKay, 2012). ALP procedures require various assumptions and considerations such as scenario dependence/independence, material non-linearities, strain rate enhancement, connection behaviors and linear/non-linear nature of analyses (Arup, 2011), creating a sizeable cluster of assumption combinations that provide design or assessment pathways corresponding to different levels of robustness (Adam et al., 2018). Most international building codes in motion opt to scenario-independent ALP approaches omitting a thorough consideration of the hazard causing the local damage, for their promise as being easy-to-implement methodologies. Utilization of linear and non-linear static procedures (LSP and NSP) is permitted along with full-fledged non-linear dynamic procedures (NDP), but with certain caveats pinpointed by comparisons. NSP methods are the primary choice,

given that they can encompass both geometric and material nonlinearities in a straightforward static way with a ductility-based robustness assessment framework.

Key element design approach is based on the identification and meticulous design of critical load-bearing structural components, which are most likely to set off progressive collapse upon failure (Ellingwood et al., 2007). In this approach, key elements are designed to be more robust and resistant to extreme loading cases, by making choices to harness the full capacity of the element in axial load, shear and flexure. Key element design is also used extensively by various building codes currently in use in many countries.

All three methods explained above are considered extensively by international codes and guidelines, but given their balance between the assumptions allowing simpler analyses and the accuracy of outputs in return, ALP methods have the most widespread use in design practices for progressive collapse. These methods generally involve the simulation of sudden column loss events in a structure by introducing subtle changes to applied loads and member layout, and linear static, non-linear static and non-linear dynamic analysis procedures could be employed in their applications, depending on the focus of the analysis.

Pushdown analysis method is among the most prominent ALP methods, which is conducted by analyzing a given structure suffering load-carrying member losses under incrementally-increased gravity loads (Khandelwal & El-Tawil, 2011). Gravity loads applied to the bays located above the location of a removed column are incremented until total collapse of the structure and, thus, capability of load redistribution and residual member capacities could be determined. This method is reckoned to be providing advantages, given that no complicated hysteretic material models or time history analyses are required, and that column loss impacts could be introduced merely by using dynamic increase factors; nevertheless, dynamic effects by the sudden nature of column losses cannot be addressed since this method is of non-linear static nature (Kim et al., 2009, McKay et al., 2012).

Another commonly employed ALP method is the pulldown method, which, in contrast to pushdown analysis method, involves application of a static load equal to the axial compression force on the removed column multiplied by a dynamic increase factor at the location of the member. Although the dynamic increase factor is required to be calculated by means of non-linear dynamic analyses, the method itself is of a non-linear static nature, making it simpler with a compromise for overall structural response accuracy. This method is deemed advantageous for its promise of yielding a satisfactory match of the peak dynamic responses of a damaged building through non-linear static analysis procedures. In addition, structural responses of members adjacent to the location of removed columns are predicted to an acceptable extent (Liu, 2014).

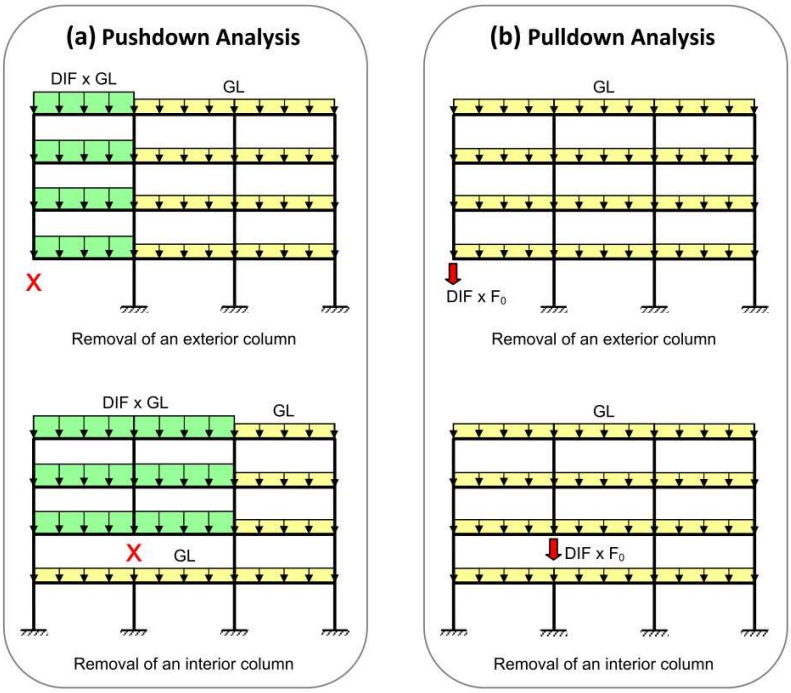

Figure 1.3 Illustration of the applications of (a) pushdown analysis; and (b) pulldown analysis (Liu, 2014)

Depending on the demands of a given research effort, pushdown or pulldown methods are employed by using different factors to ensure sufficient agreement

between the structural responses represented by these methods and those generated by full-fledged non-linear dynamic analysis efforts.

It is possible today, with the developments in the field of computing, to rapidly create accurate and reliable simulations of the progressive collapse of structures by numerical modelling, without compromising the consideration of complexities innate to progressive collapse phenomenon, such as impacts, nonlinearities and large deformations. Several numerical modelling methods are available in the literature, and finite element method (FEM), discrete element method (DEM), applied element method (AEM) and cohesive element method (CEM) are the prominent ones that are extensively employed in progressive collapse simulation endeavors (Adam et al., 2018). Among these four methods, FEM stands out as the most widely used method owing to its capability of facilitating different levels of approximation and complexity, such as the utilization of continuum or macromodels with linear or nonlinear analyses, 2D or 3D models, implicit or explicit calculation, and static or dynamic behavior (Kunnath et al., 2018). Provided that the interaction between elements is established to ensure deformation and constraint compatibility, FEM proves to be a rapid and economically viable method to benefit from.

In earthquake and building codes of Turkey, progressive collapse risk is not mentioned explicitly and no comprehensive mitigation strategy is proposed, but there exists certain performance-based design rules to increase the robustness of buildings in the presence of progressive collapse risk. Nevertheless, most of the building stock in Turkey is constructed based on older codes with more forgiving design limits, making them vulnerable to progressive collapse. The Kocaeli Earthquake back in 1999 was perhaps the most compelling example of such events to point out that building codes in motion must be adapted to such risks. In addition, the building stock is under risk also because building inspection studies to be conducted by municipalities and the governmental bodies are not planned and monitored in an ambitious fashion. Therefore, many buildings are constructed with materials having less than required strength or amount, and without complete adherence to building codes. In addition, random column removals are typical practice especially on the

ground floors of residential buildings to open up uninterrupted spaces for shops, reducing the redundancy capabilities of buildings and rendering them vulnerable to the risk of progressive collapse. Building performance assessment procedures, therefore, are required to assess and determine the performance of built and to-be-built structures, respectively, to set the ground rules for protecting the buildings against the risk of progressive collapse.

1.3 Objective and Scope

The study is concentrated on investigating the influence of reinforced concrete column properties on the collapse envelopes of the buildings. Two reinforced concrete residential buildings are selected to this end, and the entirety of the study is based on their numerical models and the variants of these models created according to the parameters reckoned to be affecting reinforced concrete column performance and building collapse envelopes.

Linear static, non-linear static and non-linear dynamic analysis procedures are employed in the analyses of the building models included in this study. Linear static procedures are followed for evaluating the performance of building models under gravity loads and in the presence of sequential column removals, while non-linear static and non-linear dynamic analysis procedures are utilized for assessing earthquake performances of the same models.

The buildings are also assessed for their structural performance according to the building codes in motion in Turkey, illuminating the structural risks posed by in-situ properties of column-type members.

Given the limited availability of buildings well-suited to the intended objectives of this study, only two buildings, on which live column removal tests could be conducted, are included in this study. Parametric studies required for discovering the influence of reinforced column details on building collapse envelopes are conceived by constructing numerical models of these two buildings with altered column details.

It is expected that this study could reveal research paths that might be followed to inquire into the impacts of reinforced concrete column details on structural performance of buildings in an expansive experimental or numerical scale, in order to be able to propose sound and robust design and assessment principles to mitigate progressive collapse risks in reinforced concrete structures with vertical load-carrying members.

1.4 Organization of the Thesis

The organization of this study can be explained as follows:

Chapter 2 is reserved for introducing the two test buildings scrutinized in this study. Structural and material details related to these buildings are presented, and live column removal tests conducted on these buildings are explained and their results are discussed. Structural performance assessment procedures applied to these two buildings according to two different building codes in motion in Turkey are also outlined. The chapter is concluded with a general discussion on the structural performance of the test buildings.

Chapter 3 elaborates on the procedures for constructing performance (building collapse) envelopes for the test buildings. Verification studies conducted on three distinct structural models to demonstrate the utility of OpenSees for this study are presented in the first three sections of the chapter. Simulations of live column removal tests for the test buildings are presented after these sections. Vertical and lateral pushover analyses of the test buildings with integrated column removal procedures are explained in the third section of the chapter, and the procedures for creating performance envelopes are shared. All analysis results are then shared and discussed in the remaining sections of this chapter.

Chapter 4 is reserved for a generalized account of the results of all the analyses conducted in this study. Comparative efforts in the previous chapter are briefly discussed, and the influence of reinforced column properties on the performances of

test buildings is summarized in the light of these discussions. The chapter is closed with remarks on future directions in this particular field of research.

CHAPTER 2

TEST BUILDINGS

2.1 Introduction

The backbone of this study is comprised of live column removal tests conducted on two reinforced concrete structures. These buildings are residential-type buildings located in Elazığ Province of Turkey, which had sustained minor to moderate damage following an earthquake event with a magnitude of Mw 6.8 occurred in January 2020. Among a cluster of residential buildings erected around the same time, these two buildings were the two standing still after the earthquake, and this occurrence warranted an in-depth scrutiny of the underlying structural mechanisms. Due to the extent of observed damage, these two buildings were evacuated after the earthquake, and then first-floor columns of these buildings were removed sequentially in a predetermined order, in an attempt to discover the reasons causing the other buildings to collapse and these two buildings to weather the earthquake event. The column removal process for each building continued until total collapse.

In this chapter, collected data about these buildings are presented in an attempt to provide insight into their structural nature. Live column removal tests conducted on the two buildings on site are explained, and structural performance assessment studies conducted for these buildings according to the procedures prescribed by the relevant building codes in motion in Turkey, namely The Principles for the Identification of Risky Structures (RYTEIE) and The Turkish Building Earthquake Code (TBDY), are explained. Results of these assessment efforts are discussed to evaluate the performance and risk status of each building.

2.1.1 Building I

The first building examined in this study is a five-story reinforced concrete residential building with a typical floor plan given in Figure 2.1. The building was damaged and found to be under high risk after the earthquake, thus making it a suitable specimen for a live column removal test. According to the available data about the building, total height is 14 meters with each floor having a height of 2.8 meters, and concrete used in the design of the building was of grade C25 (f_{ck} = 25 MPa), and longitudinal and transverse reinforcing steel bars were of grade S420 (f_{yk} = 420 MPa) and S220 (f_{yk} = 220 MPa), respectively.

A series of destructive and non-destructive tests for concrete and rebar inspection were conducted to verify these data. Six core samples extracted from the building were tested to find concrete strength, and the average concrete strength was found to be 6.5 MPa. Rebar inspections verified the steel strength and disclosed the longitudinal and transverse steel layouts for sampled members, providing data to be used for modeling the building (Table 2.1).

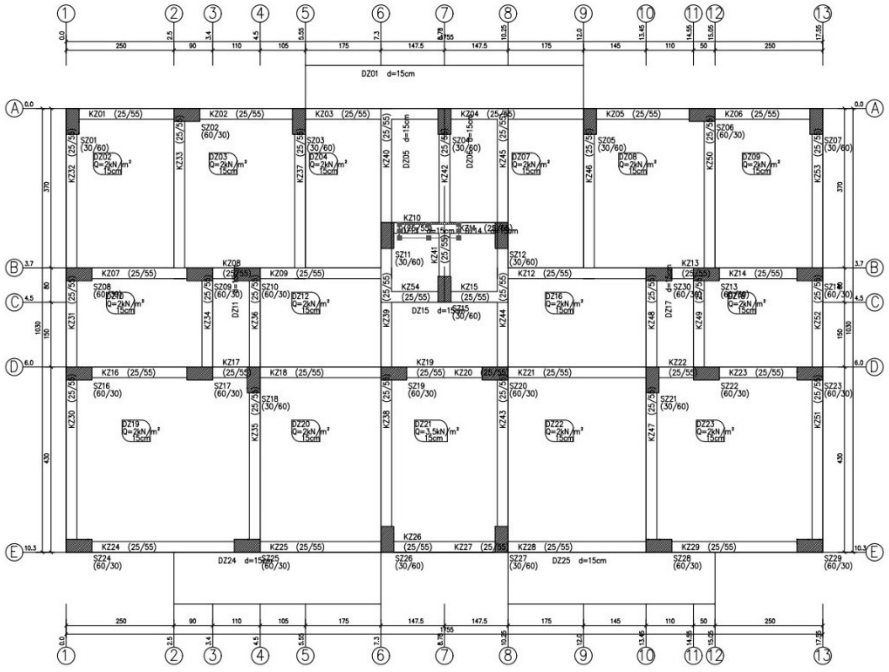

Figure 2.1 Typical Floor Plan of Building I

Columns of the building were comprised of single size but with two different orientations, and beams also had a single cross-section type. No data was available for beam rebar layout; therefore, a rebar layout with a total reinforcement ratio of 1% was selected for these members. Slabs were of simple flat type and 15 centimeters in thickness throughout the whole building. The building also had infill walls at each floor, but they were deemed not to be contributing to the performance of the building, so the infill walls of the first-floor were removed prior to the testing. Live loads imposed on the structure were concentrated on the slabs, and these loads were assumed to be between 1.5 kN/m^2 and 3.5 kN/m^2 depending on the storey and area of use.

Table 2.1 Structural member details for Building I

COLUMNS			
Type I		**Type II**	
Section Width (b) [mm]	300	Section Width (b) [mm]	600
Section Height (h) [mm]	600	Section Height (h) [mm]	300
Clear Cover (d') [mm]	46	Clear Cover (d') [mm]	46
Longitudinal Reinforcement [mm]	8ϕ14	Longitudinal Reinforcement [mm]	8ϕ14
Transverse Reinforcement [mm]	ϕ8	Transverse Reinforcement [mm]	ϕ8
Spacing (s) [mm]	280	Spacing (s) [mm]	280

BEAMS	
Section Width (b) [mm]	300
Section Height (h) [mm]	600
Clear Cover (d') [mm]	46
Longitudinal Reinforcement [mm]	4ϕ14
Transverse Reinforcement [mm]	ϕ8
Spacing (s) [mm]	280

2.1.2 Building II

The second building included in this study is, similar to Building I, a five-story reinforced concrete residential building, but with a typical floor plan (Figure 2.2) different from that of the first building. This building was light-to-moderately damaged and inhabitable in the aftermath of the earthquake event, and included in the live column removal test program. Collected data revealed that the building had a total height of 14.5 meters and each floor had a height of 2.9 meters. Concrete mixture used in the design was claimed to be of grade C25 (f_{ck} = 25 MPa), and longitudinal and transverse reinforcing steel bars were of grade S420 (f_{yk} = 420 MPa) and S220 (f_{yk} = 220 MPa), respectively.

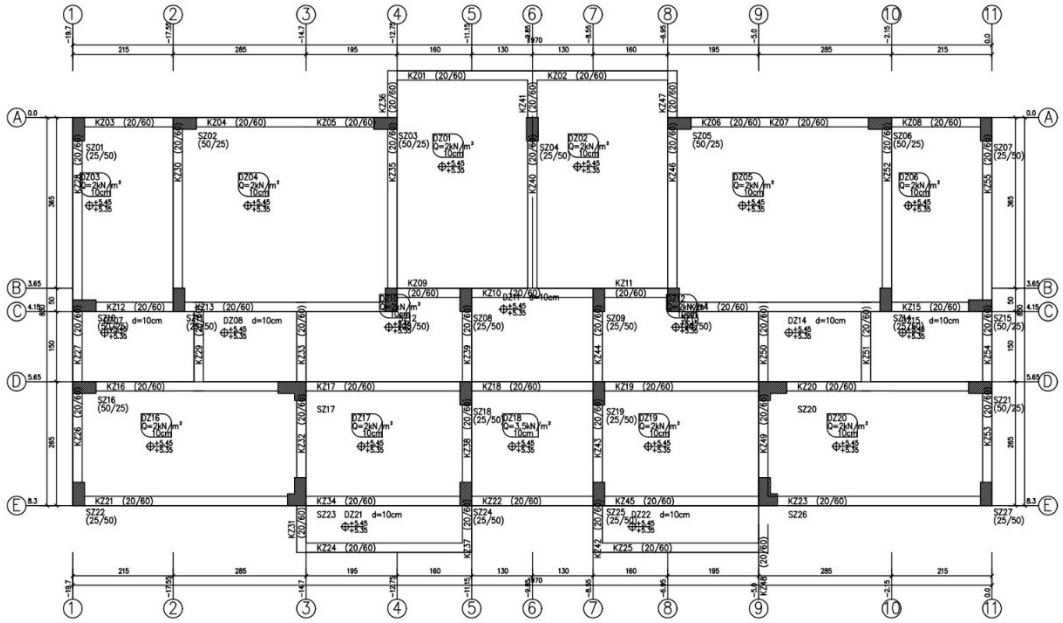

Figure 2.2 Typical Floor Plan of Building II

Destructive and non-destructive tests for concrete and rebar inspection, however, yielded different values for these properties. Six core samples taken from this building were examined to find in-situ concrete strength, and the average concrete strength was found to be approximately 7.8 MPa. Rebar inspection studies, on the other hand, verified the steel strength and provided the longitudinal and transverse

steel layouts for sampled members. These data were later used for modeling the building (Table 2.2).

Columns of the building came in two different sizes with two different orientations for each size, and beams had a single cross-section type. No data was available for beam rebar layout; therefore, a rebar layout with a total reinforcement ratio of 1% was selected for these members. Slabs were of simple flat type and 10 centimeters in thickness throughout the whole building. The building also had infill walls at each floor, but none of these was removed during the column removal tests. Live loads imposed on the structure were concentrated on the slabs, and these loads ranged from 1.5 kN/m^2 to 3.5 kN/m^2 depending on the story and area of use.

Table 2.2 Structural member details for Building II

COLUMNS			
Type I		**Type II**	
Section Width (b) [mm]	250	Section Width (b) [mm]	500
Section Height (h) [mm]	500	Section Height (h) [mm]	250
Clear Cover (d') [mm]	46	Clear Cover (d') [mm]	46
Longitudinal Reinforcement [mm]	10ϕ16	Longitudinal Reinforcement [mm]	10ϕ16
Transverse Reinforcement [mm]	ϕ8	Transverse Reinforcement [mm]	ϕ8
Spacing (s) [mm]	230	Spacing (s) [mm]	230
Type III		**Type IV**	
Section Width (b) [mm]	350	Section Width (b) [mm]	550
Section Height (h) [mm]	550	Section Height (h) [mm]	350
Clear Cover (d') [mm]	46	Clear Cover (d') [mm]	46
Longitudinal Reinforcement [mm]	14ϕ16	Longitudinal Reinforcement [mm]	14ϕ16
Transverse Reinforcement [mm]	ϕ8	Transverse Reinforcement [mm]	ϕ8
Spacing (s) [mm]	230	Spacing (s) [mm]	230

BEAMS	
Section Width (b) [mm]	200
Section Height (h) [mm]	600
Clear Cover (d') [mm]	46
Longitudinal Reinforcement [mm]	4ϕ16
Transverse Reinforcement [mm]	ϕ8
Spacing (s) [mm]	230

2.2 Live Column Removal Tests

Live column removal tests were conducted for both buildings by following a predetermined order of removal for first-floor columns. These tests involved the removal of 11 out of 30 and 10 out of 27 first-floor columns for Building I and Building II, respectively. Building I was completely collapsed upon the removal of the last (eleventh) column indicated in its respective column removal order plan (Figure 2.3). Building II was standing still at the end of the column removal test according to the determined column removal order (Figure 2.5), but it was completely collapsed after a small lateral push was imposed at the roof level by means of heavy machinery. These different end results obtained from the live column removal tests might be due to the fact that almost all infill walls located on the first-floor of Building I were removed, but those located on the first-floor of Building II were left intact. This outcome might be due to the contribution of infill walls as non-structural members to the overall structural performance of a given building.

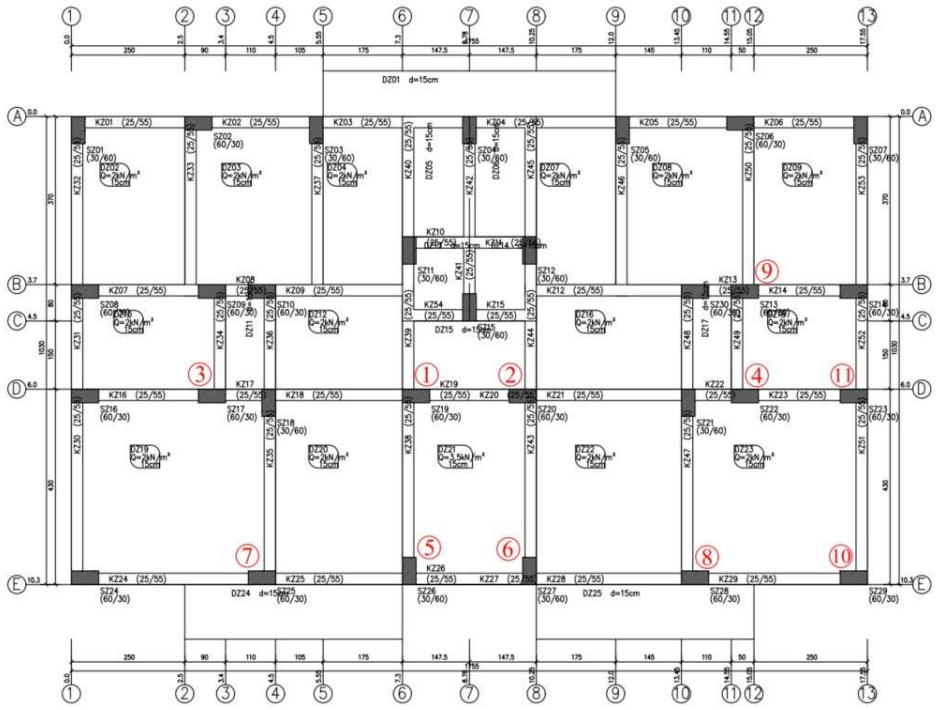

Figure 2.3 Column removal order followed in the live column removal test for Building I



Figure 2.4 A view of Building I during live column removal tests at the removal step of the last column initiating total collapse

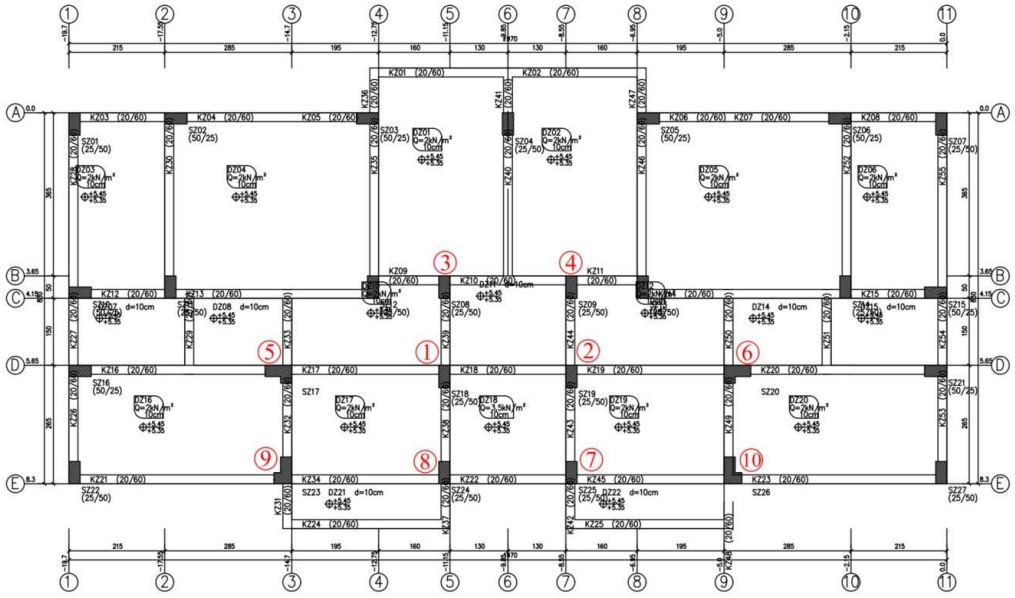

Figure 2.5 Column removal order followed in the live column removal test for Building II



Figure 2.6 A view of Building II during live column removal tests after the removal step of the last column with the building partially collapsed due to roof displacement induced by heavy machinery

2.3 Assessment of the Buildings According to the Principles for the Identification of Risky Structures (RYTEIE)

This section presents the performance assessment procedures for the two buildings located in Elazığ, Turkey according to the building assessment code in motion in Turkey, titled "Guidelines for Identification of Buildings under High Risk" (RYTEIE). The efforts herein are intended for determining the performance levels of the two buildings as per the assessment codes in use in Turkey. The results of these efforts were expected to serve as a benchmark for the results to be obtained by employing the novel assessment method proposed in this study.

In the following two subsections, these two buildings are assessed separately according to RYTEIE. Structural analyses of the buildings were conducted on an in-house platform prepared at Structural Mechanics Laboratory. All the steps of the

assessment procedure for each building are outlined in detail, and members exceeding the safe limits set by the RYTEIE are presented. Considering the relevant rules in the code, the buildings are evaluated for their risk status as a whole. Although the overall risk status of each building is not expected to reflect the underlying mechanisms or to serve as a sound benchmark, intermediate assessment steps and risk status of individual structural members are deemed significant outputs of these assessment procedures for comparing the methods in use with the method put forth in this study.

2.3.1 Building Assessment Procedure According to RYTEIE

RYTEIE encompasses two main clusters of procedures for building assessment, namely earthquake hazard determination and risk identification. Earthquake hazard determination steps for a given building could be summarized as follows:

- Live load reduction factor (n) and earthquake ground motion level of the building are determined by referring to Table 2.3 after defining the intended purpose of use,

Table 2.3 Earthquake ground motion levels to be used according to building intended purpose of use (RYTEIE)

Building Intended Purpose of Use	Live Load Reduction Coefficient, *n*	Earthquake Ground Motion Level
1. Buildings needed to be used after earthquake, buildings people populate for extended periods and in dense populations, buildings where valuable entities are stored and buildings housing hazardous materials		
a) Buildings that must be immediately used after earthquake (Hospitals, dispensaries, community clinics, fire emergency building and facilities, post offices and other communication facilities, transportation stations and facilities, energy production and distribution facilities, province, district and municipality administration buildings, first aid and disaster planning stations)	0.3	DD-1*
b) Schools, other education building and facilities, dormitories and sleeping quarters, military barracks, correctional facilities, etc.	0.6	
c) Museums	0.6	
d) Buildings where materials with toxic, explosive, flammable, etc. properties are located or stored	0.6	
2. Buildings people populate for short periods of time and in dense populations and other buildings		
a) Shopping malls, sports facilities, movie theaters, theaters, concert halls, places of worship, etc.	0.6	DD-2
b) Houses, offices, hotels, building-type industrial structures, parking lots, etc.	0.3	
c) Warehouses, bonded warehouses, etc.	0.8	

* In cases where 1.5 times the S_{DS} coefficient determined for DD-2 is smaller than the S_{DS} coefficient determined for DD-1, DD-2 earthquake ground motion level will be used by multiplying with 1.5, instead of DD-1.

- spectral acceleration coefficients (S_S and S_1) for DD-1 and DD-2 earthquake ground motion levels are obtained from Turkey Earthquake Hazard Maps in use.
- Soil class for a given building is determined by soil investigation methods. Data obtained from these investigation efforts are used in Equation 2.1 to calculate certain soil parameters in order to determine the local soil class by using Table 2.4.

$$(V_S)_{30} = \frac{30}{\sum_{i=1}^{N} \frac{h_i}{V_{S,i}}} \quad ; \quad (N_{60})_{30} = \frac{30}{\sum_{i=1}^{N} \frac{h_i}{N_{60,i}}} \quad ; \quad (c_u)_{30} = \frac{30}{\sum_{i=1}^{N} \frac{h_i}{c_{u,i}}} \qquad (2.1)$$

Table 2.4 Local soil classess according to RYTEIE

Local Soil Class	Soil Type	Average within the top 30 m		
		$(V_S)_{30}$ [m/s]	$(N_{60})_{30}$ [blow/30cm]	$(c_u)_{30}$ [kPa]
ZA	Intact, hard rocks	>1500	-	-
ZB	Lightly weathered, moderately hard rocks	760-1500	-	-
ZC	Very dense sand, gravel and rigid clay layers or weathered, highly cracked weak rocks	360-760	>50	>250
ZD	Medium dense-dense sand, gravel or very stiff clay layers	180-360	15-50	70-250
ZE	Loose sand, gravel or soft-stiff clay layers or profiles satisfying the conditions of PI > 20 and w > 40%, and including soft clay layer (c_u < 25 kPa) thicker than 3 meters in total.	<180	>15	<70
ZF	· Soils with a risk of settlement and potential collapse under earthquake effect (liquefiable soils, highly sensitive clays, collapsible soils with weak cement, etc.) · Clays with high peat and/or organic content having a total thickness greater than 3 meters · Clays with high plasticity (PI > 50) having a total thickness greater than 8 meters · Very thick (> 35 m) soft or medium dense clays.			

Table 2.5 Local soil impact coefficients for the short period range according to RYTEIE

Local Soil Class	Local Soil Impact Coefficient, F_S, for Short Period Range					
	$S_S \leq 0.25$	$S_S = 0.50$	$S_S = 0.75$	$S_S = 1.00$	$S_S = 1.25$	$S_S \geq 1.50$
ZA	0.8	0.8	0.8	0.8	0.8	0.8
ZB	0.9	0.9	0.9	0.9	0.9	0.9
ZC	1.3	1.3	1.2	1.2	1.2	1.2
ZD	1.6	1.4	1.2	1.1	1.0	1.0
ZE	2.4	1.7	1.3	1.1	0.9	0.8

Table 2.6 Local soil impact coefficients for the period of 1.0 seconds according to RYTEIE

Local Soil Class	**Local Soil Impact Coefficient, F_1, for the period of 1.0 seconds**					
	$S_1 \leq 0.10$	$S_1 = 0.20$	$S_1 = 0.30$	$S_1 = 0.40$	$S_1 = 0.50$	$S_1 \geq 0.60$
ZA	0.8	0.8	0.8	0.8	0.8	0.8
ZB	0.8	0.8	0.8	0.8	0.8	0.8
ZC	1.5	1.5	1.5	1.5	1.5	1.4
ZD	2.4	2.2	2.0	1.9	1.8	1.7
ZE	4.2	3.3	2.8	2.4	2.2	2.0

- Using the obtained S_S and S_1 values along with local soil class, local soil impact coefficients (F_S and F_1) are determined using Tables 2.5 and 2.6, and then, spectral acceleration coefficients (S_{DS} and S_{D1}) are calculated using Equation 2.2.

$$S_{DS} = S_S F_S \qquad S_{D1} = S_1 F_1 \tag{2.2}$$

- Horizontal elastic spectral acceleration value for any given period is calculated by Equation 2.3, where T_A and T_B values are calculated by Equation 2.4, to plot the horizontal elastic acceleration spectrum (Figure 2.7) for the building. T_L value is assumed to be 6 seconds.

$$S_{ae}(T) = \begin{cases} \left(0.4 + 0.6\dfrac{T}{T_A}\right) S_{DS} & T \leq T_A \\ S_{DS} & T_A \leq T \leq T_B \\ \dfrac{S_{D1}}{T} & T_B \leq T \leq T_L \\ \dfrac{S_{D1} T_L}{T^2} & T_L \leq T \end{cases} \tag{2.3}$$

$$T_A = 0.2\frac{S_{D1}}{S_{DS}} \qquad T_B = \frac{S_{D1}}{S_{DS}} \tag{2.4}$$

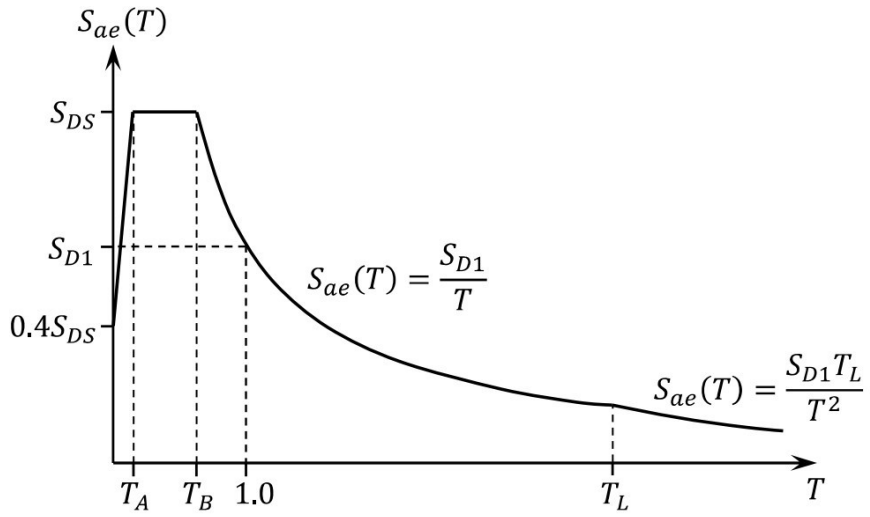

Figure 2.7 Horizontal Elastic Acceleration Spectrum according to RYTEIE

Constructing the acceleration spectrum concludes the set of procedures for earthquake hazard determination and commences the other set of procedures intended for risk identification. This process begins by defining the type of load-carrying system and building class depending on the height or the number of stories for the building. Then, the procedures outlined in the corresponding chapter specified in Table 2.7 are followed.

Table 2.7 Chapters of RYTEIE to be referred to according to the type of load-carrying system

	Building Classes		
	1	**2**	**3**
Type of Load-Carrying System	**Low-Rise** $H_T \leq 30$ m or $n_s \leq 10$	**Mid-Rise** $30 < H_T \leq 50$m or $10 < n_s \leq 17$	**High-Rise** $50 < H_T$ or $17 \leq n_s$
Reinforced Concrete	Chapter 4	Chapter 5	Chapter 6
Masonry	Chapter 7	Chapter 7	Chapter 7
Composite	Chapter 8	Chapter 5	Chapter 6

Since the buildings investigated in this study each have five stories and total heights of 14 meters for Building I and 14.5 meters for Building II, they are classified as low-rise reinforced concrete buildings (Table 2.7), and procedures for the risk

identification of this type of buildings are outlined in Chapter 4 of RYTEIE. Therefore, the procedures listed only in Chapter 4 are employed, and these procedures are explained as follows:

- Available typical floor plans for the basement and selected inspection floors are used for defining the load-carrying system features of the building. Geometries of all structural members are also defined by making use of these plans.
- Depending on the accessibility status of load-carrying system plans of the building, available info level coefficient is determined. Then, load-carrying member capacities are calculated by using available material strength values and then taken into account by being multiplied by the available info level coefficient (Table 2.8).

Table 2.8 Information Level Coefficients for buildings according to RYTEIE

Level of Information	Information Level Coefficient
Minimum	0.90
Detailed	1.00

- Destructive and non-destructive tests are conducted on members in all floors for which the floor plans are obtained. These tests are conducted in accordance with certain specifications stated in the relevant clauses of the RYTEIE text with an aim to determine in-situ reinforcing steel layouts and material properties.
- Finite element models are prepared for 3D analysis of the examined building, where beams and columns are modeled as frame elements. Rigid diaphragms are created for modeling reinforced concrete slabs. All floor masses of vertical members are distributed among the floors they are connected to, and dead and live loads are obtained in accordance with TS 498 code. Live load reduction coefficient is extracted from Table 2.3.

- Effective flexural rigidity values are used in all analyses. These values are calculated by the formulae provided in the respective clauses of the document (i.e 0.3 for beams and 0.5 for columns).
- Earthquake effects are defined by using the obtained horizontal elastic acceleration spectrum (Figure 2.5), in accordance with the building types and earthquake ground motion levels specified in Table 2.3.
- Linear elastic calculation and modal combination method are used in tandem with the specified details in the document in order to determine the risk status of the examined building. Risk status determination is carried out by considering the vertical loads and earthquake effects imposed on the building $(G + nQ \pm E)$ separately for both directions and for both ways of these directions.
- Columns are categorized according to their expected shear load to capacity ratio computed by using the transverse rebar layout at member ends in order to define the risk status determination limits (Table 2.9).

Table 2.9 Column classification table according to RYTEIE

$\frac{V_e}{V_r}$	**Columns with a spacing $s \leq 100$ mm, stirrups with 135° hooks on both ends and a total transverse reinforcement area satisfying the equation $A_{sh} \geq 0.06sb_k\ (f_{cm}/f_{ywm})$**	**Other cases**
$V_e/V_r \leq 0.7$	A	B
$0.7 < V_e/V_r \leq 1.1$	B	B
$1.1 < V_e/V_r$	B	C

- Member axial load and rotation capacities are calculated following the limits presented in tables. Then, section axial load to axial load capacity ratios and floor drift ratios for all columns are calculated. These values are compared by specified limits according to column categories (Table 2.10), and members exceeding these limits are regarded to have exceeded risk limits.

Table 2.10 m_{limit} and $(\delta/h)_{limit}$ values for columns according to RYTEIE

Columns of Group A			
$N_k/(f_{cm}A_c)$		m_{limit}	$(\delta/h)_{limit}$
≤ 0.1		5.0	0.035
≥ 0.6		2.5	0.0125
Columns of Group B			
$N_k/(f_{cm}A_c)$	$A_{sh}/(sb_k)$	m_{limit}	$(\delta/h)_{limit}$
≤ 0.1	≤ 0.0005	2.0	0.01
	≥ 0.006	5.0	0.03
≥ 0.6	≤ 0.0005	1.0	0.005
	≥ 0.006	2.5	0.0075

Columns of Group C	
m_{limit}	$(\delta/h)_{limit}$
1.0	0.005

- For each assessed floor, axial compression stresses in columns are calculated under vertical loads $(G + nQ)$. Average of axial compression stresses are calculated for these floors, and in cases where the specified limits for this average value and the risk limits of any column member on the same floor are exceeded, the building of interest is labeled to be "under risk".
- For each assessed floor, floor shear force ratio is calculated by dividing the sum of column shear forces that are found to be under high risk to the floor shear force to the shear force limit found according to Table 2.11. If the specified limit for this ratio is exceeded, the building of interest is labeled to be "under risk".

Table 2.11 Floor shear force ratio limit values depending on the average of infill wall and column axial compression stresses according to RYTEIE

Average infill wall and column axial compression stress (=Sum of infill wall and column stresses / Number of infill walls and columns)	**Floor shear force ratio limit values**
$\geq 0.65f_{cm}$	0
$0.1f_{cm} \geq$	0.35

2.3.2 Assessment Procedures for Building I

The first set of procedures required by RYTEIE is tailored for determining the earthquake danger/risk for the building. RYTEIE proposes two earthquake ground motion levels according to the intended use of buildings under scrutiny, and these levels correspond to specified live load reduction factors, *n.* This factor was found to be 0.3 for Building I, which is a residential building with the earthquake ground motion level of DD-2 (Table 2.3). Data collected from the site and available in relevant databases revealed that the soil class for the site was designated to be ZC, which indicates the presence of highly compacted sands, gravels and tough clay layers or disintegrated, highly fractured weak rocks. Map spectral acceleration coefficients, (S_S and S_1), were found to be 0.91 and 0.25 seconds, respectively. These values, along with local soil classes, are used for determining local ground impact coefficients, (F_S and F_1), to calculate spectral acceleration coefficients, S_{DS} and S_{D1} (Table 2.5 and 2.6), which were found to be 1.092 and 0.375, respectively. Then, these coefficients are inserted into Equation 2.3 to calculate horizontal elastic spectral acceleration, along with T_A and T_B values. All these values make up the critical points to construct the horizontal elastic acceleration spectrum for the building (Figure 2.8).

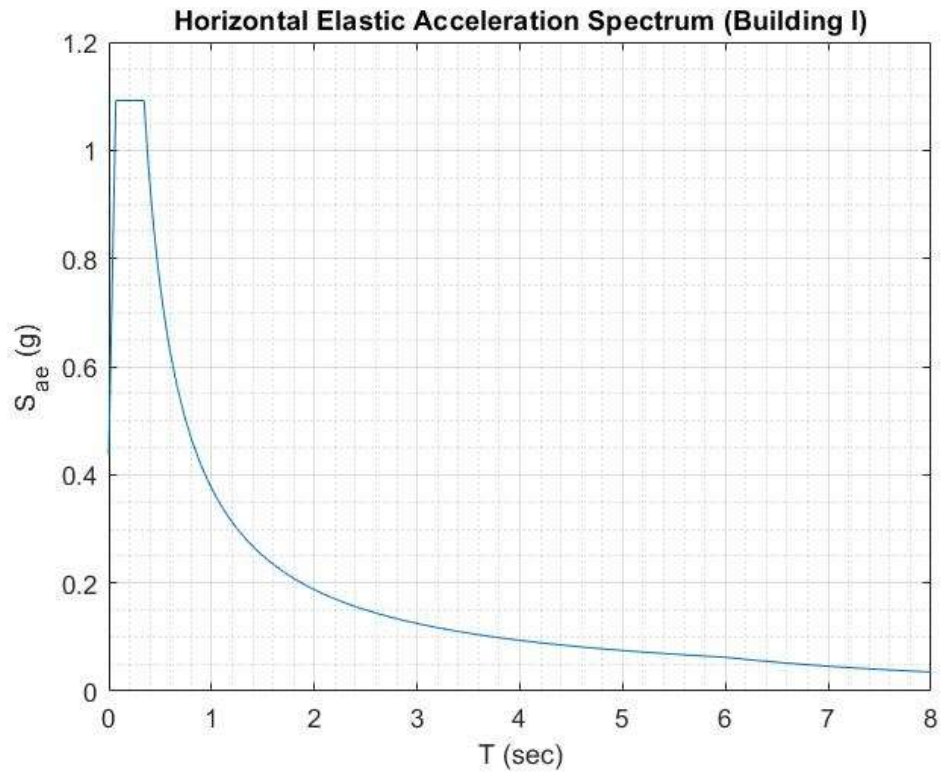

Figure 2.8 Horizontal Elastic Acceleration Spectrum for Building I according to RYTEIE

After completing this step, Building I was modeled and analyzed according to the procedure outlined in Chapter 4 of RYTEIE to conduct risk identification process. All columns in the building were identified to be Class B columns according to Table 2.9, and limit values were selected from Table 2.10 as per this information.

Results of the analysis of Building I are given in tabulated form below:

Table 2.12 Risk identification procedure results for Building I according to RYTEIE

Floor	Floor Height (m)	Loading Type	Floor Mass (Tons)	Total Floor Shear Force (kN)	Total Shear Force of Members Under Risk (kN)	Average Axial Stress (MPa)	In-situ Concrete Strength (MPa)	Floor Shear Force Limit Value	Shear Force Sum of Members Under Risk / Total Shear Force	Investigation	Floor Risk Status	Number of Members Under Risk / Total Member Count
Floor 1	2.8	G+0.3Q+(Ex+)	183.61	3862.51	427.050	1.628	6.5	0.254	0.111	✓	Under Risk	2 / 30
		G+0.3Q+(Ex-)	183.61	3862.51	395.680	1.628	6.5	0.254	0.102	✓		2 / 30
		G+0.3Q+(Ey+)	183.61	3375.94	810.200	1.628	6.5	0.254	0.240	✓		4 / 30
		G+0.3Q+(Ey-)	183.61	3375.94	1009.070	1.628	6.5	0.254	0.299	×		5 / 30
Floor 2	2.8	G+0.3Q+(Ex+)	183.61	3546.66	239.080	1.295	6.5	0.287	0.067	✓	No Risk	1 / 30
		G+0.3Q+(Ex-)	183.61	3546.66	240.550	1.295	6.5	0.287	0.068	✓		1 / 30
		G+0.3Q+(Ey+)	183.61	3084.02	672.270	1.295	6.5	0.287	0.218	✓		7 / 30
		G+0.3Q+(Ey-)	183.61	3084.02	627.560	1.295	6.5	0.287	0.203	✓		6 / 30
Floor 3	2.8	G+0.3Q+(Ex+)	183.61	2974.31	0.000	0.961	6.5	0.320	0.000	✓	No Risk	0 / 30
		G+0.3Q+(Ex-)	183.61	2974.31	0.000	0.961	6.5	0.320	0.000	✓		0 / 30
		G+0.3Q+(Ey+)	183.61	2580.53	0.000	0.961	6.5	0.320	0.000	✓		0 / 30
		G+0.3Q+(Ey-)	183.61	2580.53	0.000	0.961	6.5	0.320	0.000	✓		0 / 30
Floor 4	2.8	G+0.3Q+(Ex+)	183.61	2308.34	0.000	0.628	6.5	0.350	0.000	✓	No Risk	0 / 30
		G+0.3Q+(Ex-)	183.61	2308.34	0.000	0.628	6.5	0.350	0.000	✓		0 / 30
		G+0.3Q+(Ey+)	183.61	2043.19	0.000	0.628	6.5	0.350	0.000	✓		0 / 30
		G+0.3Q+(Ey-)	183.61	2043.19	0.000	0.628	6.5	0.350	0.000	✓		0 / 30
Floor 5	2.8	G+0.3Q+(Ex+)	180.79	1298.66	0.000	0.294	6.5	0.350	0.000	✓	No Risk	0 / 30
		G+0.3Q+(Ex-)	180.79	1298.66	0.000	0.294	6.5	0.350	0.000	✓		0 / 30
		G+0.3Q+(Ey+)	180.79	1173.21	0.000	0.294	6.5	0.350	0.000	✓		0 / 30
		G+0.3Q+(Ey-)	180.79	1173.21	0.000	0.294	6.5	0.350	0.000	✓		0 / 30

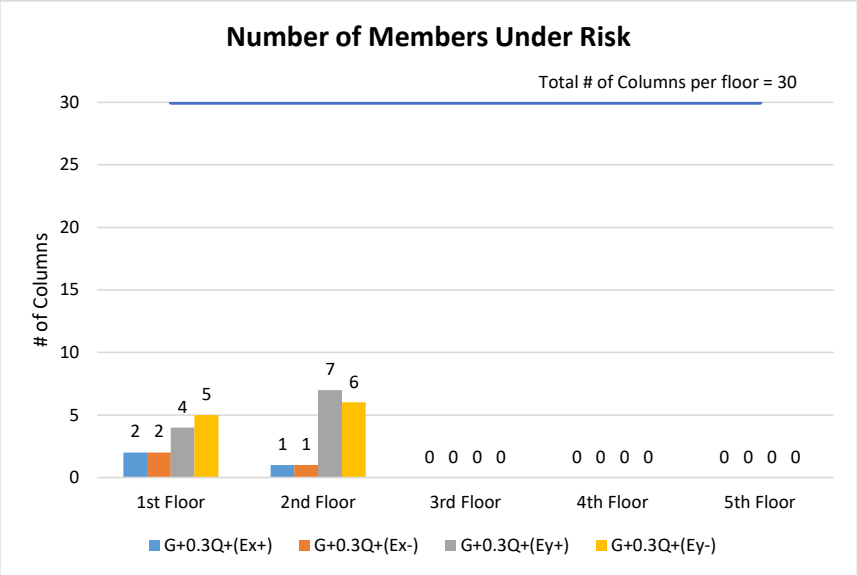

Figure 2.9 Bar chart representing the number of column-type members under risk on each floor of Building I

As indicated by the results presented in Table 2.12, shear force ratio limit was exceeded in the first floor for one of the four loading types. Therefore, this building was assessed to be under risk according to the conditions specified in RYTEIE.

The assessment procedure outlined here indicates that some of the first- and second-story columns of this building are susceptible to failure, the loss of which may set off a progressive collapse occurrence resulting in a partial or total collapse of the building. Judging by the small number of columns under risk and their concentration on the first and second floors of the building, zipper-type progressive collapse is the most possible collapse progression scenario for this case. The members under risk could be retrofitted against failure to mitigate progressive collapse risk. The remaining members and floors are observed to be demonstrating satisfactory structural performance, pointing out to good conformity to prescribed design rules and construction plans.

2.3.3 Assessment Procedures for Building II

Since Building II was also a residential building like Building I, live load reduction factor was found to be 0.3, and the earthquake ground motion level was determined to be of level DD-2 (Table 2.3). Data collected from the site and relevant databases indicated the soil class for the site to be of ZD type, pointing out to the presence of medium dense – dense sand, gravel of very stiff clay layer formations. Map spectral acceleration coefficients, S_S and S_1, were found to be 0.91 and 0.26 seconds, respectively. Using these data and the steps outlined before, spectral acceleration coefficients S_{DS} and S_{D1} were calculated to be 1.034 and 0.541, respectively. These coefficients were then used as inputs for Equation 2.3 to construct the horizontal elastic acceleration spectrum for the building, which is presented in Figure 2.10 below:

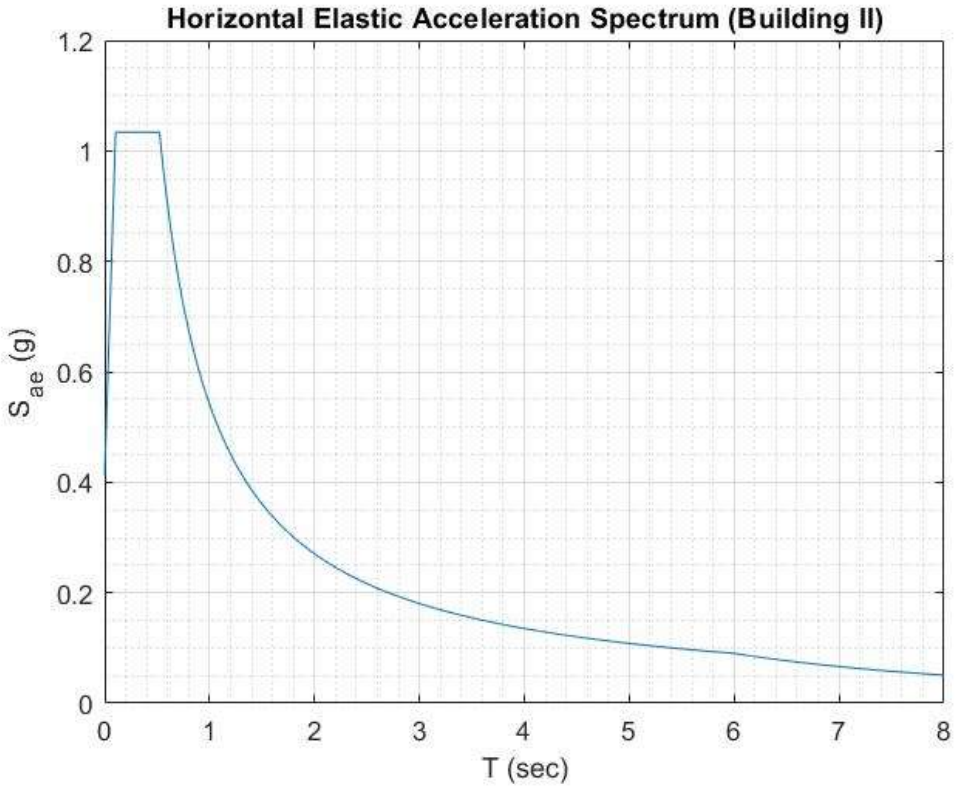

Figure 2.10 Horizontal Elastic Acceleration Spectrum for Building II according to RYTEIE

By making use of this spectrum as well, Building II was modeled and analyzed on according to Chapter 4 in RYTEIE to proceed with risk identification procedures. All columns were conforming the criteria of Class B for column types according to Table 2.9, and m_{limit} and $(\delta/h)_{limit}$ values were obtained from Table 2.10 in light of this information.

Results of the analysis of Building II are presented below:

Table 2.13 Risk identification procedure results for Building II according to RYTEIE

Floor	Floor Height (m)	Loading Type	Floor Mass (Tons)	Total Floor Shear Force (kN)	Total Shear Force of Members Under Risk (kN)	Average Axial Stress (MPa)	In-situ Concrete Strength (MPa)	Floor Shear Force Limit Value	Shear Force Sum of Members Under Risk / Total Shear Force	Investigation	Floor Risk Status	Number of Members Under Risk / Total Member Count
Floor 1	2.9	G+0.3Q+(Ex+)	144.60	3305.52	1962.730	1.909	7.8	0.258	0.594	×	Under Risk	18 / 27
		G+0.3Q+(Ex-)	144.60	3305.52	1962.740	1.909	7.8	0.258	0.594	×		18 / 27
		G+0.3Q+(Ey+)	144.60	3585.71	638.490	1.909	7.8	0.258	0.178	✓		6 / 27
		G+0.3Q+(Ey-)	144.60	3585.71	454.420	1.909	7.8	0.258	0.127	✓		4 / 27
Floor 2	2.9	G+0.3Q+(Ex+)	144.60	3042.11	2675.190	1.519	7.8	0.290	0.879	×	Under Risk	24 / 27
		G+0.3Q+(Ex-)	144.60	3042.11	2675.190	1.519	7.8	0.290	0.879	×		24 / 27
		G+0.3Q+(Ey+)	144.60	3314.73	2687.860	1.519	7.8	0.290	0.811	×		21 / 27
		G+0.3Q+(Ey-)	144.60	3314.73	2506.710	1.519	7.8	0.290	0.756	×		18 / 27
Floor 3	2.9	G+0.3Q+(Ex+)	144.60	2550.75	1510.830	1.128	7.8	0.322	0.592	×	Under Risk	15 / 27
		G+0.3Q+(Ex-)	144.60	2550.75	1510.840	1.128	7.8	0.322	0.592	×		15 / 27
		G+0.3Q+(Ey+)	144.60	2784.46	986.750	1.128	7.8	0.322	0.354	×		8 / 27
		G+0.3Q+(Ey-)	144.60	2784.46	772.200	1.128	7.8	0.322	0.277	✓		6 / 27
Floor 4	2.9	G+0.3Q+(Ex+)	144.60	1933.82	0.000	0.738	7.8	0.350	0.000	✓	No Risk	0 / 27
		G+0.3Q+(Ex-)	144.60	1933.82	0.000	0.738	7.8	0.350	0.000	✓		0 / 27
		G+0.3Q+(Ey+)	144.60	2098.31	0.000	0.738	7.8	0.350	0.000	✓		0 / 27
		G+0.3Q+(Ey-)	144.60	2098.31	0.000	0.738	7.8	0.350	0.000	✓		0 / 27
Floor 5	2.9	G+0.3Q+(Ex+)	142.09	1053.58	0.000	0.348	7.8	0.350	0.000	✓	No Risk	0 / 27
		G+0.3Q+(Ex-)	142.09	1053.58	0.000	0.348	7.8	0.350	0.000	✓		0 / 27
		G+0.3Q+(Ey+)	142.09	1135.22	0.000	0.348	7.8	0.350	0.000	✓		0 / 27
		G+0.3Q+(Ey-)	142.09	1135.22	0.000	0.348	7.8	0.350	0.000	✓		0 / 27

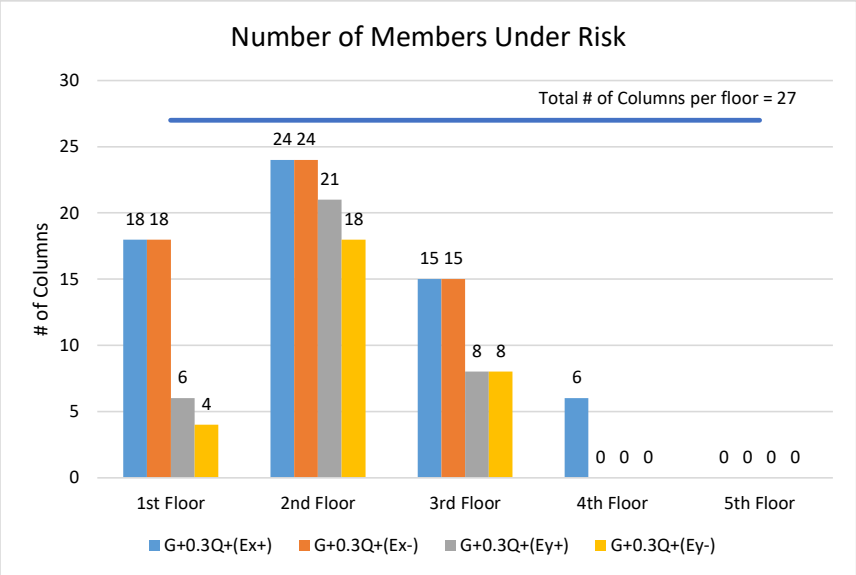

Figure 2.11 Bar chart representing the number of column-type members under risk on each floor of Building II

Results tabulated above reveals that shear force ratio limits were exceeded in the first three floors for different load combination types, indicating an objectively poor overall structural performance. Therefore, this building was assessed to be under risk according to the conditions specified in RYTEIE.

Assessment efforts for this building revealed that the first three floors are under high risk of column loss, possibly due to the use of low-strength reinforcing steel, even in the case of the least effective load combination considered, pointing out to significant risk of progressive collapse onset. Given that more than half of the columns of the first two floors are under risk according to the assessment procedures, it is possible for these floors to undergo a pancake-type of failure, if progressive collapse commences with the loss of a member located in the close vicinity of a cluster of risky members. As the case for the first building, retrofit options could be considered for members under risk, but the decision might not be a feasible one, because retrofits might be needed for a sizeable batch of columns. Only the fifth floor is observed to conform performance targets, since the loads imposed on members at this floor are at marginal levels.

2.4 Assessment of the Buildings According to the Turkish Building Earthquake Code (TBEC)

In this chapter, the two test buildings located in Elazığ, Turkey, are assessed by their structural performance according to the building earthquake code in motion in Turkey, titled “The Turkish Building Earthquake Code” and published in 2018. The assessment efforts presented in this chapter are intended for determining the performance levels of the buildings in terms of the earthquake code in use in Turkey. The results to be obtained are again expected to be compared with the outputs of the new assessment method investigated in this body of work.

The following two subsections are reserved for the performance assessment of each building according to TBEC. Structural analysis results obtained from YAPNET are

used also in this chapter. General progression of the assessment procedure is presented, and all performance metrics are checked according to the limits set by TBEC. The buildings are then evaluated for their performance levels. Similar to the case of the assessment procedure according to RYTEIE, intermediate assessment decisions and member performance limits are observed in detail to draw a comparison between these and the ones included in the assessment method proposed in this study.

2.4.1 Building Assessment Procedure According to TBEC

Rules to be implemented for the assessment of performance under earthquake impact for all existing buildings and building-type structures are defined and explained in Chapter 15 of the TBEC document (TBEC, 2018). Capacity calculations of these buildings are specified under chapters categorized according to the material type (cast-in-place or precast reinforced concrete, steel, cold-formed steel, masonry or timber). The buildings scrutinized in this study are classified as low-rise reinforced concrete frame structures; therefore, the procedures specified for this type of buildings are presented in this section. Earthquake ground motion levels to be used in assessment procedures are defined in Chapter 2, and building performance targets and earthquake design classes (EDCs) are defined in Chapter 3 of the same document.

Assessment procedures specified in TBEC require the collection of information on member details and sizes, load-carrying system geometry and material properties from building construction plans and reports, observations of and measurements taken from the building, and tests conducted on material specimens obtained from the building.

Information levels and corresponding information level coefficients (see Table 2.14) are defined according to the extent of the information on the current state of buildings collected through their inspection. Information level coefficients are applied to

member capacities according to the level of the information obtained from inspected buildings. These levels are determined by the inspection of building geometry, and a series of destructive and non-destructive tests to obtain member details and material properties, details of which for each level are presented in relevant clauses. Uncertainties in the load-carrying systems of built buildings are reflected to calculation methods by information level coefficients.

Table 2.14 Information Level Coefficients for Buildings

Information Level	**Information Level Coefficient**
Limited	0.75
Extensive	1.00

TBEC lays down three damage states and damage limits for ductile members at section level, namely Limited Damage (LD), Controlled Damage (CD) and Pre-failure Damage (PD) states and their corresponding limit values. Limited Damage state describes a limited hyperelastic behavior, Controlled Damage state a hyperelastic behavior in which section strength could be provided safely, and Pre-failure Damage state an advanced level of hyperelastic behavior in the inspected section. Section damage limits specified in TBEC mark transition boundaries between different section damage zones depicted in Figure 2.12. Sections are placed in these damage zones after the internal forces and deformations calculated according to specified procedures are compared with the numerical values corresponding to damage zone interfaces, and member damage states are determined as per the section of that member suffering the greatest damage.

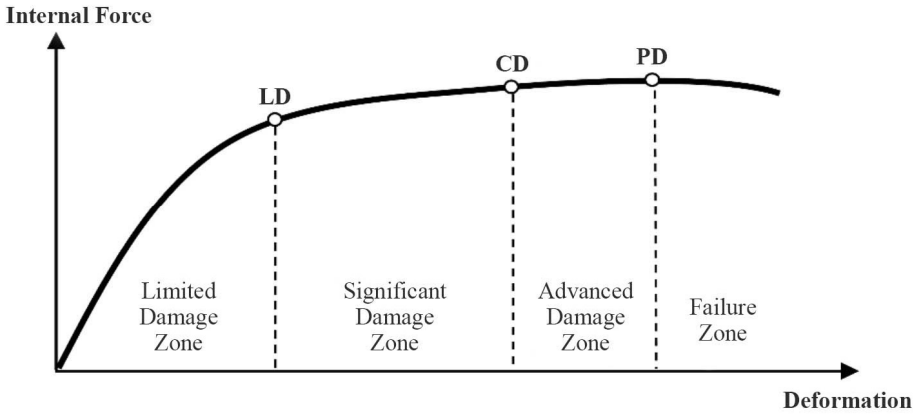

Figure 2.12 Section damage zones defined by TBEC (2018)

TBEC also requires earthquake calculations in order to determine the built or retrofitted buildings, and provides both linear and non-linear calculation methods. Horizontal elastic design spectrum provided in Chapter 2 in TBEC for the earthquake ground motion levels determined according to Clause 2.2 are employed to this end. Procedures to construct the spectrum are as follows:

- Data related to earthquake ground motions to be considered in the assessment of buildings under earthquake effect are defined under Chapter 2. There are four different earthquake ground motion levels defined in TBEC, designated as DD-1, DD-2, DD-3 and DD-4, and earthquake data, such as map spectral acceleration coefficients $S_s$and S_1, corresponding to these levels are collected from the database of the Disaster and Emergency Management Presidency (AFAD). These levels are related to the probabilities and return periods of different earthquake scenarios.
- Map spectral acceleration coefficients, S_s and S_1, are converted to design spectral acceleration coefficients by Equation 2.5. Local ground impact coefficients, F_s and F_1,, used in Equation 2.5 are picked from the Tables 2.15 and 2.16 below:

$$S_{DS} = S_S F_S \qquad S_{D1} = S_1 F_1 \tag{2.5}$$

Table 2.15 Local soil impact coefficients for the short period range according to RYTEIE

Local Soil Class	**Local Soil Impact Coefficient, F_S, for Short Period Range**					
	$S_S \leq 0.25$	$S_S = 0.50$	$S_S = 0.75$	$S_S = 1.00$	$S_S = 1.25$	$S_S \geq 1.50$
ZA	0.8	0.8	0.8	0.8	0.8	0.8
ZB	0.9	0.9	0.9	0.9	0.9	0.9
ZC	1.3	1.3	1.2	1.2	1.2	1.2
ZD	1.6	1.4	1.2	1.1	1.0	1.0
ZE	2.4	1.7	1.3	1.1	0.9	0.8

Table 2.16 Local soil impact coefficients for the period of 1.0 seconds according to RYTEIE

Local Soil Class	**Local Soil Impact Coefficient, F_1, for the period of 1.0 seconds**					
	$S_1 \leq 0.10$	$S_1 = 0.20$	$S_1 = 0.30$	$S_1 = 0.40$	$S_1 = 0.50$	$S_1 \geq 0.60$
ZA	0.8	0.8	0.8	0.8	0.8	0.8
ZB	0.8	0.8	0.8	0.8	0.8	0.8
ZC	1.5	1.5	1.5	1.5	1.5	1.4
ZD	2.4	2.2	2.0	1.9	1.8	1.7
ZE	4.2	3.3	2.8	2.4	2.2	2.0

- Horizontal elastic design spectrum for any earthquake ground motion level under consideration is constructed by using Equation 2.6 and 2.7 (Figure 2.13). Period of transition to constant displacement zone T_L is assumed to be 6 seconds.

$$S_{ae}(T) = \begin{cases} \left(0.4 + 0.6\dfrac{T}{T_A}\right) S_{DS} & T \leq T_A \\ S_{DS} & T_A \leq T \leq T_B \\ \dfrac{S_{D1}}{T} & T_B \leq T \leq T_L \\ \dfrac{S_{D1} T_L}{T^2} & T_L \leq T \end{cases} \tag{2.6}$$

$$T_A = 0.2\frac{S_{D1}}{S_{DS}} \qquad T_B = \frac{S_{D1}}{S_{DS}} \tag{2.7}$$

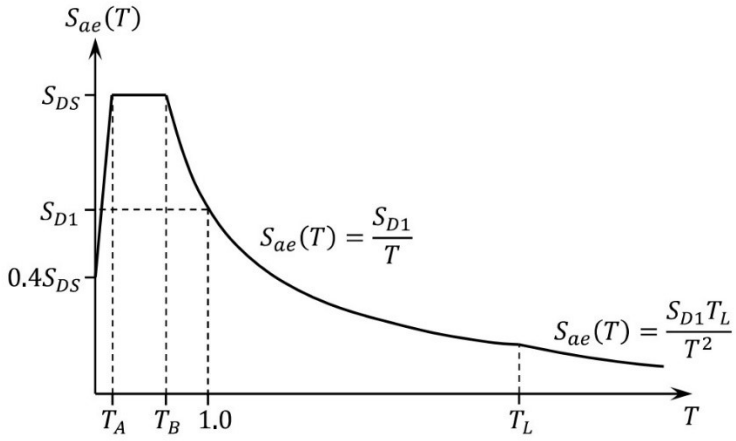

Figure 2.13 Horizontal Elastic Acceleration Spectrum according to TBEC

Earthquake performance of buildings are assessed under the combined effects of applied vertical loads and earthquake effects. Earthquake forces are applied to the building in both orientations and in both directions for each orientation.

Finite element models are created for 3D analysis of the examined building using multi-mode pushover method, with beams and columns modeled as frame elements. Rigid diaphragms are used for modeling reinforced concrete slabs. All floor masses of vertical members are distributed among the floors they are connected to, and dead and live loads are obtained in accordance with TS 498 code.

Earthquake Design Classes are determined according to Building Use Classes (BUC) presented in Table 2.17.

Table 2.17 Building Use Classes and Building Importance Coefficients

Building Use Class	Building Purpose of Use	Building Importance Coefficient (I)
BUC = 1	**Buildings needed to be used after earthquake, buildings people populate for extended periods and in dense populations, buildings where valuable entities are stored and buildings housing hazardous materials** **a)** Buildings that must be immediately used after earthquake (Hospitals, dispensaries, community clinics, fire emergency building and facilities, post offices and other communication facilities, transportation stations and facilities, energy production and distribution facilities, province, district and municipality administration buildings, first aid and disaster planning stations) **b)** Schools, other education building and facilities, dormitories and sleeping quarters, military barracks, correctional facilities, etc. **c)** Museums **d)** Buildings where materials with toxic, explosive, flammable, etc. properties are located or stored	1.5
BUC = 2	**Buildings people populate for short periods of time and in dense populations and other buildings** Shopping malls, sports facilities, movie theaters, theaters, concert halls, places of worship, etc.	1.2
BUC = 3	**Other buildings** Other buildings that do not conform the definitions provided for BUC = 1 and BUC = 2 (Houses, offices, hotels, building-type industrial structures, etc.)	1.0

Earthquake Design Classes (EDC) to be considered in design under earthquake impact are determined according to BUCs and short period design spectral acceleration coefficient defined for DD-2 earthquake ground motion level (Table 2.18).

Table 2.18 Earthquake Design Classes (EDCs)

Short Period Design Spectral Acceleration Coefficient at DD-2 Earthquake Ground Motion Level (S_{DS})	Building Use Class	
	BUC = 1	BUC = 2, 3
$S_{DS} < 0.33$	EDC = 4a	EDC = 4
$0.33 \le S_{DS} < 0.50$	EDC = 3a	EDC = 3
$0.50 \le S_{DS} < 0.75$	EDC = 2a	EDC = 2
$0.75 \le S_{DS}$	EDC = 1a	EDC = 1

Buildings are categorized into eight Building Height Classes (BHC) according to their total height in design under earthquake impact. These classes are defined in Table 2.19 according to their Earthquake Design Classes (EDCs).

Table 2.19 Building Height Ranges Defined According To Building Height Classes and Earthquake Design Classes

Building Height Class	Building Height Ranges Defined According To Building Height Classes and Earthquake Design Classes [m]		
	EDC = 1, 1a, 2, 2a	EDC = 3, 3a	EDC = 4, 4a
BHC = 1	$H_N > 70$	$H_N > 91$	$H_N > 105$
BHC = 2	$56 < H_N \leq 70$	$70 < H_N \leq 91$	$91 < H_N \leq 105$
BHC = 3	$42 < H_N \leq 56$	$56 < H_N \leq 70$	$56 < H_N \leq 91$
BHC = 4	$28 < H_N \leq 42$	$42 < H_N \leq 56$	
BHC = 5	$17.5 < H_N \leq 28$	$28 < H_N \leq 42$	
BHC = 6	$10.5 < H_N \leq 17.5$	$17.5 < H_N \leq 28$	
BHC = 7	$7 < H_N \leq 10.5$	$10.5 < H_N \leq 17.5$	
BHC = 8	$H_N \leq 7$	$H_N \leq 10.5$	

Building Performance Levels are defined for building load-carrying systems under earthquake impact to be the basis for the definition of Building Performance Targets. These levels are:

- Uninterrupted Use (UU) Performance Level corresponds to the state where there is zero or negligible structural damage on building load-carrying system members,
- Limited Damage (LD) Performance Level corresponds to the state where there is limited damage on building load-carrying system members; i.e. where non-linear behavior remains limited,
- Controlled Damage (CD) Performance Level corresponds to the state where there is damage on building load-carrying system members that is not heavy and mostly possible to retrofit,

- Collapse Prevention (CP) Performance Level corresponds to the precollapse state where there is advanced heavy damage on building load-carrying system members. Partial or total collapse of the building is prevented at this level.

Building Performance Targets and corresponding assessment/design approaches are defined according to the building performance levels explained above and presented in Table 2.20.

Table 2.20 Performance Targets and Assessment/Design Approaches to be Applied for Built Cast-In-Place Reinforced Concrete, Precast Reinforced Concrete and Steel Buildings (Except High Buildings - BHC ≥ 2)

Earthquake Ground Motion Level	EDC = 1, 2, 3, 3a, 4, 4a		EDC = 1a, 2a	
	Normal Performance Target	Assessment/Design Approach	Advanced Performance Target	Assessment/Design Approach
DD-3	-	-	LD	PBD
DD-2	CD	PBD	-	-
DD-1	-	-	CD	PBD

Since the buildings scrutinized within the scope of this study require the performance-based assessment and design approach (PBD) according to Table 2.20, the procedures of only this approach will be detailed here. PBD involves the following principles:

- Force-deformation correlations of current or previously predesigned load-carrying system members, which are compatible with non-linear modeling approaches, are determined,
- Calculations of the load-carrying system are done by static or time history dynamic incremental methods, under earthquake ground motion(s) selected in a compatible way with dictated performance target(s), and deformation demands related to non-linear ductile behavior and strength demands related to brittle behavior.

- Obtained deformation and internal force demands are compared with deformation and strength capacities defined in aggreement with prescribed performance target(s),
- For built buildings, deformation-based assessment is completed by demonstrating that deformation and strength demands are below or above the corresponding deformation and strength capacities.
- For the assessment of load-carrying system members, earthquake effects are combined with gravity and live loads, and these load combinations are applied to the structure for all calculations ($G + nQ \pm E$) for each orientation in both directions of earthquake force. Active live loads are calculated by multiplying these loads with a live load mass participation coefficient, n, specified in Table 2.21.

Table 2.21 Live load mass participation coefficients

Building Purpose of Use	*n*
Warehouse, bonded warehouse, etc.	0.80
School, dormitory, sports hall, cinema, theater, concert hall, place of worship, restaurant, shop, etc.	0.60
House, office, hotel, hospital, parking lot, etc.	0.30

- All structural members are modeled as frame elements with lumped plasticity behavior (plastic hinge) model. Hinge lengths are taken half of the effective depth of the section in the active orientation ($L_p = 0.5h$).
- Allowed concrete and reinforcing steel total unit deformations calculated according to lumped plasticity model for collapse prevention (CP) performance level are as follows for rectangular columns and beams:
    - For concrete:

$$\varepsilon_c^{(CP)} = 0.035 + 0.04\sqrt{\omega_{we}} \leq 0.018 \qquad (2.8)$$

where;

$$\omega_{we} = \alpha_{se}\rho_{sh,min}\frac{f_{ywe}}{f_{ce}} \quad (2.9)$$

$$\alpha_{se} = \left(1 - \frac{s}{2D}\right)^{n} \quad ; \quad \rho_{sh} = \frac{2A_{os}}{Ds} \quad (2.10)$$

- For steel:

$$\varepsilon_s^{(CP)} = 0.4\varepsilon_{su} \quad (2.11)$$

- Plastic rotation limit is calculated by Equation 2.12 according to lumped plasticity behavior model for reinforced concrete limits and used in performance assessment for collapse prevention (CP) performance level.

$$\theta_p^{(CP)} = \frac{2}{3}\left[(\varphi_u - \varphi_y)L_p\left(1 - 0.5\frac{L_p}{L_s}\right) + 4.5\varphi_u d_b\right] \quad (2.12)$$

- Allowed concrete and reinforcing steel total unit deformations and plastic rotation limits to be used for the performance assessment conducted for controlled damage (CD) performance level are defined in relation to the values calculated for CP performance level and these limits are given in Equations 2.13 and 2.14.

$$\varepsilon_c^{(CD)} = 0.75\varepsilon_c^{(CP)} \quad ; \quad \varepsilon_s^{(CD)} = 0.75\varepsilon_s^{(CP)} \quad (2.13)$$

$$\theta_p^{(CD)} = 0.75\theta_p^{(CP)} \quad (2.14)$$

- Allowed concrete and reinforcing steel total unit deformations calculated for performance assessment conducted for limited damage (LD) performance level are given in Equation 2.15. In addition, plastic hinge formation is not allowed in the load-carrying system for this performance level (Equation 2.16).

$$\varepsilon_c^{(LD)} = 0.0025 \quad ; \quad \varepsilon_s^{(LD)} = 0.0075 \tag{2.15}$$

$$\theta_p^{(LD)} = 0 \tag{2.16}$$

Earthquake ground motion levels and minimum performance targets prescribed for buildings at these earthquake ground motion levels to be considered in the determination of earthquake performances of built or retrofitted buildings were presented in Table 2.20.

Earthquake performance of built buildings are related to the state of the damages expected to occur in the building under earthquake impact, and defined by considering four different damage states. Building performance level is determined by the application of calculation methods defined in clauses 15.5 and 15.6, and the decisions made on member performances according to Clause 15.7.

In any floor of reinforced concrete buildings, at most 20% of the beams are permitted to cross into Significant Damage Zone in the end of the calculations done for each earthquake direction, but all other load-carrying members are within limited damage zone. Provided that members damaged in a brittle fashion, if any, are retrofitted, buildings in such state may assumed to be at limited damage performance level.

The buildings satisfying the condition below are assumed to be at controlled damage performance level, provided that members damaged in a brittle fashion, if any, are retrofitted:

(a) On any floor of reinforced concrete buildings, as a result of the calculations carried out for each direction of the applied earthquake, except for the secondary beams (not located within horizontal load-carrying system), at most 35% of the beams and the amount of vertical members (columns, walls and retrofitted infill walls) speficied in paragraph (b) are permitted to move to advanced damage zone.

(b) Total contribution of vertical members to the shear force carried by vertical members on each floor must be below 20%. On the top floor, the ratio of the

shear force sum for vertical elemants within the zone of advanced damage state to the sum of shear forces all vertical members on the same floor can be at most 40%.

(c) All other load-carrying members are within the limited damage zone or significant damage zone. However, on any floor, the ratio of shear forces carried by vertical members both at the top and bottom sections of which significant damage limit is exceeded, to the shear forces carried by all vertical members should not exceed 30%.

Provided the consideration that all members damaged in a brittle fashion are within failure zone, buildings conforming to the following conditions are assumed to be at collapse prevention performance level:

(a) As a result of the calculations done for each applied earthquake direction on any floor of reinforced concrete buildings, except for secondary (not located within the load-carrying system) beams, at most 20% of the beams can transition into failure zone.

(b) All other load-carrying members are within limited damage zone, significant damage zone or advanced damage zone. However, on any floor, the ratio of shear forces carried by vertical members both at the top and bottom sections of which significant damage limit is exceeded, to the shear forces carried by all vertical members should not exceed 30%.

(c) Use of the building in its current state is hazardous in respect to life safety.

The building is in failure state if it cannot satisfy collapse prevention performance level. Use of the building is hazardous in respect to life safety.

2.4.2 Assessment Procedures for Building I

According to the assessment procedures outlined by TBEC, earthquake data related to the assessment of Building I are the same as those obtained in the assessment efforts by RYTEIE, corresponding to the response spectrum given in Figure 2.8. The

building has a live load reduction factor of 0.3 according to Table 2.21, and map spectral acceleration coefficients, S_S and S_1, were found to be 0.91 and 0.25 seconds, respectively. These values are used to calculate spectral acceleration coefficients, S_{DS} and S_{D1} (Tables 2.15 and 2.16), which were found to be 1.092 and 0.375, respectively. Building Use Class of this building was determined to be BUC = 3, given that it is a residential building (Table 2.17), and earthquake design class of the building, according to these data and Table 2.18, was found to be EDC = 1. Table 2.20 shows that this design class requires the performance-based design and assessment approach to be adopted. Therefore, limits specified in TBEC for this approach are used in assessing the performance of members comprising this building. Results of the assessment study conducted for Building I are presented in Table 2.22.

Results given in Table 2.22 reveal that the first floor of the building cannot satisfy collapse prevention (CP) performance level for any load combination considered, indicating that the building is susceptible to total collapse due to poor performance even in the presence of service level (DD-2 level) earthquakes. The eleven first-floor columns which have failed to satisfy collapse prevention limits and poor performance of some of the second-floor columns point out that all progressive collapse types are possible to be observed in the building depending on the location of the column that may initiate collapse progression with its failure. In cases where poorly-performing first-floor columns are not closely packed, domino-type failure may occur, while in the other case, pancake-type failure might take place.

Table 2.22 Performance assessment procedure results for Building I according to TBEC

Floor	Floor Height (m)	Loading Type	Number of Beams / Number of Primary Beams	Number of Beams in Limited Damage Zone	Number of Beams in Significant Damage Zone	Number of Beams in Advanced Damage Zone	Number of Beams in Failure Zone	Total Number of Columns	Number of Columns in Limited Damage Zone	Number of Columns in Significant Damage Zone	Number of Columns in Advanced Damage Zone	Number of Columns in Failure Zone	Limited Damage Performance Level	Controlled Damage Performance Level	Collapse Prevention Performance Level
Floor 1	2.8	G+0.3Q+(Ex+)	33 / 31	27	6	0	0	30	11	3	5	11	NO	NO	NO
		G+0.3Q+(Ex-)	33 / 31	27	6	0	0	30	11	5	3	11	NO	NO	NO
		G+0.3Q+(Ey+)	28 / 22	28	0	0	0	30	9	9	0	12	NO	NO	NO
		G+0.3Q+(Ey-)	28 / 22	28	0	0	0	30	10	8	2	10	NO	NO	NO
Floor 2	2.8	G+0.3Q+(Ex+)	33 / 31	26	7	0	0	30	9	18	2	1	NO	NO	NO
		G+0.3Q+(Ex-)	33 / 31	26	6	1	0	30	8	18	4	0	NO	NO	YES
		G+0.3Q+(Ey+)	28 / 22	28	0	0	0	30	3	25	2	0	NO	YES	YES
		G+0.3Q+(Ey-)	28 / 22	28	0	0	0	30	5	21	3	1	NO	NO	NO
Floor 3	2.8	G+0.3Q+(Ex+)	33 / 31	27	6	0	0	30	11	19	0	0	NO	YES	YES
		G+0.3Q+(Ex-)	33 / 31	26	7	0	0	30	11	19	0	0	NO	YES	YES
		G+0.3Q+(Ey+)	28 / 22	28	0	0	0	30	6	24	0	0	NO	YES	YES
		G+0.3Q+(Ey-)	28 / 22	28	0	0	0	30	7	22	1	0	NO	YES	YES
Floor 4	2.8	G+0.3Q+(Ex+)	33 / 31	30	3	0	0	30	16	14	0	0	NO	YES	YES
		G+0.3Q+(Ex-)	33 / 31	30	3	0	0	30	15	15	0	0	NO	YES	YES
		G+0.3Q+(Ey+)	28 / 22	28	0	0	0	30	16	14	0	0	NO	YES	YES
		G+0.3Q+(Ey-)	28 / 22	28	0	0	0	30	14	16	0	0	NO	YES	YES
Floor 5	2.8	G+0.3Q+(Ex+)	33 / 31	33	0	0	0	30	30	0	0	0	YES	YES	YES
		G+0.3Q+(Ex-)	33 / 31	33	1	0	0	30	30	0	0	0	YES	YES	YES
		G+0.3Q+(Ey+)	28 / 22	28	0	0	0	30	30	0	0	0	YES	YES	YES
		G+0.3Q+(Ey-)	28 / 22	28	0	0	0	30	28	2	0	0	NO	YES	YES

2.4.3 Assessment Procedures for Building II

As in the case of Building I, earthquake data related to the assessment of Building II are the same as those obtained in the assessment efforts by RYTEIE, corresponding to the response spectrum given in Figure 2. The building has a live load reduction factor of 0.3 according to Table 2.21, and map spectral acceleration coefficients, S_S and S_1, were found to be 0.91 and 0.26 seconds, respectively. These values are used to calculate spectral acceleration coefficients, S_{DS} and S_{D1} (Tables 2.15 and 2.16), which were found to be 1.034 and 0.541, respectively. Building Use Class of this building was determined to be BUC = 3, for it is a residential building (Table 2.17), and earthquake design class of the building, according to these data and Table 2.18, was found to be EDC = 1. Table 2.20 shows that this design class requires the performance-based design and assessment approach to be adopted. Therefore, limits specified in TBEC for this approach are used in assessing the performance of members comprising this building. Results of the assessment study conducted for Building II are presented in Table 2.23.

Results presented in Table 2.23 show that Building II cannot satisfy collapse prevention (CP) performance level in the first three floors for any load combination considered, indicating that the building is highly susceptible to total collapse due to sub-par performance even in cases of service level (DD-2) earthquakes. Given that the number of columns in the first two floors, which are located in the failure zone in terms of damage levels, it is possible to observe all progressive collapse types in this building. In addition, distribution of a considerable number of poorly-performing columns among floors is likely to cause domino-type failure, yet, in cases of closely-packed weak columns, it is possible to observe pancake-type failure.

Table 2.23 Performance assessment procedure results for Building II according to TBEC

Floor	Floor Height (m)	Loading Type	Number of Beams / Number of Primary Beams	Number of Beams in Limited Damage Zone	Number of Beams in Significant Damage Zone	Number of Beams in Advanced Damage Zone	Number of Beams in Failure Zone	Total Number of Columns	Number of Columns in Limited Damage Zone	Number of Columns in Significant Damage Zone	Number of Columns in Advanced Damage Zone	Number of Columns in Failure Zone	Limited Damage Performance Level	Controlled Damage Performance Level	Collapse Prevention Performance Level
Floor 1	2.9	G+0.3Q+(Ex+)	32 / 24	17	15	0	0	27	1	4	10	12	NO	NO	NO
		G+0.3Q+(Ex-)	32 / 24	17	15	0	0	27	1	4	10	12	NO	NO	NO
		G+0.3Q+(Ey+)	28 / 25	28	0	0	0	27	2	6	0	19	NO	NO	NO
		G+0.3Q+(Ey-)	28 / 25	28	0	0	0	27	0	8	2	17	NO	NO	NO
Floor 2	2.9	G+0.3Q+(Ex+)	32 / 24	16	16	0	0	27	1	3	4	19	NO	NO	NO
		G+0.3Q+(Ex-)	32 / 24	16	16	0	0	27	1	3	4	19	NO	NO	NO
		G+0.3Q+(Ey+)	28 / 25	28	0	0	0	27	0	6	6	15	NO	NO	NO
		G+0.3Q+(Ey-)	28 / 25	28	0	0	0	27	0	6	4	17	NO	NO	NO
Floor 3	2.9	G+0.3Q+(Ex+)	32 / 24	21	11	0	0	27	1	6	10	10	NO	NO	NO
		G+0.3Q+(Ex-)	32 / 24	20	12	0	0	27	1	6	10	10	NO	NO	NO
		G+0.3Q+(Ey+)	28 / 25	28	0	0	0	27	0	6	12	9	NO	NO	NO
		G+0.3Q+(Ey-)	28 / 25	28	0	0	0	27	0	10	9	8	NO	NO	NO
Floor 4	2.9	G+0.3Q+(Ex+)	32 / 24	25	7	0	0	27	2	22	3	0	NO	YES	YES
		G+0.3Q+(Ex-)	32 / 24	25	7	0	0	27	2	22	3	0	NO	YES	YES
		G+0.3Q+(Ey+)	28 / 25	28	0	0	0	27	4	15	6	2	NO	NO	NO
		G+0.3Q+(Ey-)	28 / 25	28	0	0	0	27	0	23	4	0	NO	NO	YES
Floor 5	2.9	G+0.3Q+(Ex+)	32 / 24	32	0	0	0	27	20	7	0	0	NO	YES	YES
		G+0.3Q+(Ex-)	32 / 24	32	0	0	0	27	20	7	0	0	NO	YES	YES
		G+0.3Q+(Ey+)	28 / 25	28	0	0	0	27	12	15	0	0	NO	YES	YES
		G+0.3Q+(Ey-)	28 / 25	28	0	0	0	27	20	7	0	0	NO	YES	YES

2.5 Discussion

Assessment studies explained in this chapter reveal that the two buildings introduced in the beginning of the chapter are under considerable progressive collapse risk, and the risk status of each building is expected to be reflected in corresponding building collapse envelopes to be constructed in the next chapter. Load combinations and structural configurations investigated by the assessment guidelines followed in this chapter are observed to be site- and case-specific, hinting that the use of these procedures has limitations in these respects. Therefore, the need for assessment tools encompassing a wider spectrum of cases looms.

The structural assessment efforts for the two buildings according to the RYTEIE and TBEC specifications currently in motion demonstrate also that available assessment procedures are considerably arduous, since they require soil investigation tests, rebar identification, extensive core sampling and earthquake analyses. Therefore, in an assessment code to be in effect and at the disposal of engineers from a wide spectrum of experience, simpler, faster and easier-to-implement procedures are needed to be able to assess structural performance of commonly encountered types of buildings, in our case, low-rise reinforced concrete buildings.

Building collapse envelopes are robust candidates for rapid and reliable structural performance assessment endeavors, and the following chapter is devoted to exploring their promise and the influence of reinforced concrete column members on their capabilities.

CHAPTER 3

BUILDING COLLAPSE ENVELOPES

3.1 Introduction

Building collapse envelope could be defined as a simple structural performance assessment tool created by using data points corresponding to different limit states of a given building. Each data point in these envelopes is obtained by conducting a numerical analysis of the building with a selected structural configuration and under different loading conditions. Envelopes constructed in this fashion, then, could be compared with demand data to determine the performance of the building under investigation in a reliable and rapid manner. Being refined representations of sizeable batches of complex and arduous structural analyses, building collapse envelopes have promise for providing the engineers from relevant fields with an accessible and easy-to-use assessment method to carry out structural performance assessment studies. However, the prospects of this tool are yet to be discovered, requiring research efforts towards determining the influence of parameters affecting their reliability and accuracy.

This chapter is intended to make an attempt to examine the impact of changes in certain structural parameters on building collapse envelopes by demonstrating the variations caused by tweaks in a selected set of parameters in the numerical models of two test buildings. The first section is devoted to verification studies for the analysis tool used in this study. Analysis efforts to construct building collapse envelopes for the two test buildings and their numerical variants are presented in detail in the following section. The chapter is concluded with an extensive curation of the data obtained from these analyses to demonstrate the influence of reinforced concrete column details on building collapse envelopes.

3.2 Verification Studies

Pushover analyses of the buildings assessed in the following chapters of this study were conducted on OpenSees, short for 'The Open System for Earthquake Engineering Simulation'. OpenSees is an open-source software suite capable of conducting a wide range of analysis types for structural or geotechnical systems. Efficient and rapid in terms of computations, OpenSees allows its users to select among an expansive variety of modeling and analysis choices while performing an analysis. Having an open-sourced and scripting-based nature, OpenSees occasionally resembles a black box software, warranting verification efforts to ensure sound analyses and results.

Albeit not complex ones, the buildings examined in this study required a sizeable batch of computations on OpenSees, with many modeling and analysis choices made in a meticulous fashion. This deemed another round of confirmatory checks necessary to make sure that the outputs of the analyses conducted on OpenSees were sound and relevant. To this end, two simple structural models with their experimental data of pushover analyses readily available and one three-dimensional structural model, which is the first test building investigated in this study were selected to be modeled on OpenSees. These models were then analyzed with different modeling and analysis preferences, until the outputs of these analyses and the experimental data matched to an acceptable level. The results of these efforts were conducted to observe whether OpenSees is capable of capturing the real-life behavior of structures modeled on the platform, and, therefore, can be relied on while conducting the pushover analyses of the buildings under scrutiny.

In this section, properties of the verification models, and the modeling and analysis preferences on OpenSees are presented in detail.

3.2.1 Verification Model I: Cantilever Beam

The first model was chosen to be a cantilever beam, given its simplicity and its promise as an easy-to-experiment-on nature as a specimen type. The cantilever beam used for verification in this study was selected out of the group of specimens prepared and analyzed within the scope of a doctoral dissertation by Bayrak (1998). The beam, designated by the label AS-2HT in this text, consists of a stub representing a discontinuity similar to a footing or a beam-column joint, and a column part that represents the length of a column between the section of maximum moment and the point of contraflexure (Figure 3.1). High-strength concrete and commercial grade steel reinforcing bars were used in the manufacturing of the specimen, details of which are presented in Table 3.1.

Table 3.1 Details of the AS-2HT specimen

f_c' (MPa)	Lateral Steel				Longitudinal Steel			Axial Load	
	Size (mm)	Spacing (mm)	ρ_s (%)	f_{yh} (MPa)	No. & Size (mm)	ρ_l (%)	f_{yl} (MPa)	$\frac{P}{f_c' * A_g}$	$\frac{P}{P_0}$
71.7	11.2	90	2.84	542	8-19.5	2.58	454	0.36	0.36

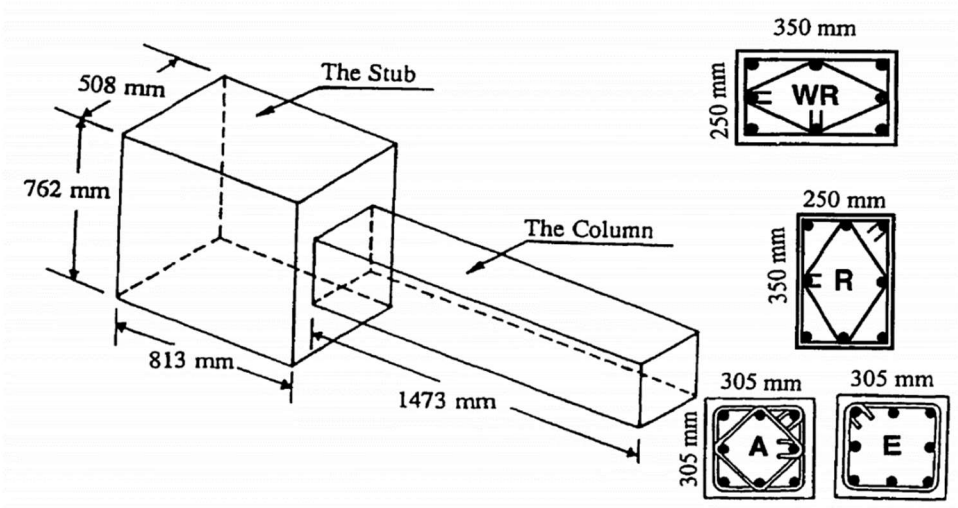

Figure 3.1 General layout of the AS-2HT test specimen

Certain testing preferences for this specimen are, for the sake of simplicity, changed in the OpenSees verification model: A monotonic loading at the tip of the column was applied in the model instead of the cyclic one at the stub-column interface, and the stub was represented by a fixed support. P-Delta effects were also included to introduce the effect of axial load on the behavior of the model. OpenSees code for the model of this specimen is presented in Appendix X.

Shear force versus tip deflection plot created by the experimental results in Bayrak's dissertation was extracted to get the data, and the outermost points of the plot were selected to construct the pushover curve for the experiment (Figure 3.2). Data recorded during the analysis on OpenSees was plotted together with this curve to assess the verification efforts for this specimen (Figure 3.3).

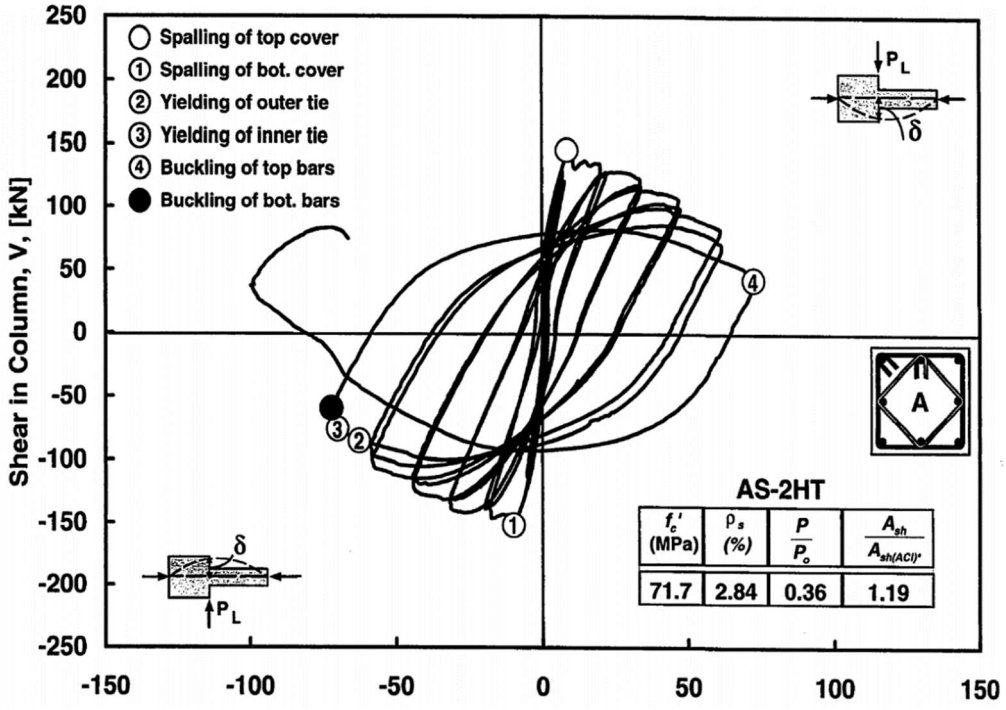

Figure 3.2 Shear Force versus Tip Deflection Behavior of Specimen AS-2HT

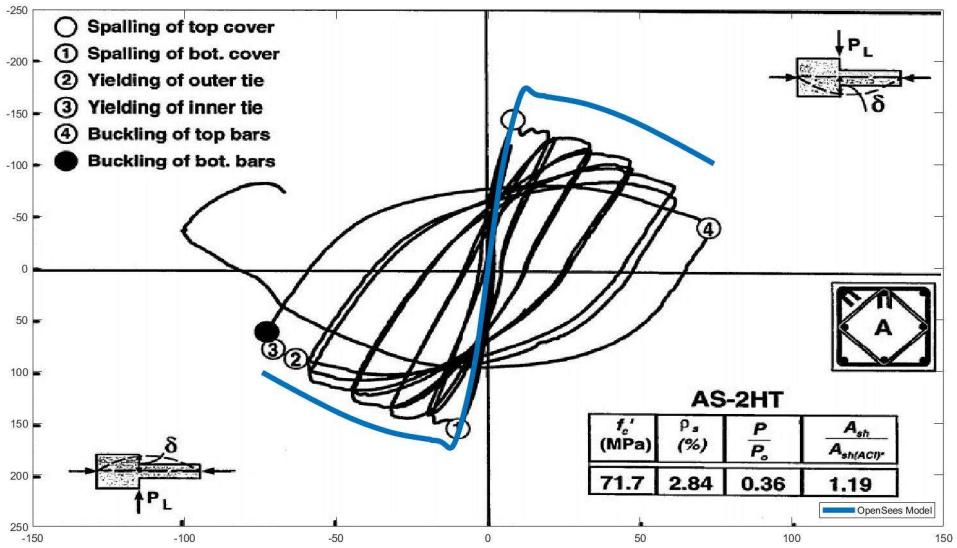

Figure 3.3 Comparison of shear Force versus tip deflection behavior represented by experimental data and OpenSees analysis outputs

Figure 3.3 demonstrates that the initial stiffness of the specimen was reflected correctly by the model and the descending portions of both curves after the peak shear force level was also in agreement without large deviations. The difference between the peak shear force values can be explained by strength degradation introduced to the experimental data by cyclic loading; therefore, the results of the OpenSees model proved to be in good agreement with available experimental data.

3.2.2 Verification Model II: Portal Frame

A simple portal frame comprised of two identical columns and an overlying beam with a slab deck (Figure 3.4) constituted the second model to be used in verification efforts, with its promise to demonstrate the pushover analysis capabilities of OpenSees in the presence of interconnected members within a somewhat complex structure. The frame was tested at METU Structural Mechanics Laboratory.

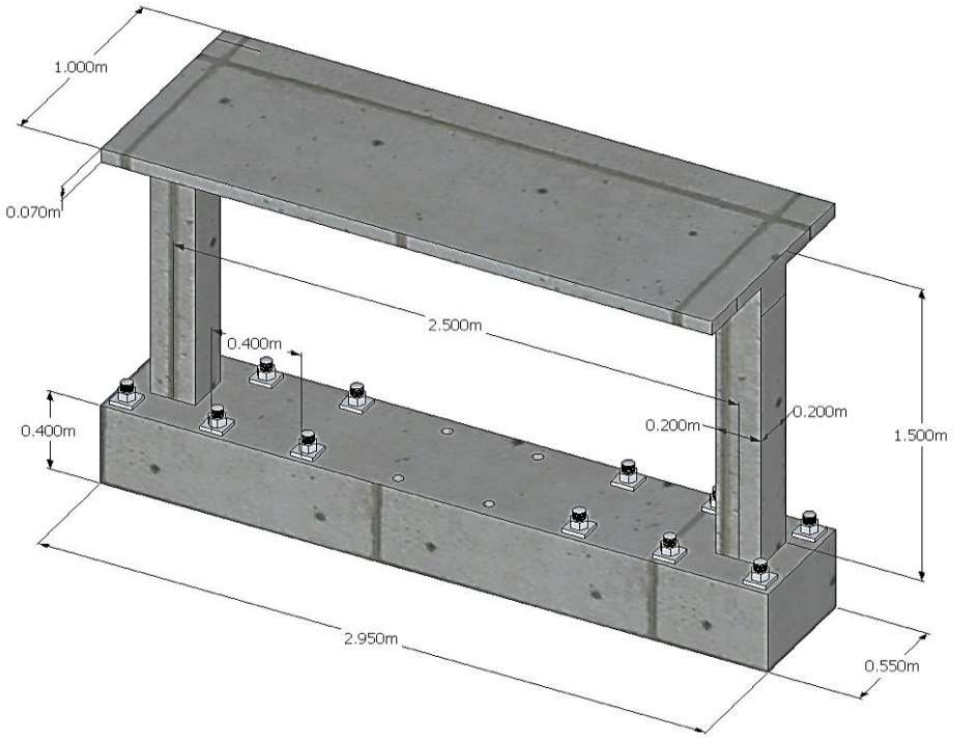

Figure 3.4 General layout of the portal frame

The frame was erected by using commercial grade concrete and steel reinforcing bars, mechanical properties and details of which are presented in Figure 3.5 and Table 3.2

Table 3.2 Mechanical properties of the materials of the portal frame

f_{ck} (MPa)	Lateral Steel			Longitudinal Steel		
	f_{yk} (MPa)	f_{su} (MPa)	ε_{su}	f_{yk} (MPa)	f_{su} (MPa)	ε_{su}
28.0	330	466	0.40	405	558	0.24

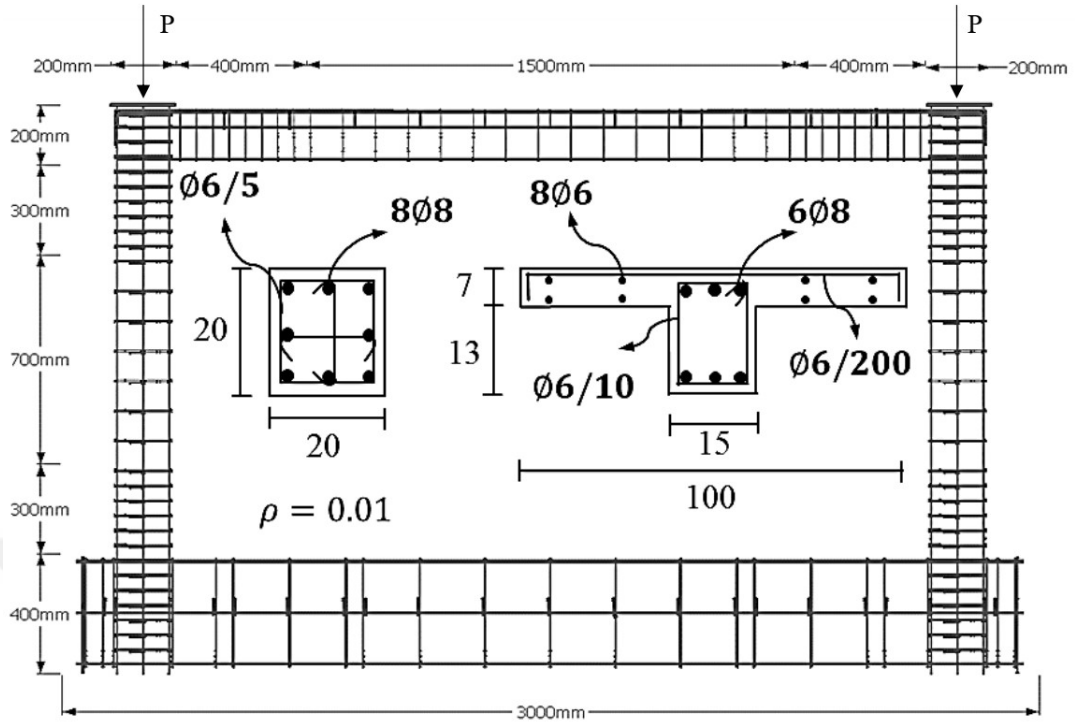

Figure 3.5 Details of the portal frame

Two point loads at the top nodes of the two columns and a distributed load in the downward direction on the slab deck were also introduced to the frame.

While the distributed load was exerted via immobile chunks of concrete placed on top of the slab, the two point loads on the columns were applied by means of two force-controlled hydraulic cylinders connected via pins to solely transfer the loads. A displacement-controlled hydraulic actuator was employed to introduce lateral cyclic loading to the system. Data were recorded by means of LVDTs installed at several points of interest on the frame.

In the construction of the OpenSees verification model for this frame, a number of modeling decisions, again, were altered in favor of a simpler model: Firstly, a monotonic loading regime was imposed at the tip of one of the columns instead of the cyclic loading pattern in the real-time experiment. The slab on top of the beam was omitted, for its inclusion would not affect the pushover performance of the overall structural system. The spacing of transverse steel in all members was

decreased at the beam-column joints to control shear failure in the constructed frame, but transverse steel bars were spaced evenly in all members in the OpenSees model. Finally, the beam was modelled as an elastic section for its real behavior was of no concern for the results of the pushover analysis. P-Delta effects were included to observe the second-degree effects of the point loads imposed on the columns.

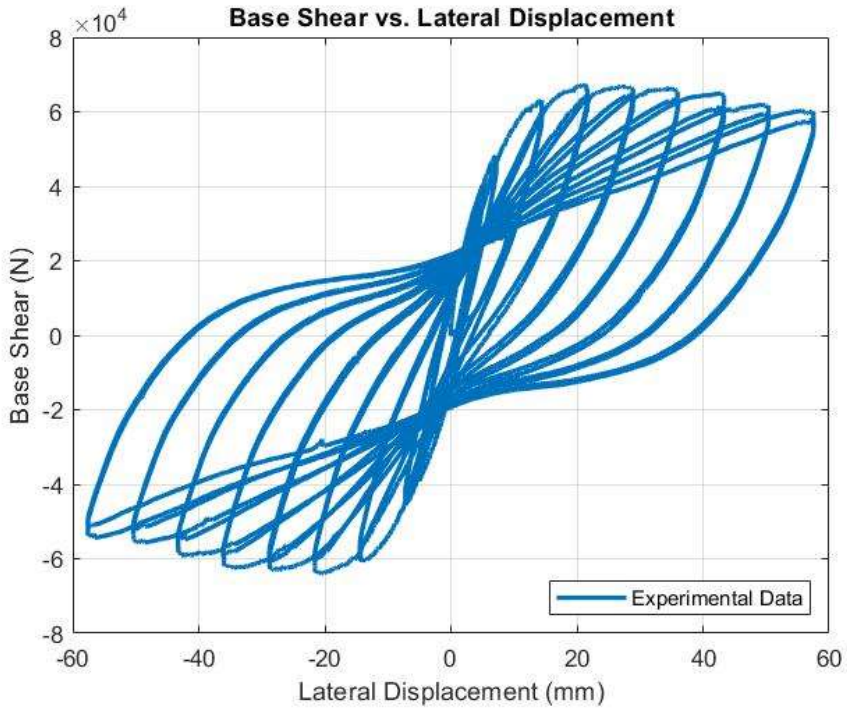

Figure 3.6 Base Shear versus Lateral Displacement response of the Portal Frame according to experiment results

Data recorded during the pushover analysis of the frame were used, following simple calibrations, to create shear force versus lateral displacement plot of the structural system (Figure 3.6). Results obtained from the numerical analysis were also refined to create the same plot, and these two plots were juxtaposed to assess the capabilities of OpenSees (Figure 3.7).

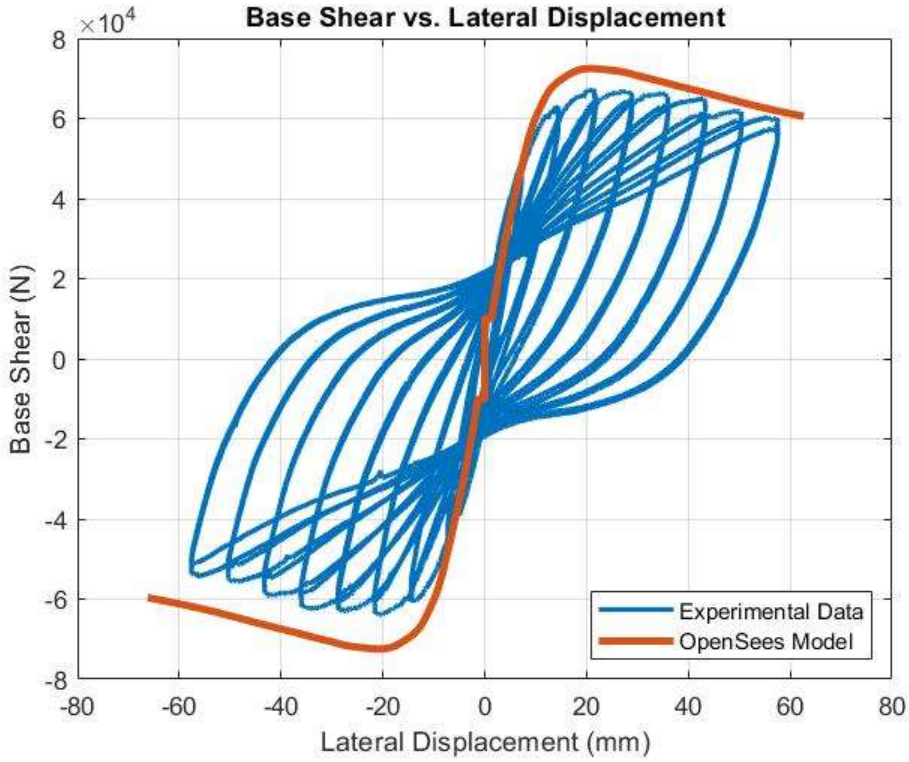

Figure 3.7 Comparison of shear force versus lateral displacement response of the portal frame represented by experimental data and OpenSees analysis outputs

The close agreement of the trends displayed by both sets of data in terms of initial stiffness responses and descending portions reflects a satisfactory depiction of the structural system by OpenSees. The difference between peak shear values can be addressed, as in the previous section, by strength degradation brought about by the cyclic loading regime utilized in the laboratory experiment. Therefore, it is verified that the capabilities of OpenSees in conducting a pushover analysis can be relied upon in conducting pushover analyses for the buildings to be assessed within the scope of this study.

3.2.3 Verification Model III: Five-Story Residential Building

The third verification model is the first test building examined within the scope of this study, which is a five-story reinforced concrete residential building composed

of beams and columns. This building was tested for its load redistribution capabilities in a live column removal test, and 11 first-story columns were removed in a predetermined order to this end (Figure 2.3). The building was collapsed upon the removal of the eleventh column in this order. For the verification of live column removal test, the building is modeled in the OpenSees environment, and the selected 11 first-story columns are removed following the same sequence as the live test. At each step, axial demand-to-capacity ratio (DCR) values for each first-story column were monitored. DCR values of first-story columns at each column removal step are presented in the figures below. It should be noted that the predetermined column removal order is indicated by the columns marked with the letter 'R':

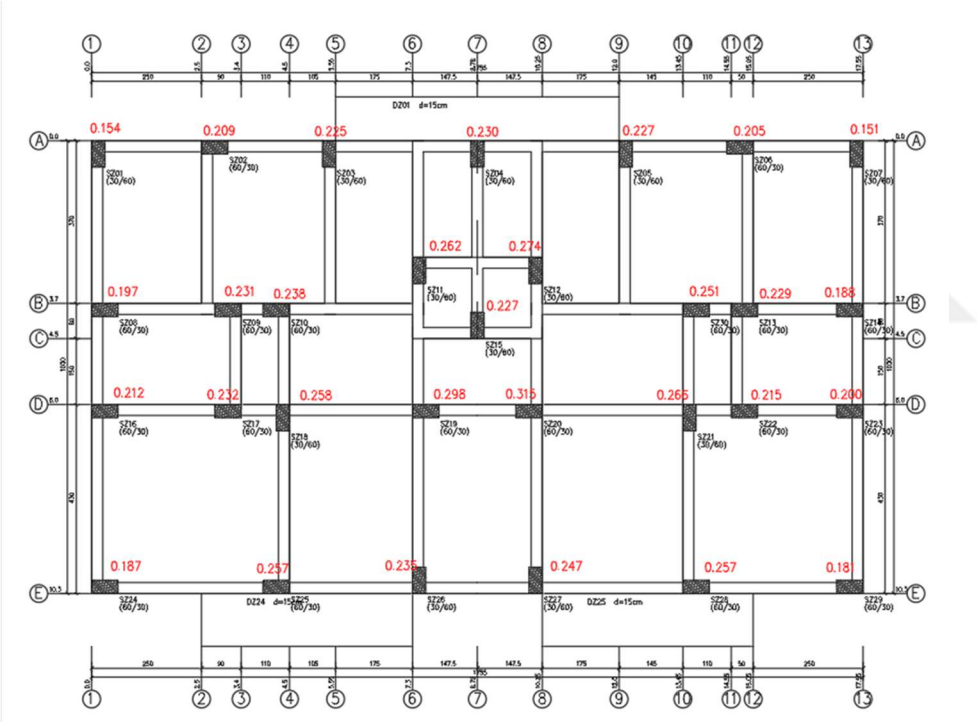

Figure 3.8 DCR values for the first-story columns in the verification of live column removal test (Initial state with no column removal)

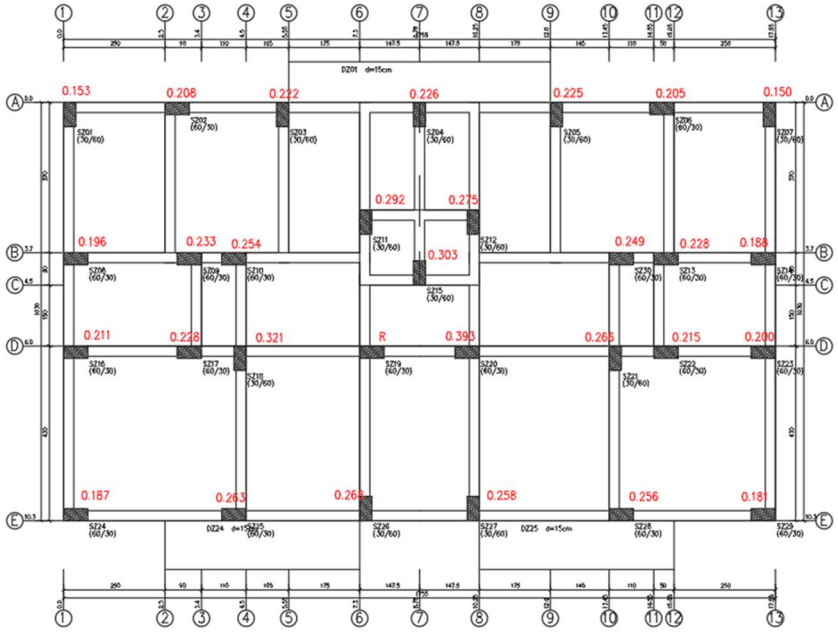

Figure 3.9 DCR values for the first-story columns in the verification of live column removal test (Step 1)

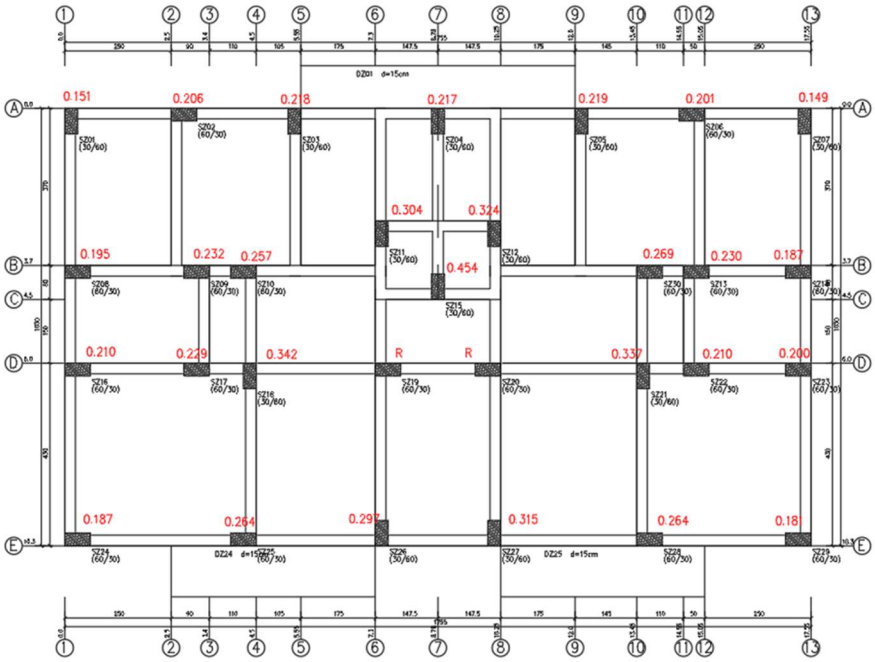

Figure 3.10 DCR values for the first-story columns in the verification of live column removal test (Step 2)

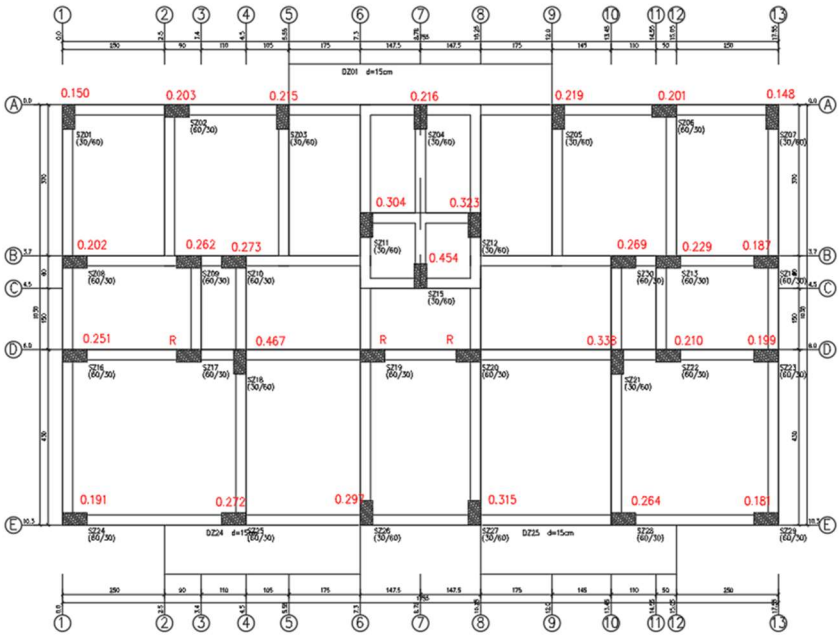

Figure 3.11 DCR values for the first-story columns in the verification of live column removal test (Step 3)

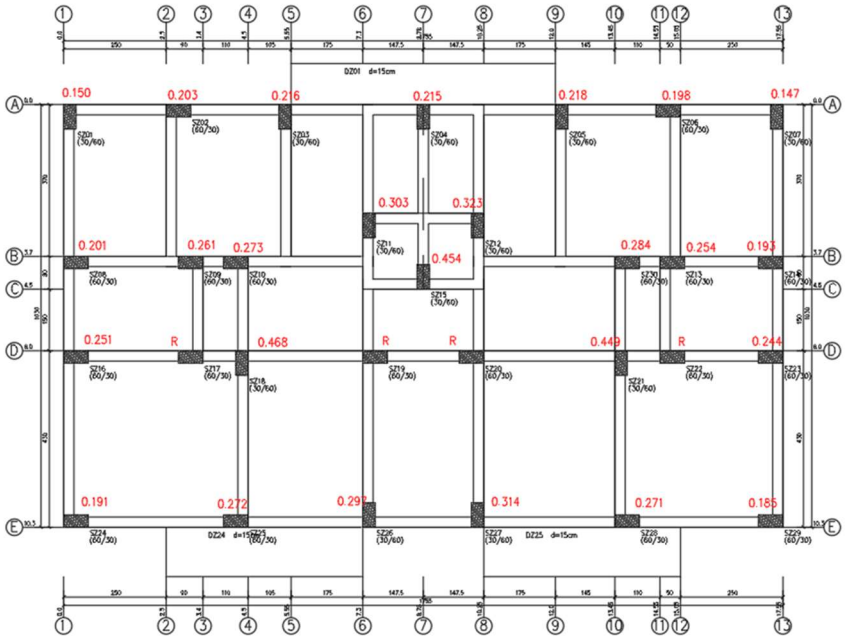

Figure 3.12 DCR values for the first-story columns in the verification of live column removal test (Step 4)

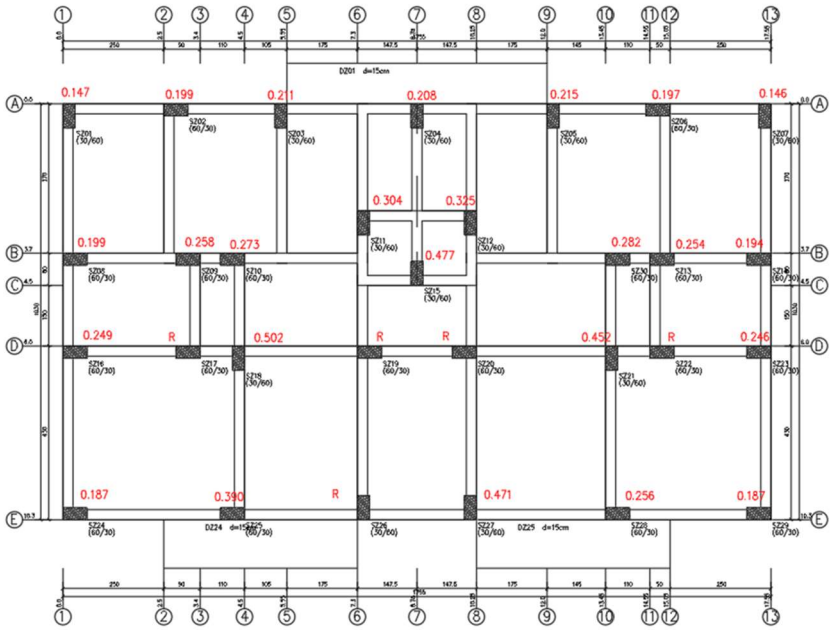

Figure 3.13 DCR values for the first-story columns in the verification of live column removal test (Step 5)

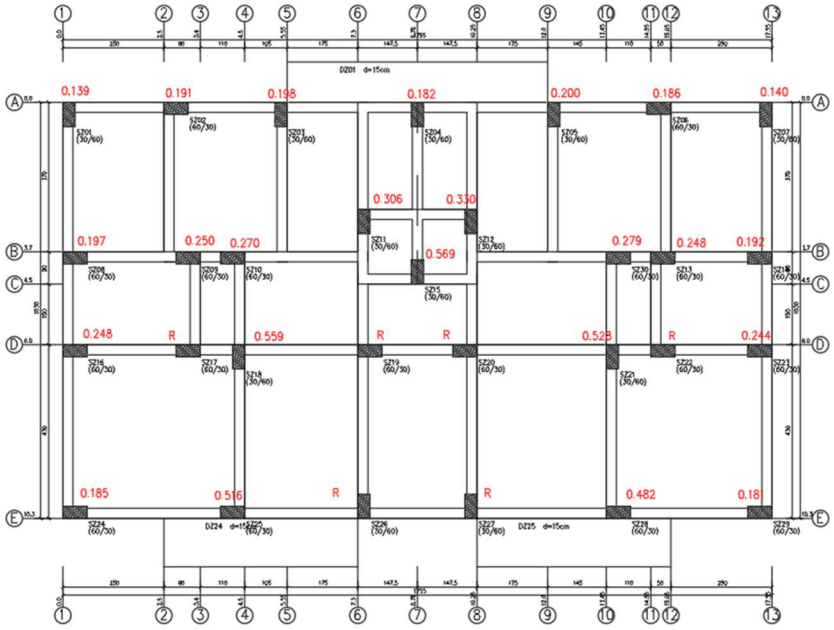

Figure 3.14 DCR values for the first-story columns in the verification of live column removal test (Step 6)

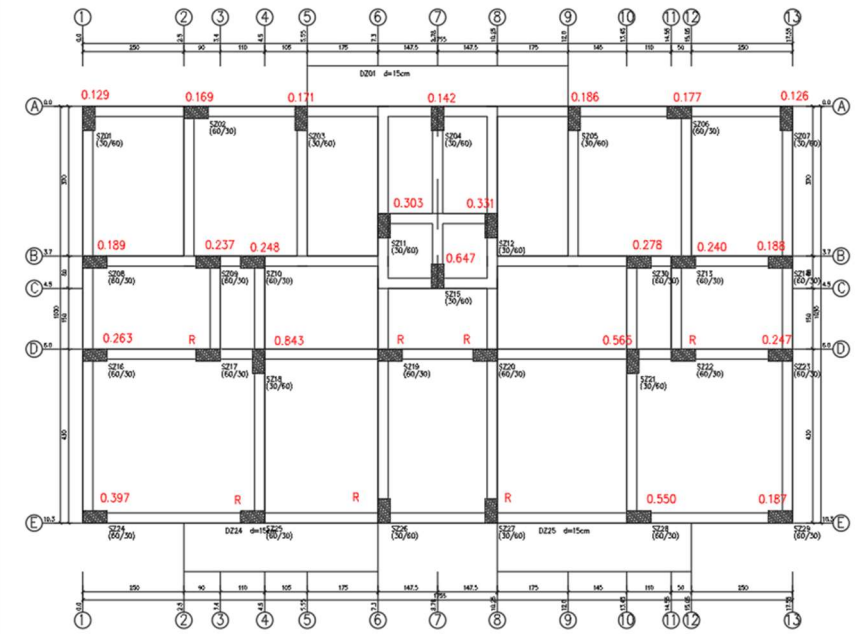

Figure 3.15 DCR values for the first-story columns in the verification of live column removal test (Step 7)

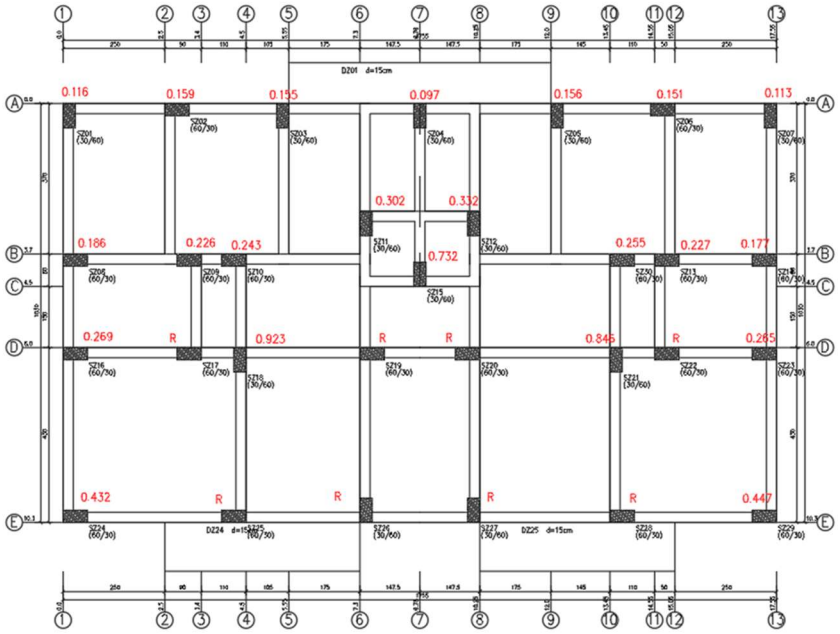

Figure 3.16 DCR values for the first-story columns in the verification of live column removal test (Step 8)

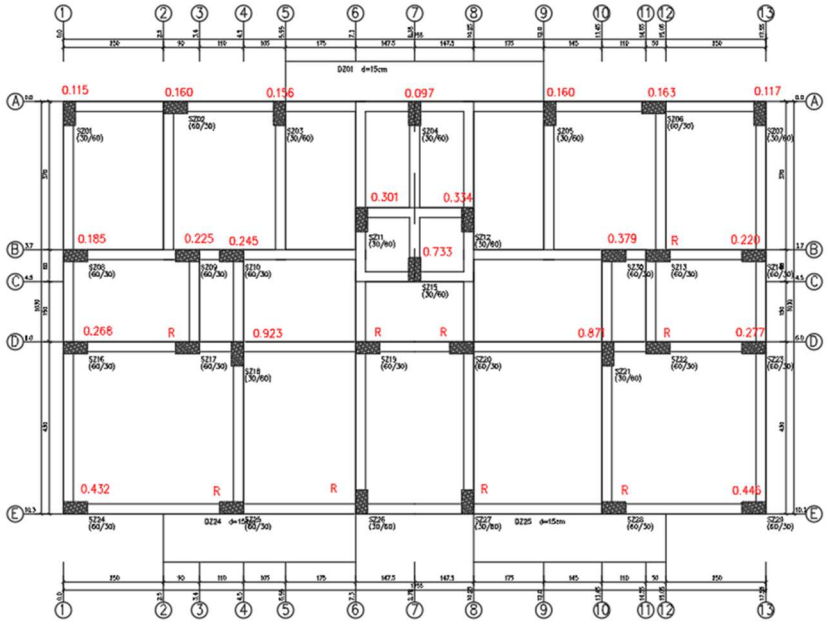

Figure 3.17 DCR values for the first-story columns in the verification of live column removal test (Step 9)

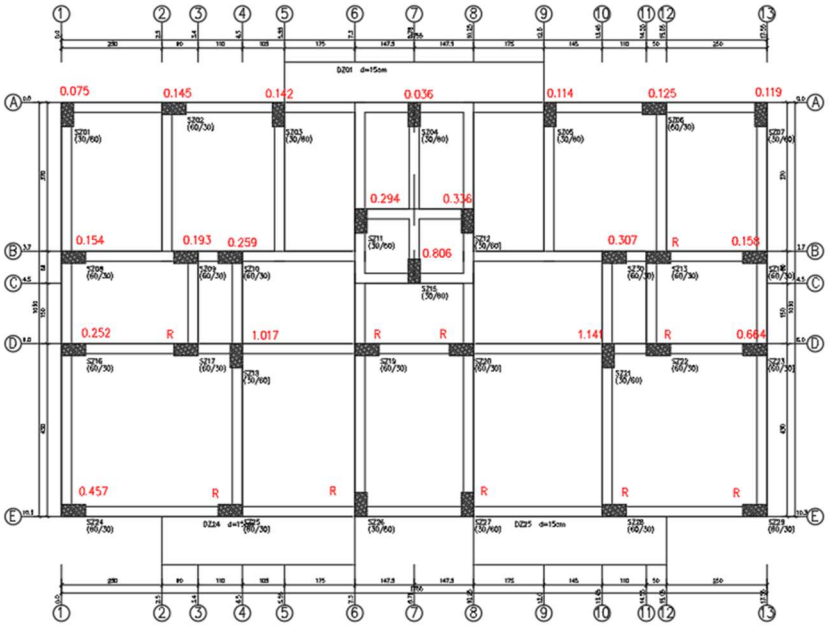

Figure 3.18 DCR values for the first-story columns in the verification of live column removal test (Step 10)

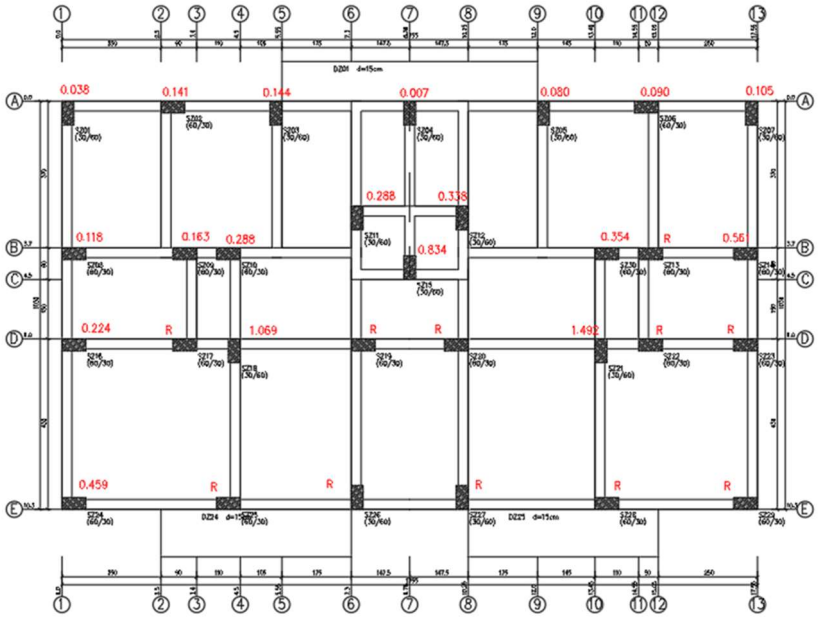

Figure 3.19 DCR values for the first-story columns in the verification of live column removal test (Step 11)

As indicated in Figure 3.18 presenting the DCR values at Step 10, two of the columns which were not included in the predetermined column removal order had reached DCR values exceeding unity. It is thought that the demand fractions exceeding the capacities of these columns may be compensated for by the overall response of the structure and may not result in an immediate onset of total collapse progression. Therefore, these columns were kept in the model for the last step. At Step 11, it is observed that one of these columns reached a DCR value of 1.492, with the other column recording a slight increase in its DCR value, signalling the onset of progressive collapse for this structure. Given that the total collapse of the building had taken place upon the removal of the eleventh column in the column removal sequence, it can be stated that the verification study successfully simulated the real-time collapse progression of the test building, proving that OpenSees is capable of representing structural response of a given three-dimensional building.

3.3 Pushover Analyses of Test Buildings with Column Removal Procedure

Two low-rise reinforced concrete buildings which sustained structural damage after the earthquake event in Elazığ, Turkey back in January 2020 were put under scrutiny to assess their performance under gravity and earthquake loads. Results of these efforts are expected to illuminate the influence of reinforced concrete column members on building collapse envelopes. To this end, a number of non-linear static (pushover) analyses are planned to determine horizontal drift capacities of the selected buildings under different levels of vertical loads. Data obtained from these analyses are used for creating case-specific building collapse envelopes.

OpenSees software was utilized for conducting these analyses; therefore, the first section of this chapter is reserved for a brief introduction to this software and its working principles. The section to follow will include modeling and analysis preferences for the tested buildings. Then, pushover analyses to be used for constructing the building collapse envelopes will be explained in detail. In the final section of the chapter, results of these analyses will be presented.

3.3.1 OpenSees® Software

The numerical models of the buildings investigated within the scope of this study were created by utilizing OpenSees® (Mazzoni et al., 2006). OpenSees®, short for The Open System for Earthquake Engineering Simulation, is an object-oriented, is an open-source software suite created by the Pacific Earthquake Engineering Research Center (PEER) at UC Berkeley. This software is intended for performing finite element analyses using a simple language in order to simulate the real-time responses of geotechnical and structural systems in the presence of earthquakes or other hazards.

Despite having a nature similar to what is called a “black box” in the realm of programming, OpenSees provides the users familiar with its working mechanisms with a tool that helps construct structural models in a rapid and sound fashion, and

offers an open-sourced structure to review and alter, if necessary, its core elements according to the needs of the user.

With a wide variety of features for facilitating linear and non-linear modeling, OpenSees allows representing both component and material behavior by non-linear force-deformation relationships. Fiber section assignment capability of OpenSees facilitates rapid determination of N-M and N-M-M interactions for 2D and 3D models, respectively, eliminating the need for long computation durations and high computational power without compromising analysis accuracy.

Model parameters and modeling preferences to be used in OpenSees for the buildings were selected by capitalizing on the verification studies conducted also on OpenSees within the scope of this work, and these parameters and preferences are explained in detail in the following subsections.

3.3.1.1 Structural Elements

OpenSees offers a myriad of structural elements to the user, and these element types were examined to find the suitable ones to be employed in the building models for this study. Given that the type of the analyses to be conducted in this study is non-linear, the focus was concentrated on selecting an element type among the non-linear beam-column element types.

OpenSees users can select either force-based or displacement-based elements for beam-column type members in their models. Force-based element types are based on iterative force-based formulations and distinguished mainly by the manner they simulate plasticity. Distributed plasticity is represented by “nonlinearBeamColumn” or “forceBeamColumn” element types, which consider a distribution of plasticity along the entire member in question. Concentrated plasticity, on the other hand, is represented by “beamWithHinges” element type, which allows the plasticity to be concentrated over specified plastic hinge lengths at the ends of a given element, but modeling the interior as elastic. Displacement-based element types are based on the

displacement formulation, and there are two types of such elements, namely "dispBeamColumn" and "dispBeamColumnInt". The difference between these two types is that the latter type includes interaction between flexural and shear components.

For modeling the beams (and girders) and columns in the test buildings, "beamWithHinges" element type was selected (Figure 3.8), for it captures the largest moment values at the ends, accurately portrays linear curvature distributions, and allows modeling different reinforcement layouts at joints (Scott & Fenves, 2006). This element type consists of two hinge regions at the ends and a linear-elastic region in between. The hinge regions require assigning an element section and hinge lengths, and these lengths are calculated by the formula proposed by Paulay and Priestley (1992).

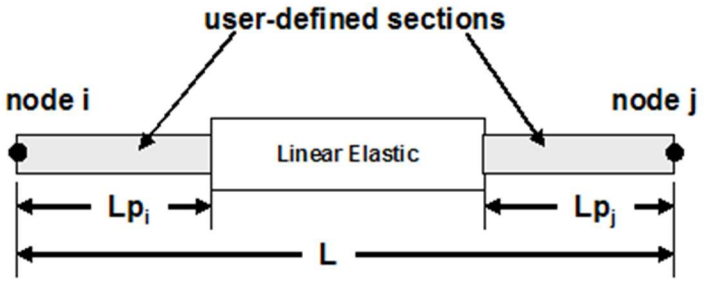

Figure 3.20 General layout of the beamWithHinges element type

Fiber cross-sections were used to assign non-linear hyperelastic behavior to hinge sections (Figure 3.9), since this section type also allows to model multiple material types within a single section. This selection also helped omitting moment-curvature analyses for each section, saving computational time and effort.

Slabs in the models were created by using the "rigidDiaphragm" command in OpenSees. All nodes of a given floor in the models were constrained by this command except one master node for each slab, resulting in a slab which is capable of transferring the imposed loads to the beams and columns, but unable to undergo deformations. It could thus be stated that slabs are not modeled in a meticulous fashion within the scope of this study, since the focus is concentrated on the columns.

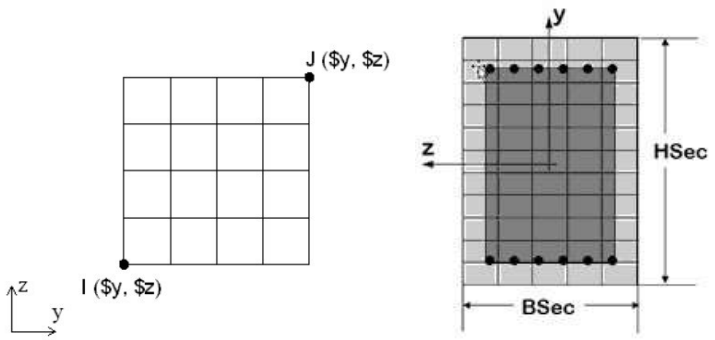

Figure 3.21 Rectangular fiber layout (left) and fiber section of a rectangular column with multiple material types

3.3.1.2 Materials

Reinforced concrete structural members comprising the test buildings, namely beams (girders) and columns are composed of unconfined concrete, confined concrete and reinforcing steel materials. The material model used for concrete (Concrete01) follows the rules of Kent-Scott-Park concrete material model (Scott et al., 1982), which has linear unloading/reloading stiffness along with plastic offset depending on damage according to the work of Karsan-Jirsa (1969). This model also has no tensile strength (Figure 3.10). Both confined and unconfined concrete sections are modeled using this material with different input parameters. The material model used for steel (Steel01), on the other hand, is a material model of uniaxial bilinear steel material with kinematic hardening (Figure 3.10).

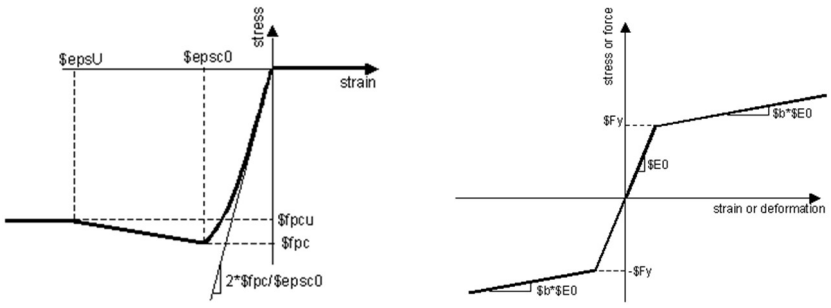

Figure 3.22 Stress-strain relationships of Concrete01 (left) and Steel01 (right) material models in OpenSees

Unconfined and confined concrete behavior of the reinforced concrete member cross-section, along with reinforcing steel material behavior, are separately defined via fiber elements, and then cross-sectional capacities are calculated for all members.

3.3.2 Building Model Variants

To be able to investigate the influence of reinforced concrete column details on building collapse envelopes, variants of the building models in hand were needed to be created. For this purpose, four different parameters are defined to create these variants, namely concrete compressive strength, number of floors, longitudinal rebar ratio and stirrup spacing for transverse reinforcement. Two different variants are prepared for each parameter, making up a total of eight artificial variants for each test building. Details of the variants are given in Table 3.3.

Table 3.3 Details of model variants in comparison to original building models

	Building I	Building II
Floor Number Variants	Original (5-story)	Original (5-story)
	8-story	8-story
	10-story	10-story
Stirrup Spacing Variants	Original (280 mm)	Original (230 mm)
	100 mm	100 mm
	200 mm	200 mm
Concrete Compressive Strength Variants	Original (6.5 MPa)	Original (7.8 MPa)
	10 MPa	10 MPa
	20 MPa	20 MPa
Longitudinal Rebar Ratio Variants	Original (d = 14mm)	Original (d = 16mm)
	16 mm	14 mm
	22 mm	18 mm

Numerical models of all variants are created by using the models of the two original buildings, and building collapse envelopes for each of these variants are constructed separately to compare their structural performances.

3.3.3 Numerical Models

Numerical models of the buildings investigated in this study are created in the OpenSees environment with certain general assumptions and alterations to the workflow of a standard pushover analysis. The assumptions related to these models can be listed as follows:

- First story columns of the numerical models examined in this chapter are assumed to have attained their point of collapse, when they exceed the specified limits marking collapse onset. In cases of such events during the course of analyses, these members are removed from the models,
- Building models attain the state of collapse when they become unable to carry the total imposed vertical load.

Structural members of these models are defined such that endpoints are basically fiber-section-based plastic hinge elements, while the middle portions exhibit linear elastic behavior. This preference allows modeling non-linear hyper-elastic behavior of these members, but hinders the modeling of axial collapse state, necessitating the use of an additional model to simulate the state of axial collapse for a given member. To this end, axial collapse criterion was checked at the endpoints of all members at each step of the analyses; therefore, a model of drift ratio at which axial collapse takes place, which depends on column axial load and rebar layout, is required. Matamoros and Ghannoum (2011) developed such a model by augmenting the mechanical model put forth by Elwood and Moehle (2007). The model defines the floor drift ratio at which collapse occurs with the following formula:

$$\frac{\delta}{h} = \frac{0.5}{5 + \left(\frac{N}{f_c * A_g}\right) * \left(\frac{b * s}{A_{sw}}\right) * \left(\frac{f_c}{f_y}\right)} \tag{3.1}$$

At each step of the gravity load and pushover analyses of the test buildings, the limit specified by Equation 3.1, along with axial load to capacity ratio, was checked for

each column-type member. Axial load to capacity or demand-to-capacity ratios (DCR) for the columns are calculated by dividing the demand on any column at any analysis step to the capacity value calculated manually in the OpenSees codes by Equation 3.2. In cases where these limits were exceeded, the member was removed from the model and the analysis was continued. Analyses were conducted until the point of total collapse, which was indicated mostly by a major convergence warning issued by OpenSees following the removal of a considerable number of first-story columns.

$$Column\ axial\ load\ capacity = 0.85 f_c A_c + f_y A_{st} \tag{3.2}$$

Numerical model building and analysis procedure for each building involved two different type of pushover analyses. The first type of these analyses can be called vertical pushover analysis, since it involves incrementally increasing the loads imposed on all floors of a given building until total collapse. In these analyses, the aim is to find the point of collapse of the building under scrutiny without considering horizontal drift. Column-type members exceeding the specified axial load ratio and rotation limits were removed also in this type of analysis, and the analyses were carried on until total collapse occurred. A maximum load factor, α, was determined at the end of these analyses, which represented the vertical load carrying capacity of the analyzed building.

The second type of these analyses was conventional pushover analysis, with the addition of the aforementioned column collapse point checks. These analyses were conducted for a number of different maximum load multipliers, representing a spectrum between a case with normal loading and one with the maximum load factor. For each analysis, vertical load analysis was performed in the beginning and columns reaching their collapse points were removed. Then, a displacement-controlled pushover analysis was conducted with a horizonal loading profile applied in accordance with the first modal response of the building. Columns are checked for

the exceedance of collapse limits also in these steps, and the analysis was executed until the point of total collapse.

At the end of each of these analyses, average drift ratio and axial load ratios for all first-floor columns were recorded. Then, the average values of four different sets of axial load ratios are recorded separately and each of these data constituted a data point coupled with the average drift ratio for the first-floor columns. Given that each of these data points represent the collapse point of the respective analysis, these points collectively correspond to an envelope representing the ultimate performance points, providing a useful figure for assessing the performance of the building under investigation. The four axial average demand-to-capacity ratio (DCR) sets are defined as follows:

- Average of DCR values of all first-floor columns recorded under the application of gravity loads only,
- Average of DCR values of 30% of first-floor columns with highest DCR values under the application of gravity loads only,
- Average of DCR values of all first-floor columns recorded at the first column failure event during pushover analyses.
- Average of DCR values of 30% of first-floor columns with highest DCR values recorded at the first column failure event during pushover analyses.

Maximum vertical load multipliers are used to create six data points for constructing each collapse envelope by selecting six equally-spaced multipliers in the load multiplier domain. These load multiplier values are then used for finding averages of DCR values for the four cases specified above. These values are coupled with ultimate drift ratios of first-floor columns obtained from pushover analyses, which correspond to the onset of total collapse of the analyzed structure, and plots of these data points yield building collapse envelope for the examined building model variant.

3.4 Results

3.4.1 Vertical Pushover Analyses

The first two average DCR value sets and maximum vertical load multipliers are determined by vertical pushover analyses conducted on each variant. Results of these analyses are tabulated below:

Table 3.4 Vertical pushover analysis results for Building I

		Maximum Vertical Load Multiplier (α)	Average DCR for all columns in gravity analysis	Average DCR for columns with the highest 30% DCR values in gravity analysis
Original (5-story)		4.4	0.795	0.938
Floor Number Variants	8-story	2.7	0.846	0.970
	10-story	2.1	0.857	0.980
Stirrup Spacing Variants	100 mm	4.4	0.795	0.938
	200 mm	4.4	0.795	0.938
Concrete Compressive Strength Variants	10 MPa	7.0	0.783	0.939
	20 MPa	14.3	0.799	0.947
Longitudinal Rebar Ratio Variants	16 mm	4.4	0.794	0.939
	22 mm	4.4	0.794	0.939

Table 3.5 Vertical pushover analysis results for Building II

		Maximum Vertical Load Multiplier (α)	Average DCR for all columns in gravity analysis	Average DCR for columns with the highest 30% DCR values in gravity analysis
Original (5-story)		4.1	0.630	0.800
Floor Number Variants	8-story	2.5	0.702	0.879
	10-story	1.9	0.724	0.892
Stirrup Spacing Variants	100 mm	4.1	0.630	0.801
	200 mm	4.1	0.630	0.801
Concrete Compressive Strength Variants	10 MPa	5.3	0.622	0.794
	20 MPa	10.9	0.615	0.790
Longitudinal Rebar Ratio Variants	14 mm	4.1	0.629	0.802
	18 mm	4.1	0.630	0.800

Both Table 3.4 and Table 3.5 show that average DCR values for the two specified cases for both buildings do not exhibit noticeable changes for different variants except for the floor variants. Maximum vertical load multipliers, on the other hand, are increased by increasing concrete strength for both buildings, which is plausible given the capacity increases introduced by greater concrete compressive strength values. Floor number variants received smaller multipliers by increasing floor numbers, which is due to the loads imposed on members by additional floors. Load multipliers and DCR value averages obtained by these analyses are used to create the points for constructing building collapse envelopes.

3.4.2 Building Collapse Envelopes

Building collapse envelopes created for the two original building models and their variants are presented in this section, and pushover curves corresponding to each data point created for constructing these envelopes are presented together with the envelopes to examine the impacts of changes introduced to reinforced concrete

column details. Envelopes and pushover curves for each selected parameter type are grouped together to better draw meaningful conclusions brought about by tweaking these parameters.

3.4.2.1 Envelopes for the Models of Building I

Envelopes created for the original model of Building I and its variants created by parameter changes are presented and compared in this subsection. Envelope of the original model of Building I and pushover curves corresponding to each data point used in plotting this envelope are presented in Figure 3.23 and Figure 3.24 below:

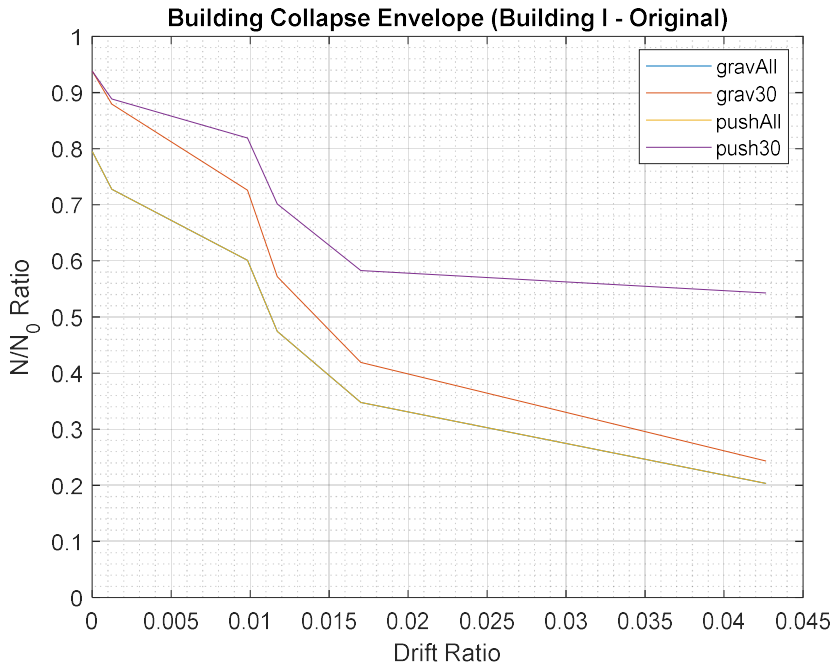

Figure 3.23 Building collapse envelope for the original model of Building I

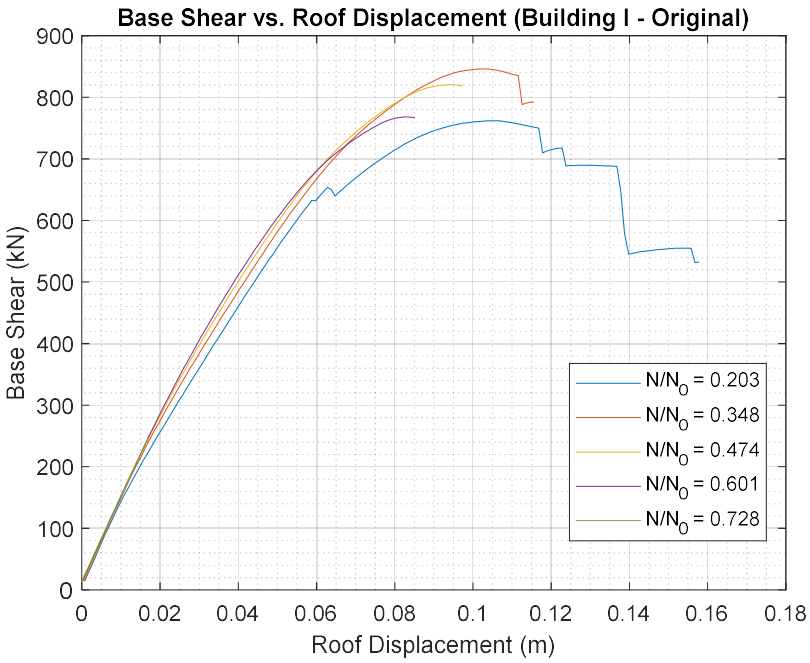

Figure 3.24 Pushover curves for the original model of Building I for data points used in corresponding envelope

In Figure 3.23, N/N_0 ratios given in the vertical axis belong to the four different sets of DCR values defined under the section reserved for explaining numerical models of the buildings, and the drift ratios on the horizontal axis are the average drift ratios for the first-floor columns. Legend provided on the plot lists the aforementioned four DCR value sets. Each pushover curve given in Figure 3.24 corresponds to a data point used in Figure 3.23 for constructing the envelope for the averages of DCR values of all columns recorded under the application of gravity loads only. All plot duos for model variants to be presented from this point on are created according to this convention.

3.4.2.1.1 Envelopes for Concrete Strength Variants

Envelopes for the variants of the original model of Building I with concrete strength values of 10 MPa and 20 MPa are presented in Figures 3.25 and 3.26, respectively, and corresponding pushover curves at their data points are given in Figures 3.27 and 3.28.

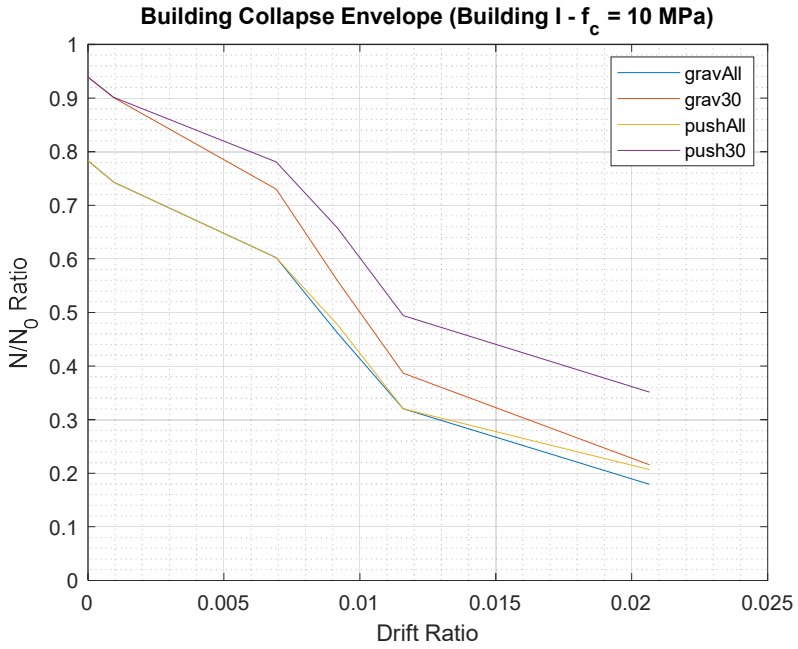

Figure 3.25 Building collapse envelope for the modified model of Building I with f_c=10 MPa

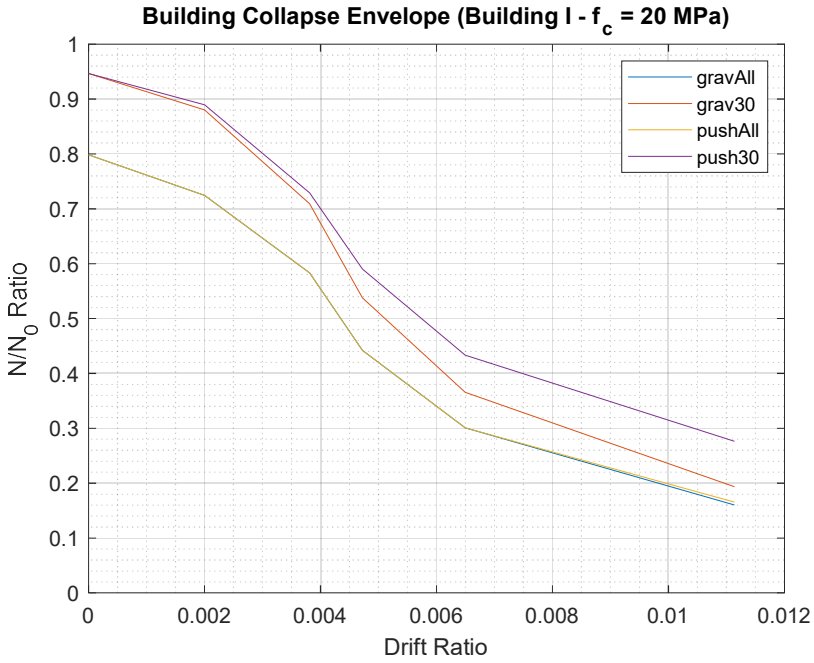

Figure 3.26 Building collapse envelope for the modified model of Building I with f_c=20 MPa

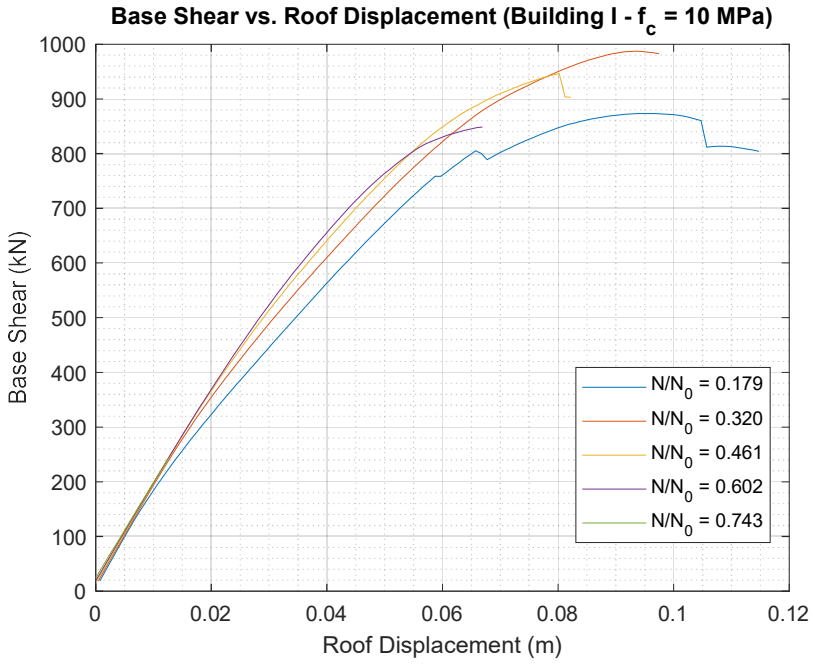

Figure 3.27 Pushover curves for the modified model of Building I with f_c = 10 MPa for data points used in corresponding envelope

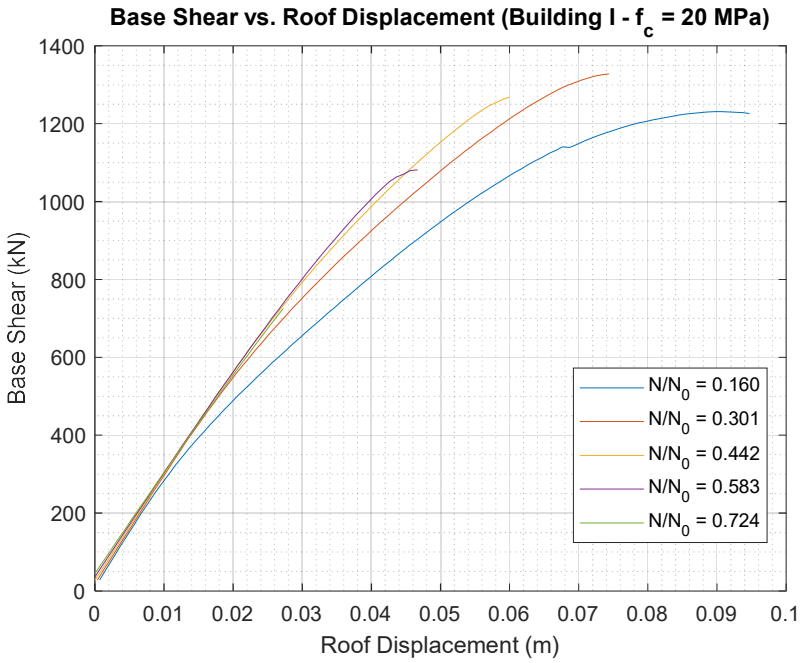

Figure 3.28 Pushover curves for the modified model of Building I with f_c = 20 MPa for data points used in corresponding envelope

Comparative plots for building collapse envelopes for the concrete strength variants of Building I for the DCR averaging cases according to gravity analysis results are presented below:

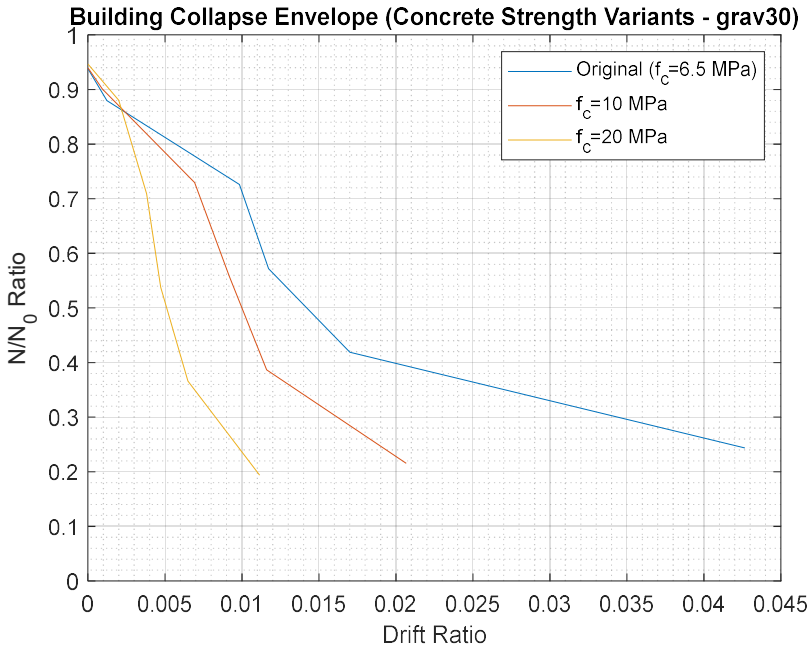

Figure 3.29 Building collapse envelopes of the concrete strength variants of Building I for the average of DCR values of 30% of first-floor columns with highest DCR values under the application of gravity loads only

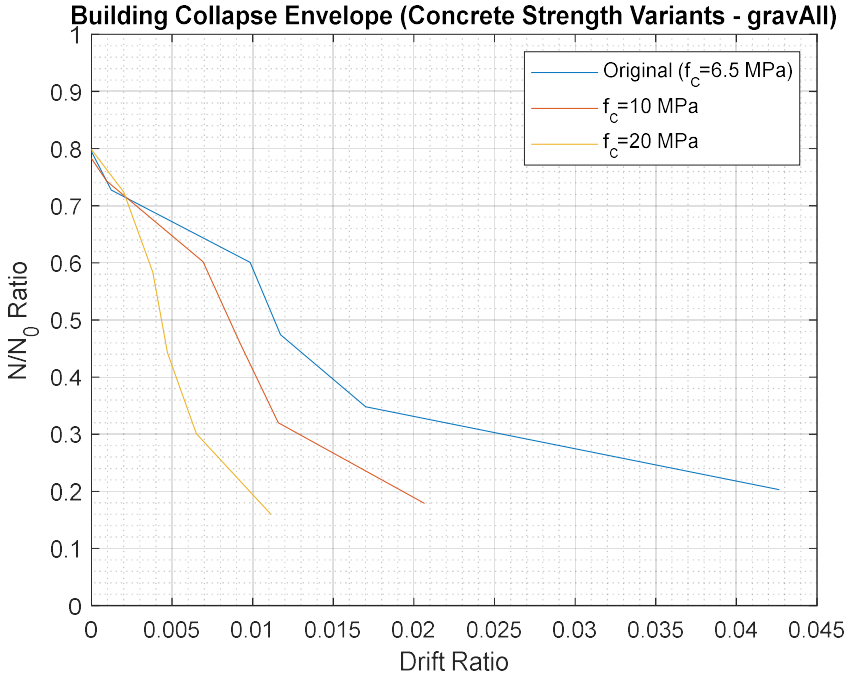

Figure 3.30 Building collapse envelopes of the concrete strength variants of Building I for the average of DCR values of all first-floor columns recorded under the application of gravity loads only

Comparison of Figures 3.23, 3.25 and 3.26 reveals at first glance that the maximum drift ratio the building envelope can extend to is decreased with increased concrete compressive strength. This change could be attributed to the fact that increased concrete compressive strength values result in the utilization of a smaller fraction of column capacities, meaning that the internal axial loads in columns are greater with increasing concrete strength for a given N/N_0 value. Greater internal axial loads result in amplified P-Delta effects, thus attaining the state of failure at smaller drift ratios. This observation is supported by the increased capacity and decreased roof displacement values portrayed by the pushover curves for the smallest N/N_0 values in Figures 3.24, 3.27 and 3.28. In addition, for a given drift ratio value, corresponding N/N_0 values on the envelopes decrease with increasing concrete strength values, which could be explained by the fact that the fraction of column capacities that could be utilized decreases.

3.4.2.1.2 Envelopes for Floor Number Variants

Envelopes for the variants of the original model of Building I with 8 stories and 10 stories are presented in Figures 3.31 and 3.32, respectively, and corresponding pushover curves at their data points are given in Figures 3.33 and 3.34.

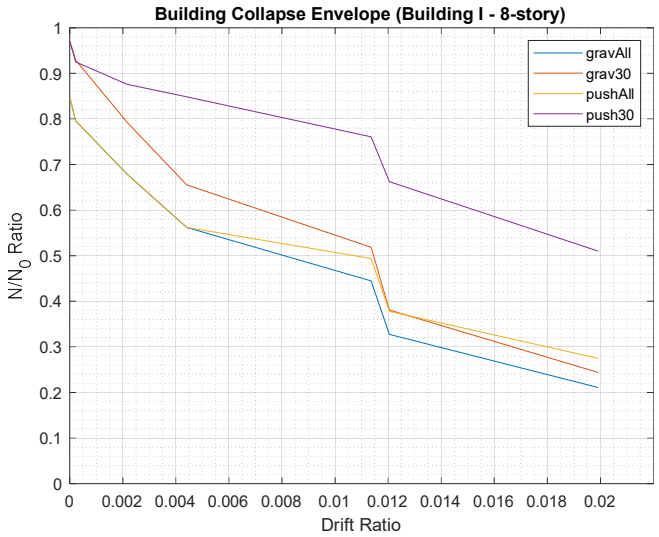

Figure 3.31 Building collapse envelope for the modified model of Building I with 8 stories

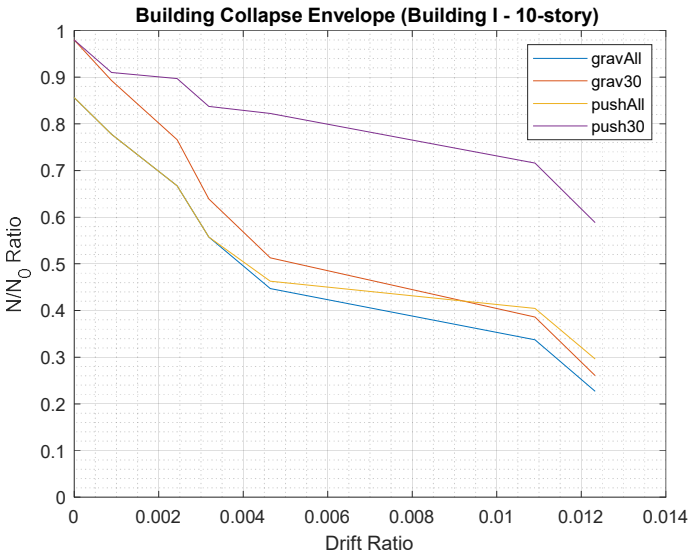

Figure 3.32 Building collapse envelope for the modified model of Building I with 10 stories

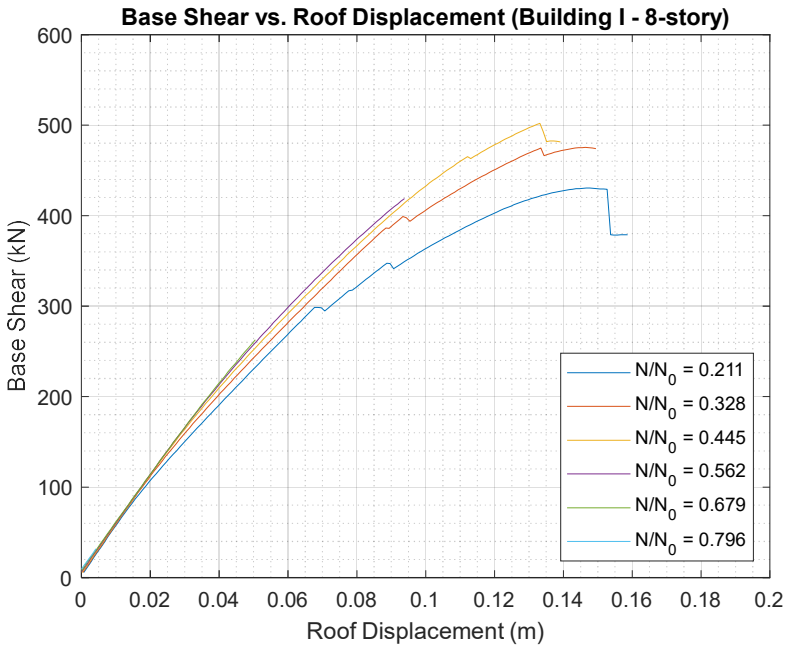

Figure 3.33 Pushover curves for the modified model of Building I with 8 stories for data points used in corresponding envelope

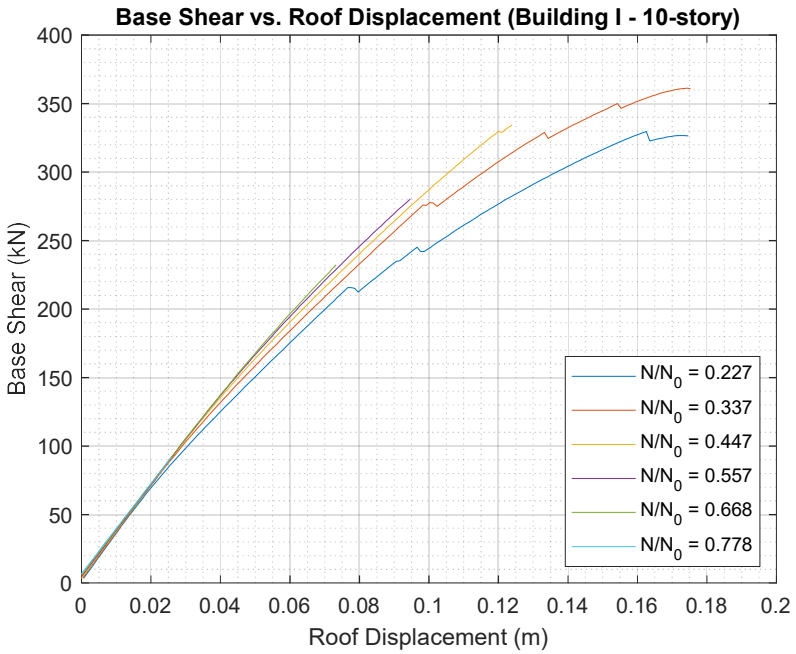

Figure 3.34 Pushover curves for the modified model of Building I with 10 stories for data points used in corresponding envelope

Comparative plots for building collapse envelopes for the floor number variants of Building I for the DCR averaging cases according to gravity analysis results are presented below:

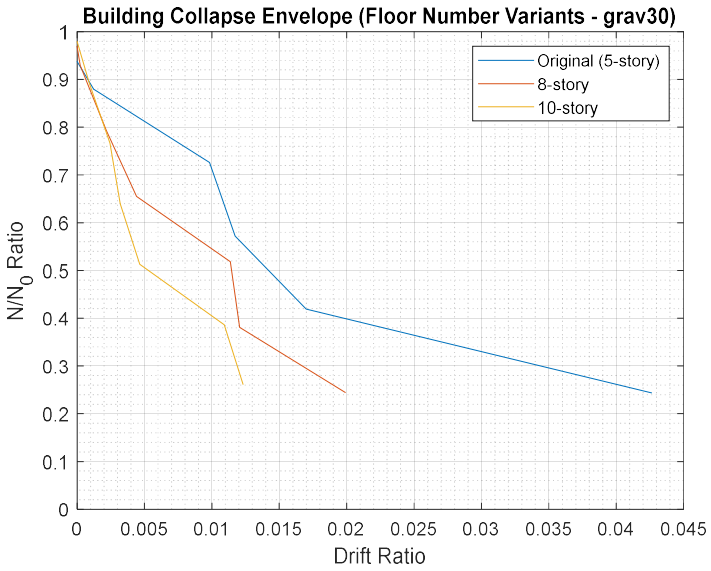

Figure 3.35 Building collapse envelopes of the floor number variants of Building I for the average of DCR values of 30% of first-floor columns with highest DCR values under the application of gravity loads only

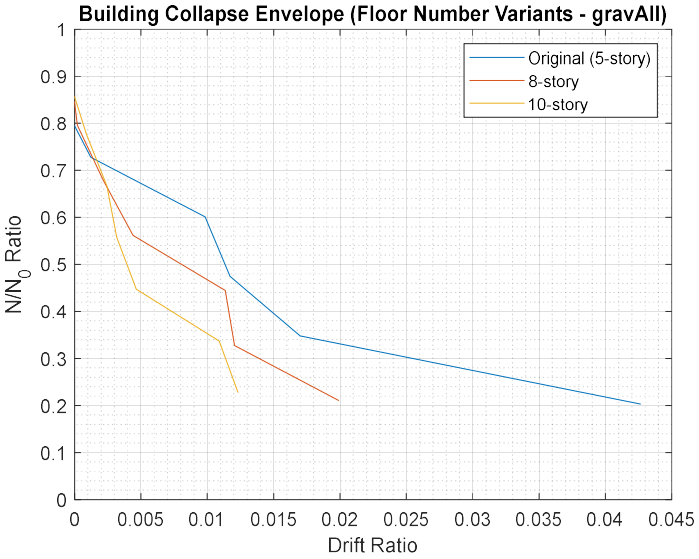

Figure 3.36 Building collapse envelopes of the floor number variants of Building I for the average of DCR values of all first-floor columns recorded under the application of gravity loads only

Similar to the case of concrete compressive strength changes, addition of stories to the original building resulted in amplified P-Delta effects on first-floor columns due to additional loads introduced to the system, as seen in Figures 3.31 and 3.32; therefore, ultimate drift ratio values for the first-floor columns represented in the envelopes decreased with increased number of stories. For the same reason, N/N_0 values for any given drift ratio value were decreased with increased number of stories, indicating that utilization levels of available axial load-carrying capacities of first-floor columns exhibited decline. Pushover curves presented in Figures 3.33 and 3.34 support this observation by depicting a downward trend in maximum base shear values, although ultimate roof displacement values displayed slight deviations from that of the original building.

3.4.2.1.3 Envelopes for Longitudinal Reinforcing Steel Ratio Variants

Envelopes for the variants of the original model of Building I with longitudinal reinforcing steel ratio values corresponding to rebar diameters of d=16 mm (steel ratio ≈ 1.12%) and d=22 mm (steel ratio ≈ 2.11%) are presented in Figures 3.37 and 3.38, respectively, and corresponding pushover curves at their data points are given in Figures 3.39 and 3.40.

Comparative plots for building collapse envelopes for the floor number variants of Building I for the DCR averaging cases according to gravity analysis results are given in Figures 3.41 and 3.42.

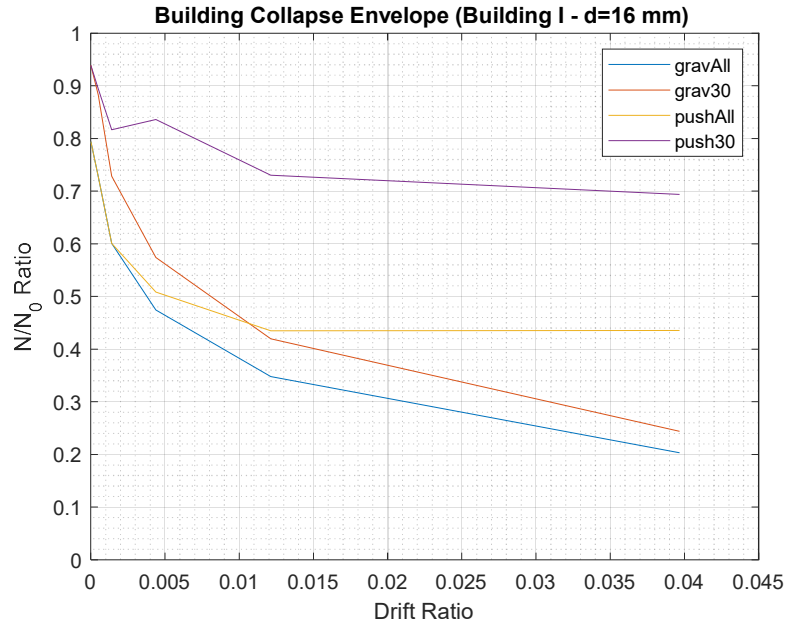

Figure 3.37 Building collapse envelope for the modified model of Building I with d=16 mm for longitudinal reinforcing steel bars

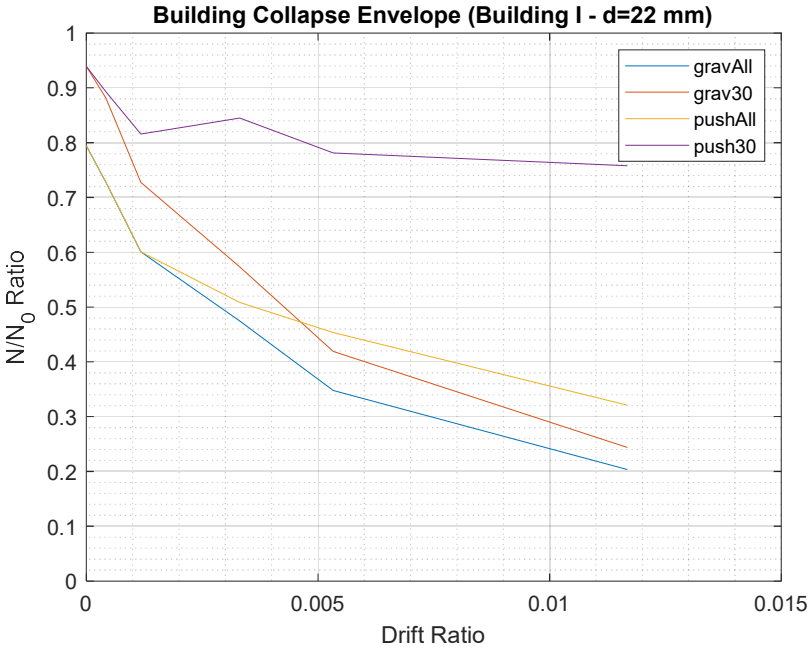

Figure 3.38 Building collapse envelope for the modified model of Building I with d=22 mm for longitudinal reinforcing steel bars

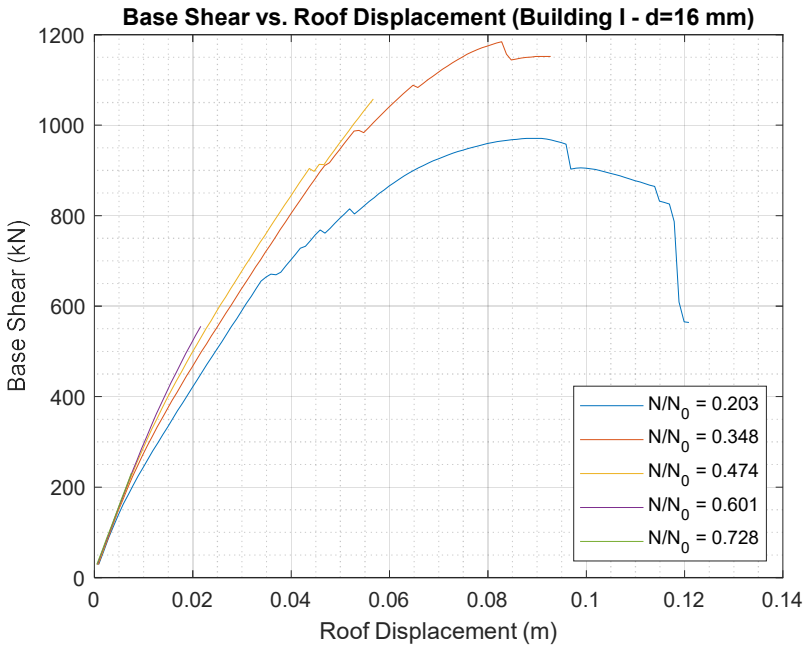

Figure 3.39 Pushover curves for the modified model of Building I with d=16 mm for data points used in corresponding envelope

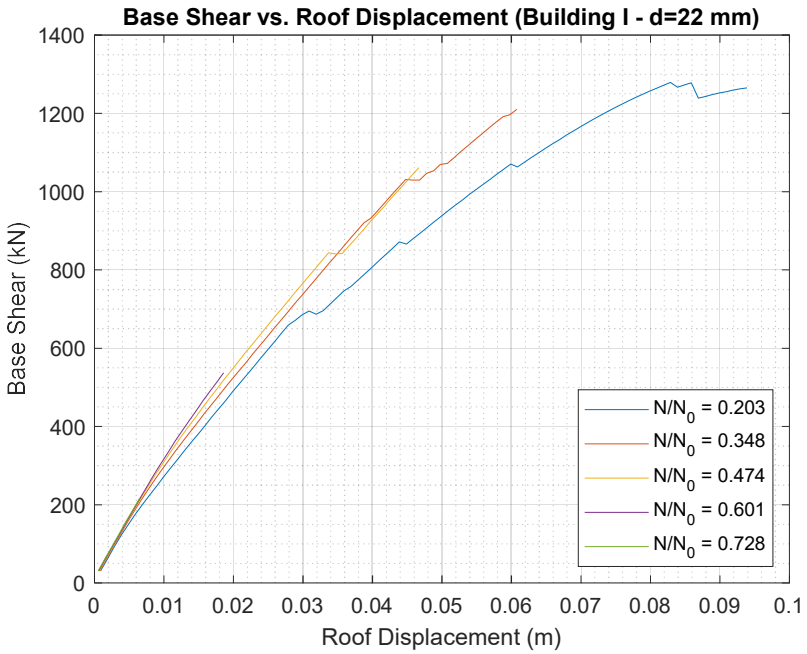

Figure 3.40 Pushover curves for the modified model of Building I with d=22 mm for data points used in corresponding envelope

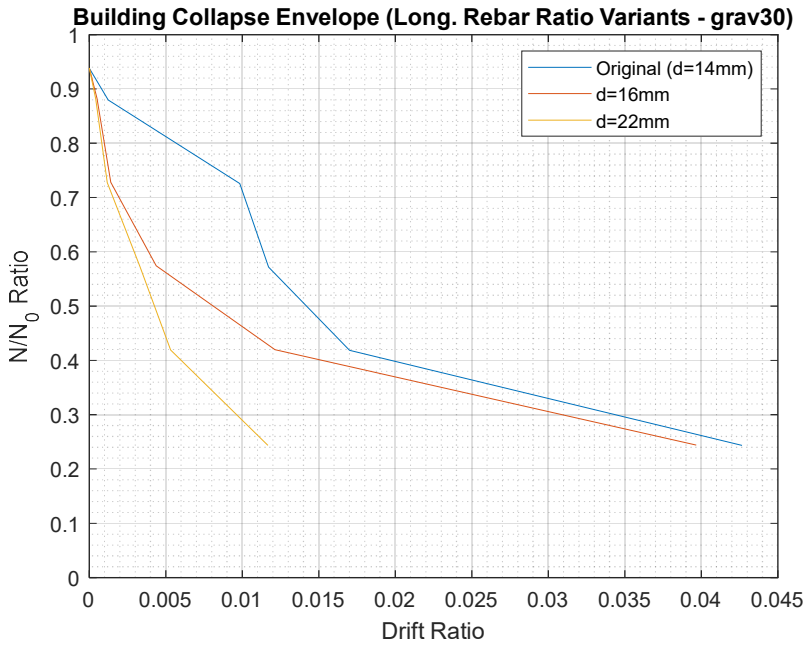

Figure 3.41 Building collapse envelopes of the longitudinal rebar ratio variants of Building I for the average of DCR values of 30% of first-floor columns with highest DCR values under the application of gravity loads only

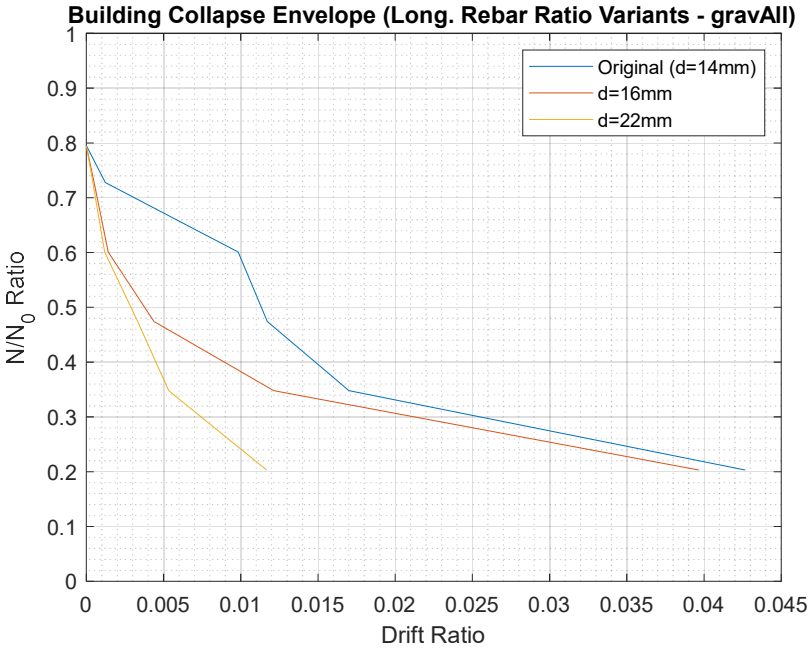

Figure 3.42 Building collapse envelopes of the longitudinal rebar ratio variants of Building I for the average of DCR values of all first-floor columns recorded under the application of gravity loads only

Figures 3.37 and 3.38 demonstrate that, compared to the envelope of the original model with a longitudinal reinforcing steel diameter of 14 mm (steel ratio ≈ 0.86%), envelopes of buildings with columns having increased longitudinal steel diameters extend to smaller drift ratio values, although N/N_0 values corresponding to these ultimate drift ratio values do not change. This change could be explained by reduced ductility (increased stiffness) in columns introduced by additional rebar presence. This observation is supported by the building structural responses represented in the pushover curves in Figures 3.39 and 3.40. In addition, N/N_0 values for particular drift ratio values are reduced with increasing longitudinal steel ratios (or diameters), indicating that increased capacities in first-floor columns result in capacity use levels less than the original case.

3.4.2.1.4 Envelopes for Stirrup Spacing Variants

Envelopes for the variants of the original model of Building I with stirrup spacing values of s=100 mm and s=200 mm are presented in Figures 3.43 and 3.44, respectively, and corresponding pushover curves at their data points are given in Figures 3.45 and 3.46.

Comparative plots for building collapse envelopes for the stirrup spacing variants of Building I for the DCR averaging cases according to gravity analysis results are given in Figures 3.47 and 3.48.

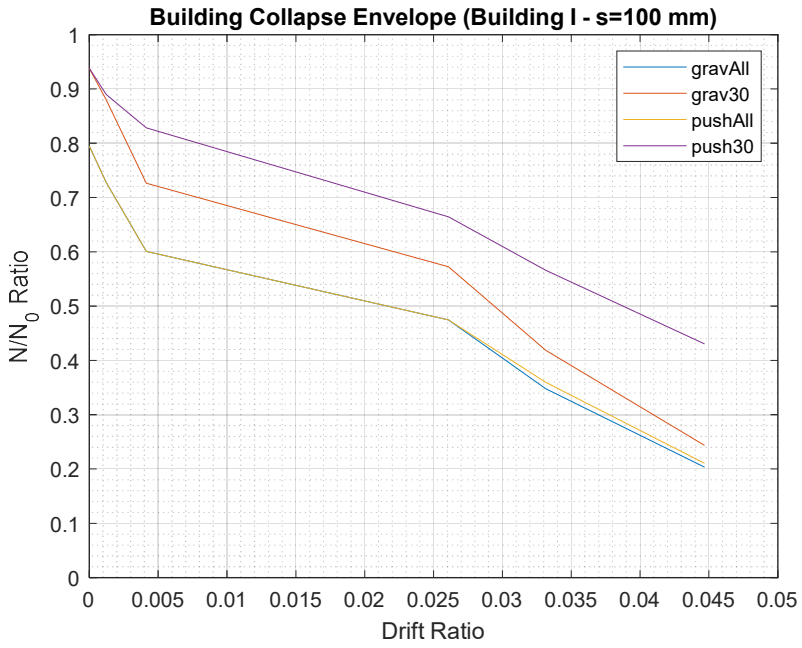

Figure 3.43 Building collapse envelope for the modified model of Building I with s=100 mm

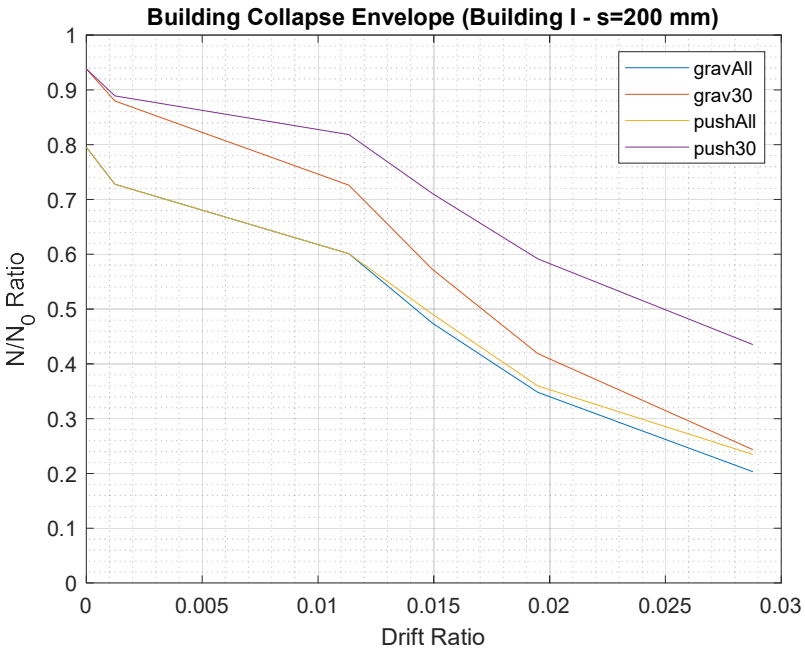

Figure 3.44 Building collapse envelope for the modified model of Building I with s=200 mm

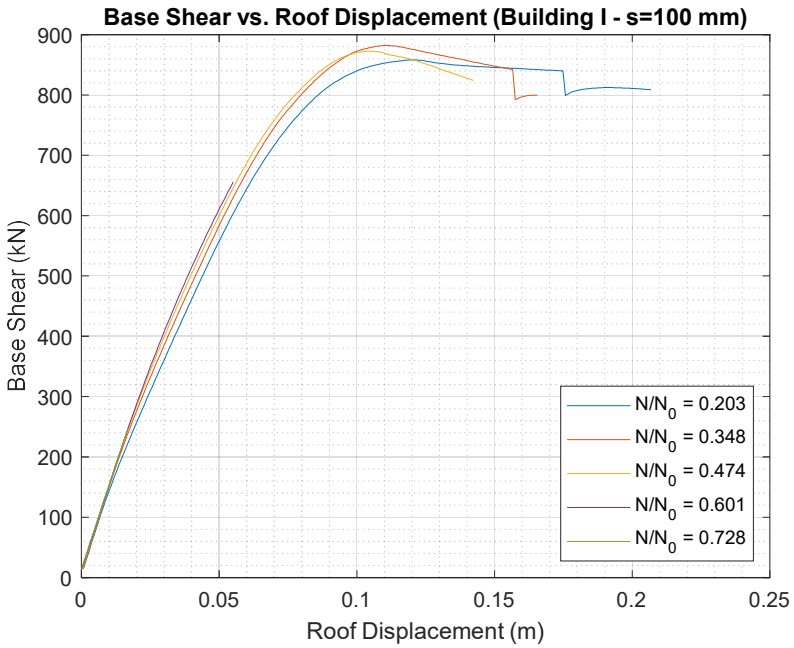

Figure 3.45 Pushover curves for the modified model of Building I with s=100 mm for data points used in corresponding envelope

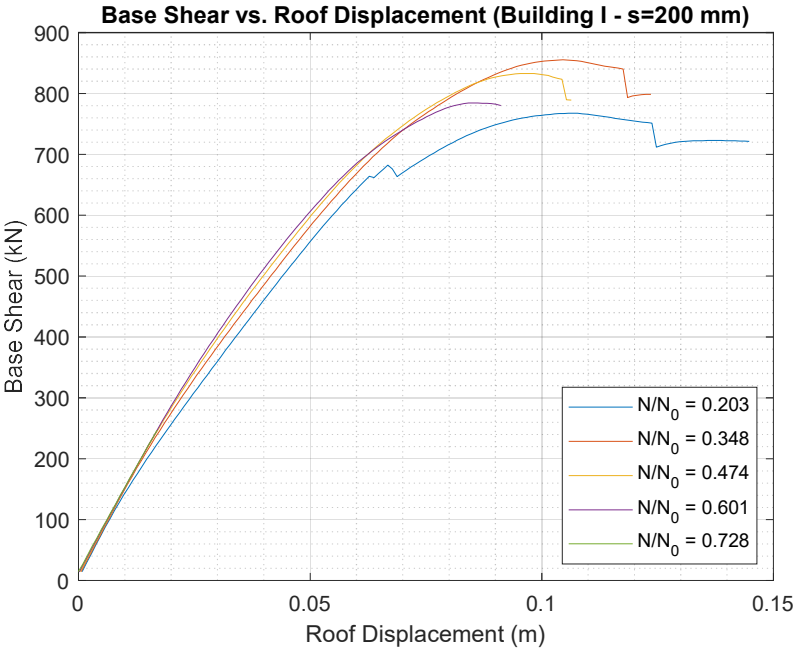

Figure 3.46 Pushover curves for the modified model of Building I with s=200 mm for data points used in corresponding envelope

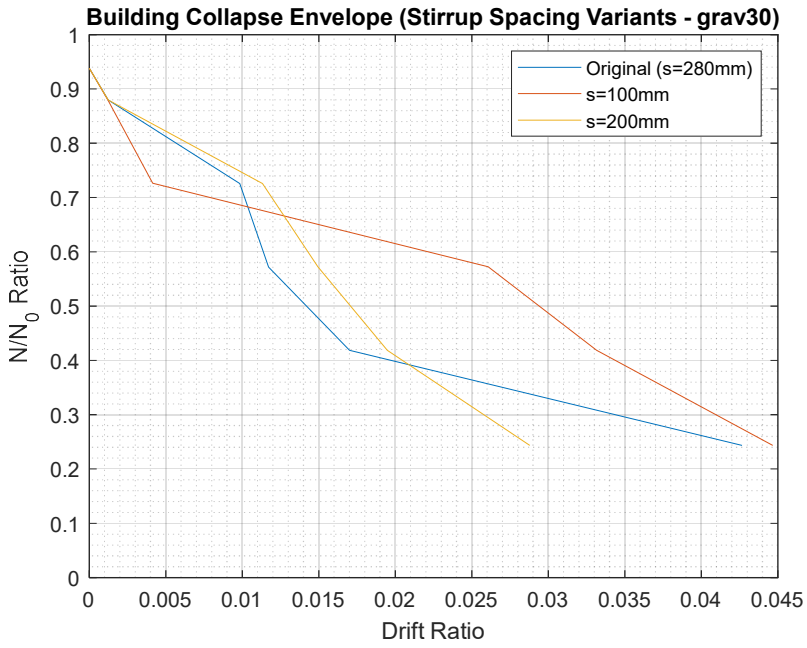

Figure 3.47 Building collapse envelopes of the stirrup spacing variants of Building I for the average of DCR values of 30% of first-floor columns with highest DCR values under the application of gravity loads only

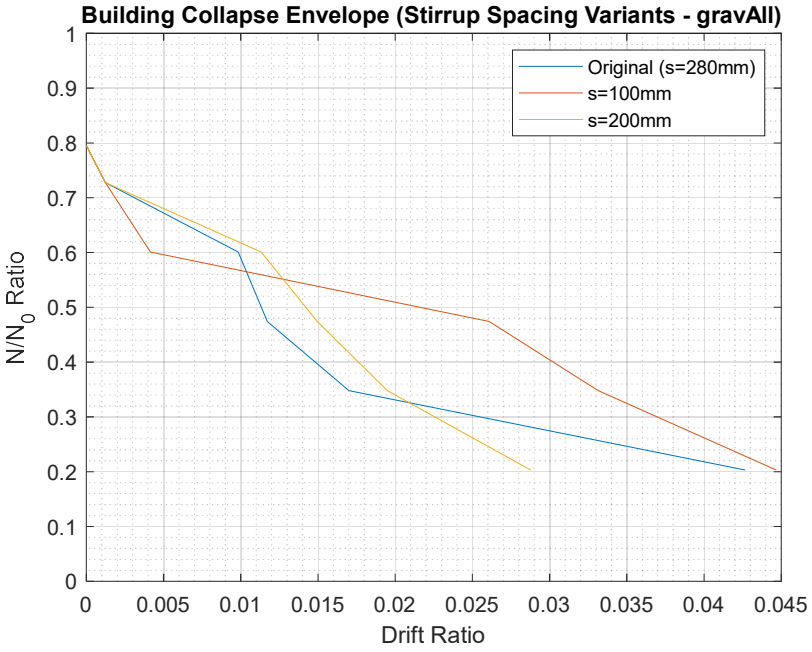

Figure 3.48 Building collapse envelopes of the stirrup spacing variants of Building I for the average of DCR values of all first-floor columns recorded under the application of gravity loads only

Comparison of Figures 3.43 and 3.44 shows that a more closely-packed stirrup configuration results in larger drift ratios in corresponding envelopes, with no changes in N/N_0 values, but when compared to the envelope of the original model, there seems to be a contradicting pattern. However, the original building model demonstrated a partial collapse pattern at smaller drift ratios during the analyses, which yielded results that are in agreement with the pattern shown in Figures 3.43 and 3.44. Since the analyses for the original model did not exhibit total failure indicated by convergence or compatibility problems in OpenSees, the envelope for the model was created with the first set of obtained results, without omitting any data, hence the contradiction explained here. Smaller stirrup spacing values resulted in slightly larger N/N_0 values for certain drift ratio values, but this observation could not support a conclusive comment. Pushover curves given in Figures 3.45 and 3.46 exhibit that ultimate roof displacement values are improved with decreased stirrup spacing values, supporting the first observation stated above.

3.4.2.2 Envelopes for the Models of Building II

Envelopes created for the original model of Building II and its variants created by parameter changes are presented and compared in this subsection. Envelope of the original model of Building II and pushover curves corresponding to each data point used in plotting this envelope are presented in Figure 3.49 and Figure 3.50 below:

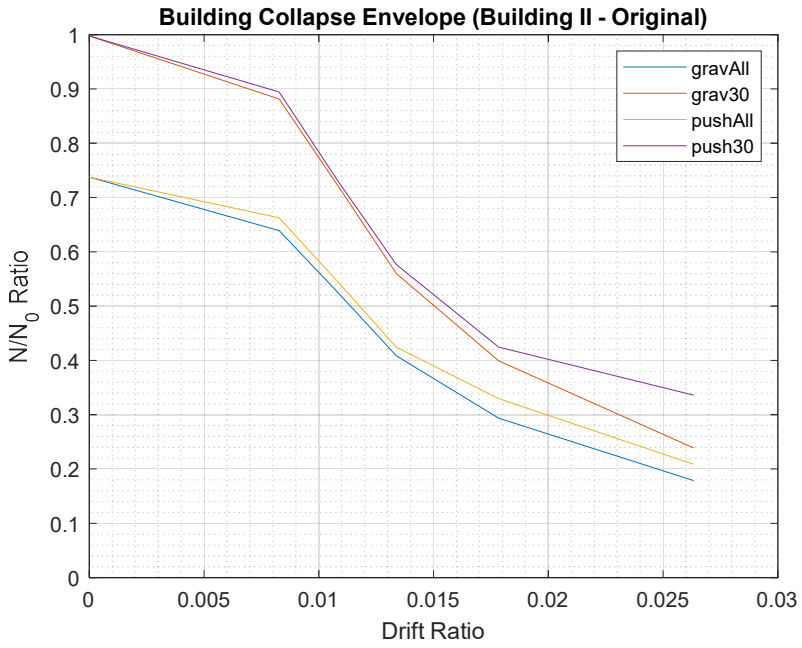

Figure 3.49 Building collapse envelope for the original model of Building II

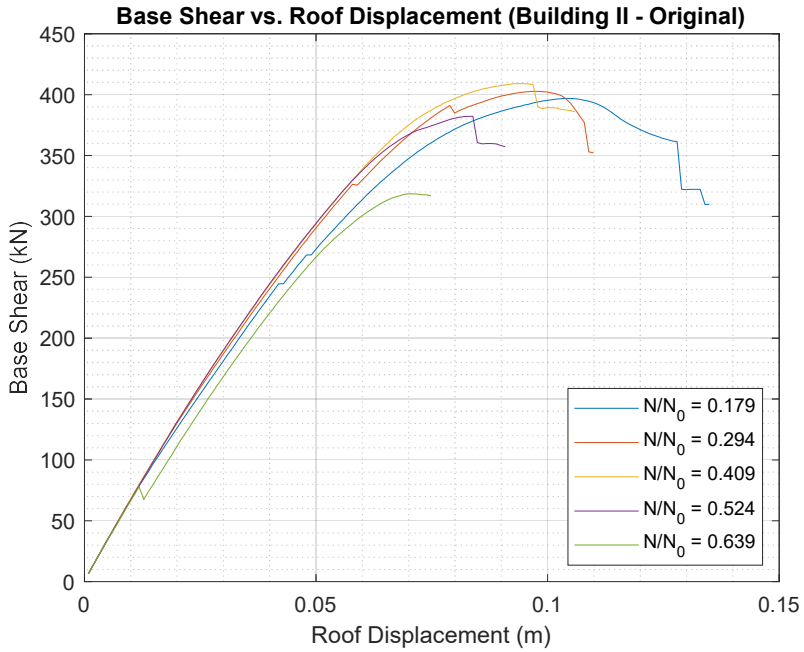

Figure 3.50 Pushover curves for the original model of Building II for data points used in corresponding envelope

3.4.2.2.1 Envelopes for Concrete Strength Variants

Envelopes for the variants of the original model of Building II with concrete strength values of 10 MPa and 20 MPa are presented in Figures 3.51 and 3.52, respectively, and corresponding pushover curves at their data points are given in Figures 3.53 and 3.54.

Comparative plots for building collapse envelopes for the concrete strength variants of Building II for the DCR averaging cases according to gravity analysis results are given in Figures 3.55 and 3.56.

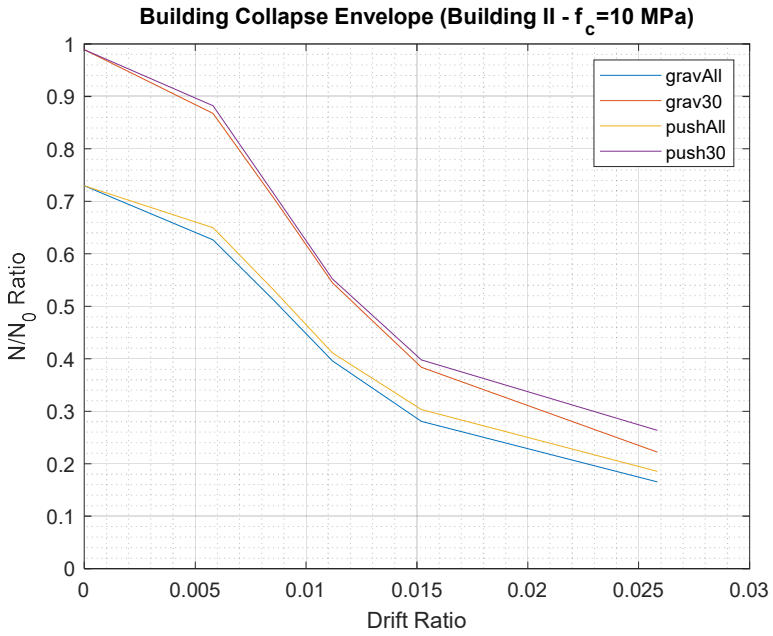

Figure 3.51 Building collapse envelope for the modified model of Building II with fc=10 MPa

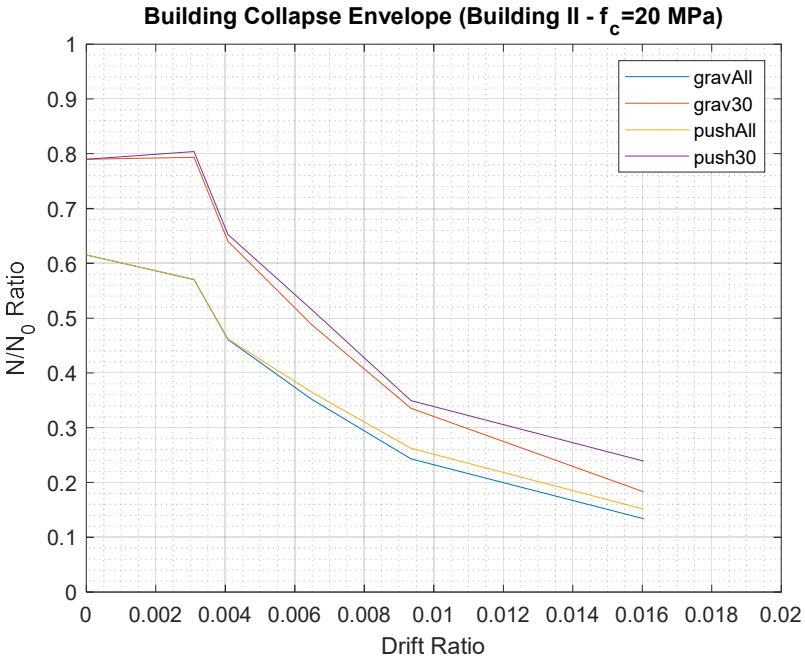

Figure 3.52 Building collapse envelope for the modified model of Building II with fc=20 MPa

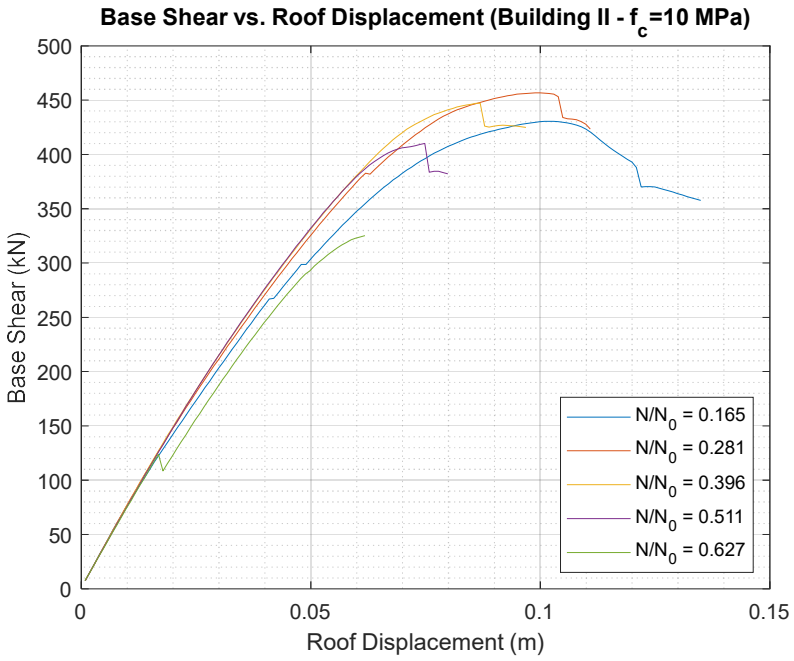

Figure 3.53 Pushover curves for the modified model of Building II with fc=10 MPa for data points used in corresponding envelope

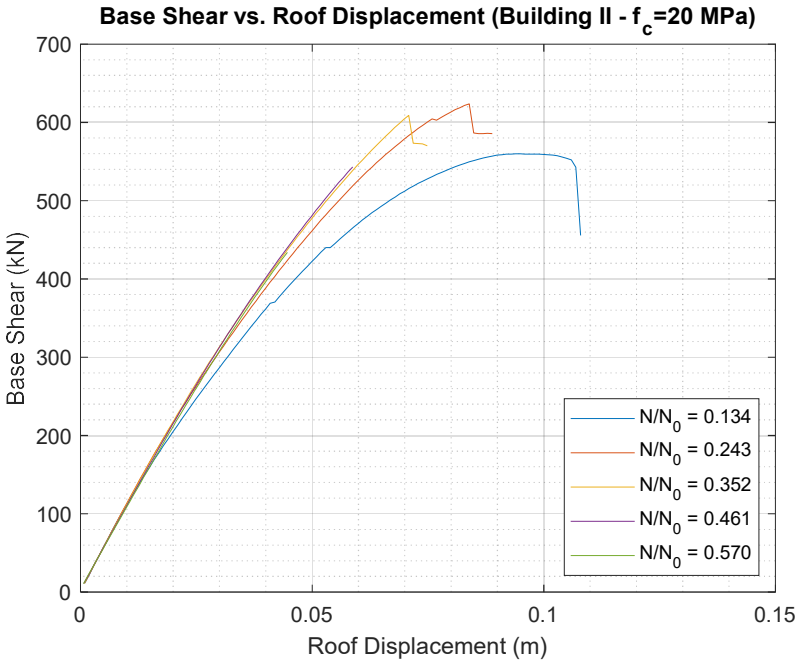

Figure 3.54 Pushover curves for the modified model of Building II with fc=20 MPa for data points used in corresponding envelope

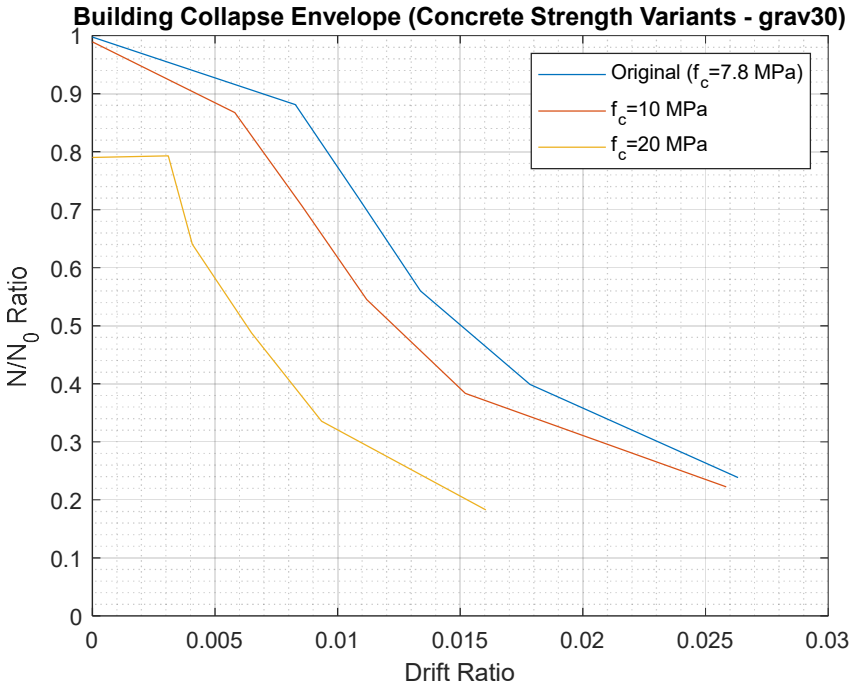

Figure 3.55 Building collapse envelopes of the concrete strength variants of Building II for the average of DCR values of 30% of first-floor columns with highest DCR values under the application of gravity loads only

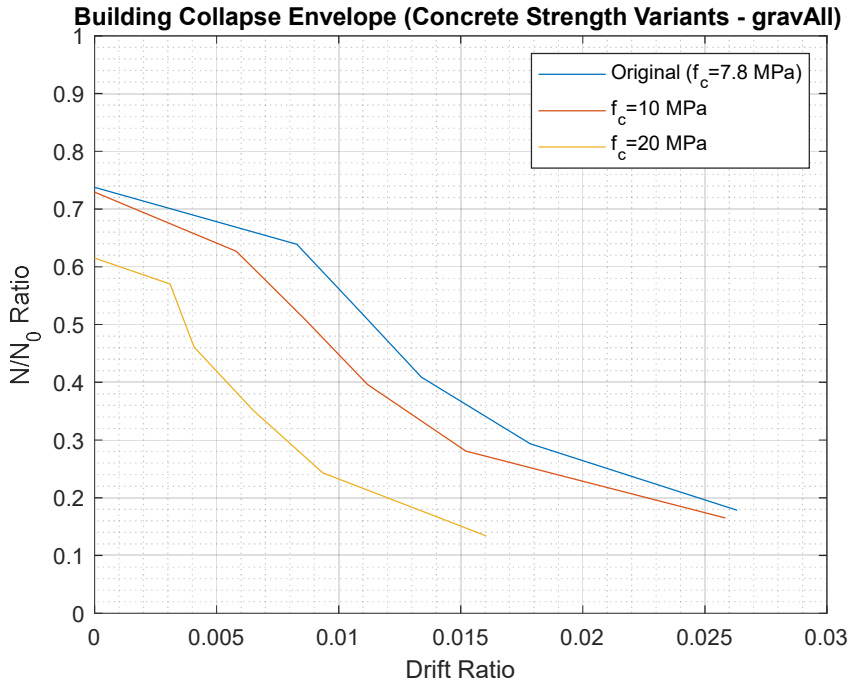

Figure 3.56 Building collapse envelopes of the concrete strength variants of Building II for the average of DCR values of all first-floor columns recorded under the application of gravity loads only

In agreement with the observations put forth for the concrete strength parameter group created from the original model of Building I, variants of the original model of Building II with different concrete strength values exhibited decreasing ultimate drift ratios in their envelopes with increasing concrete strength values (Figures 3.51, 3.52, 3.55 and 3.56). This observation is again supported by the increased capacity and decreased roof displacement values portrayed by the pushover curves for the smallest N/N_0 values in Figures 3.50, 3.53 and 3.54. Corresponding N/N_0 values on the envelopes for a given drift ratio value decrease with increasing concrete strength values, as was the case for the variants of Building I.

3.4.2.2.2 Envelopes for Floor Number Variants

Envelopes for the variants of the original model of Building II with 8 stories and 10 stories are presented in Figures 3.57 and 3.58, respectively, and corresponding pushover curves at their data points are given in Figures 3.59 and 3.60.

Comparative plots for building collapse envelopes for the floor number variants of Building II for the DCR averaging cases according to gravity analysis results are given in Figures 3.61 and 3.62.

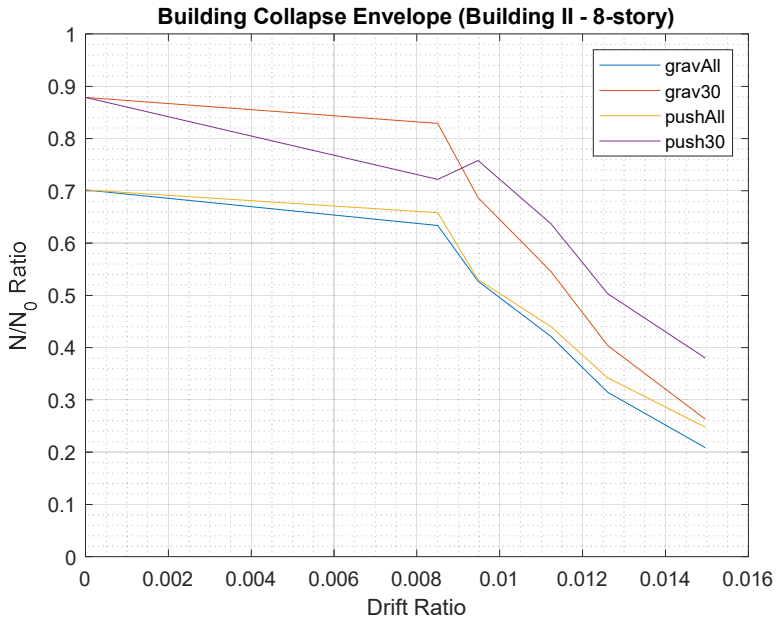

Figure 3.57 Building collapse envelope for the modified model of Building II with 8 stories

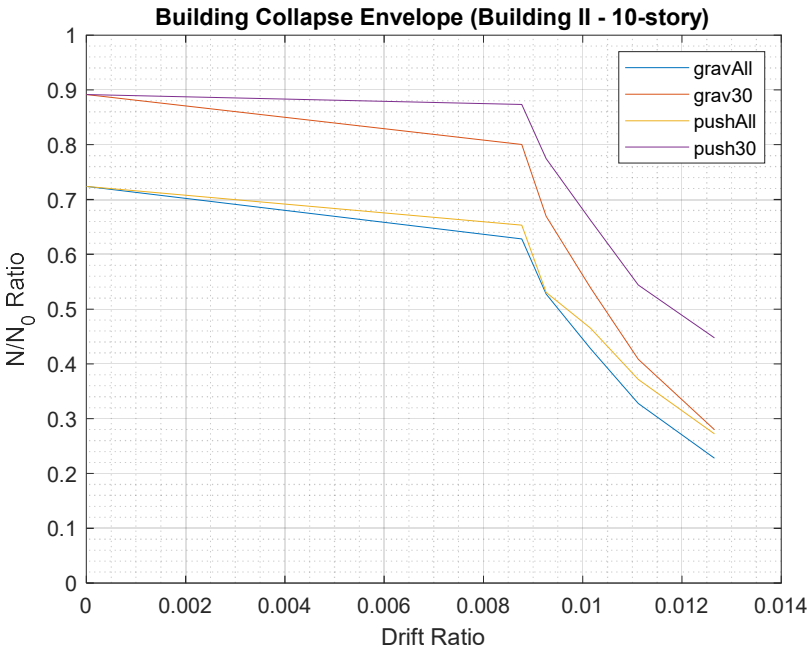

Figure 3.58 Building collapse envelope for the modified model of Building II with 10 stories

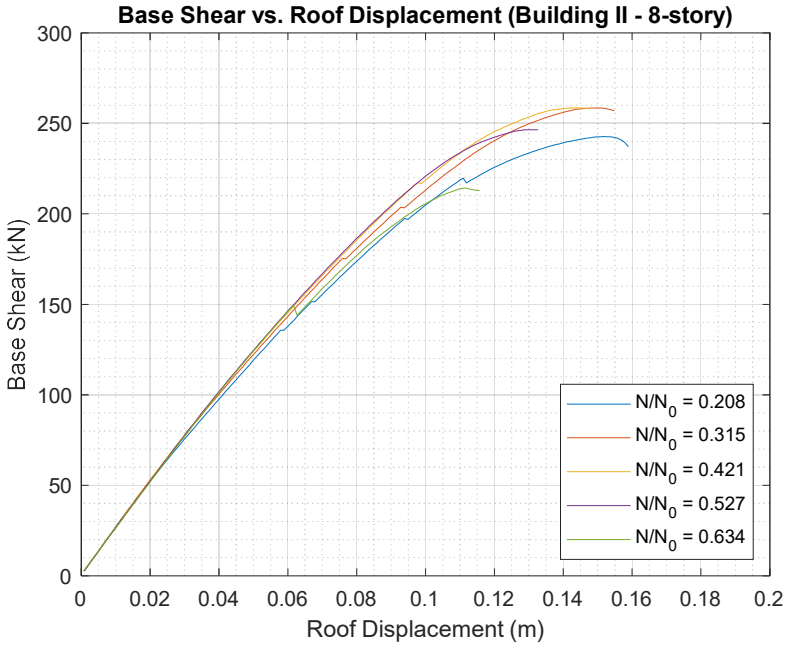

Figure 3.59 Pushover curves for the modified model of Building II with 8 stories for data points used in corresponding envelope

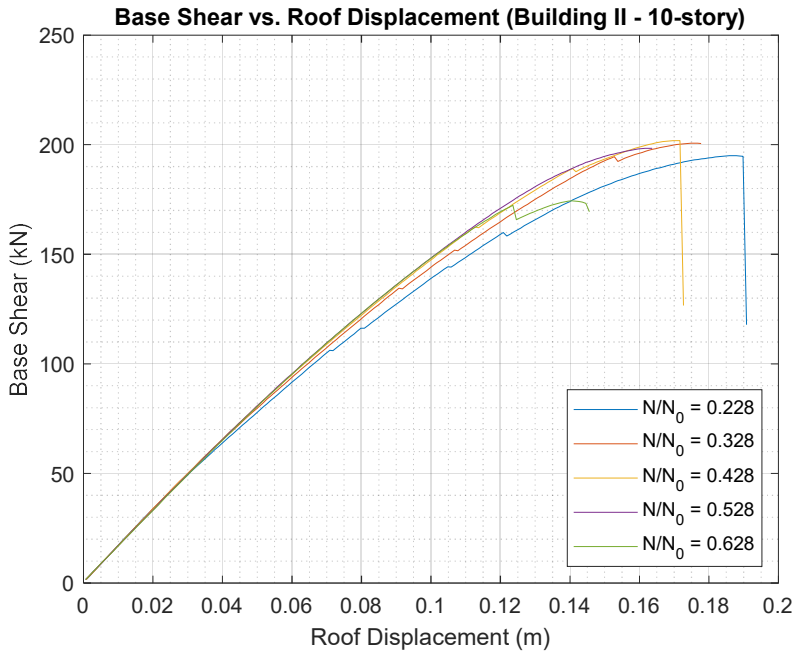

Figure 3.60 Pushover curves for the modified model of Building II with 10 stories for data points used in corresponding envelope

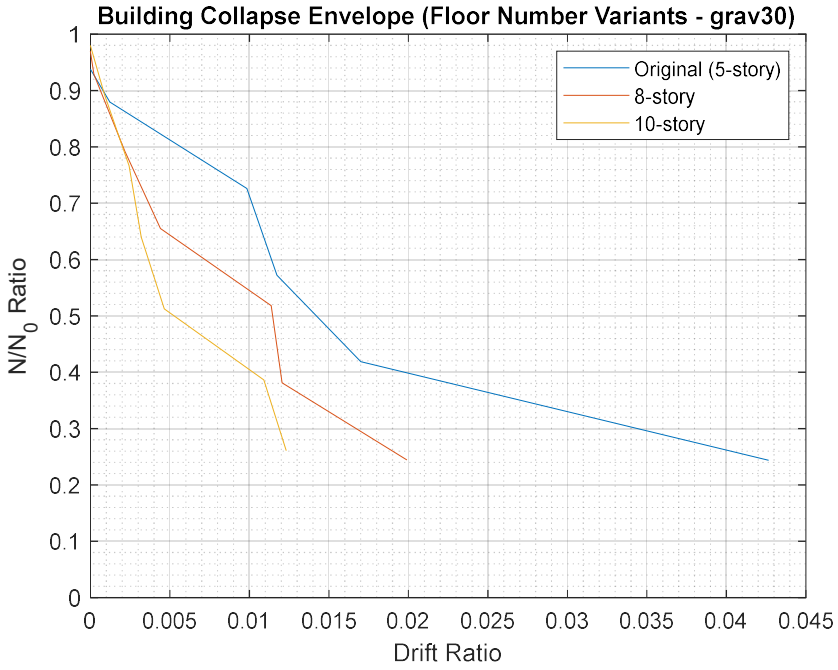

Figure 3.61 Building collapse envelopes of the floor number variants of Building II for the average of DCR values of 30% of first-floor columns with highest DCR values under the application of gravity loads only

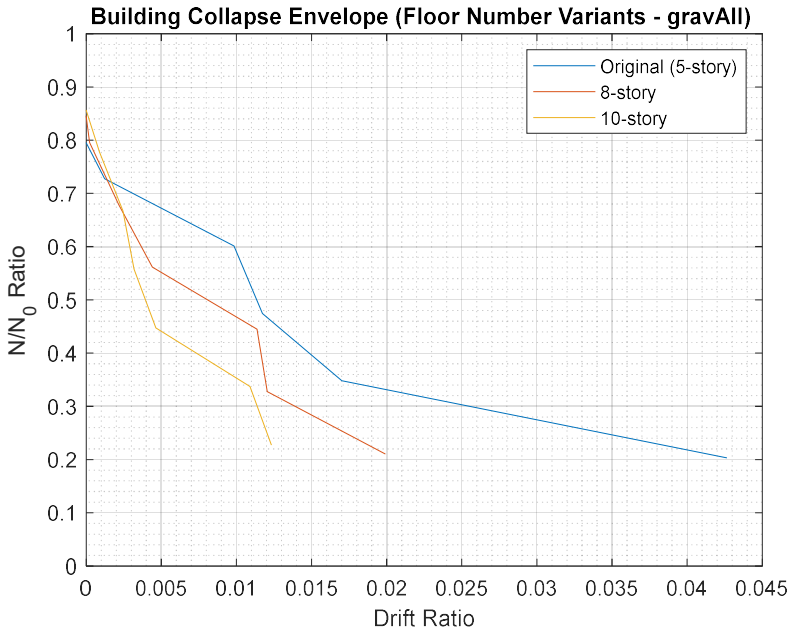

Figure 3.62 Building collapse envelopes of the floor number variants of Building II for the average of DCR values of all first-floor columns recorded under the application of gravity loads only

Similar to the case of concrete compressive strength changes and the comparison drawn for the same parameter group for Building I, ultimate drift ratio values for the first-floor columns represented in the envelopes decreased with increased number of stories. For the same reason, N/N_0 values for any given drift ratio value were decreased with increased number of stories in the envelopes given in Figures 3.57 and 3.58, indicating that the amount of used load-carrying capacities of first-floor columns decreased. Pushover curves presented in Figures 3.59 and 3.60 reinforce this observation by presenting a downward trend in maximum base shear values, and deviations from the roof displacement value of the original model within a narrow range.

3.4.2.2.3 Envelopes for Longitudinal Reinforcing Steel Ratio Variants

Envelopes for the variants of the original model of Building II with longitudinal reinforcing steel ratio values corresponding to rebar diameters of d=14 mm (average steel ratio ≈ 1.2%) and d=18 mm (average steel ratio ≈ 1.9%) are presented in Figures 3.63 and 3.64, respectively, and corresponding pushover curves at their data points are given in Figures 3.65 and 3.66.

Comparative plots for building collapse envelopes for the longitudinal reinforcing steel ratio variants of Building II for the DCR averaging cases according to gravity analysis results are given in Figures 3.67 and 3.68.

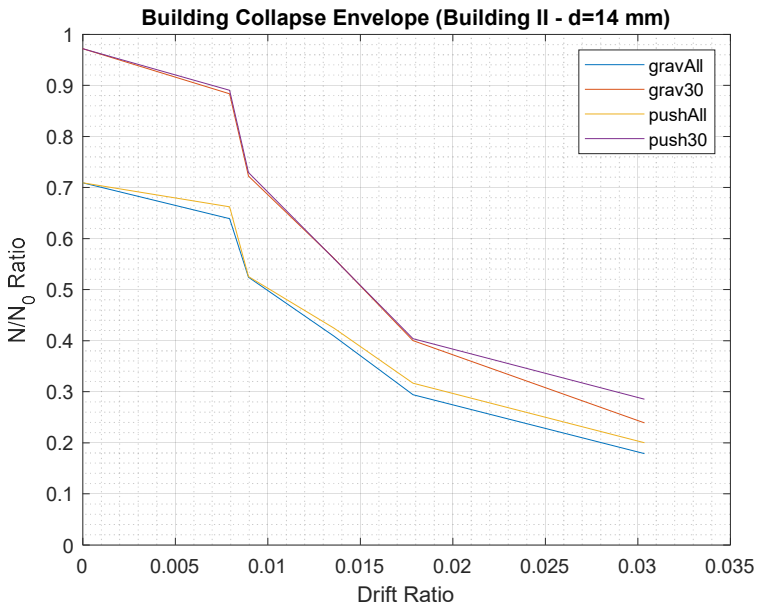

Figure 3.63 Building collapse envelope for the modified model of Building II with d=14 mm for longitudinal reinforcing steel bars

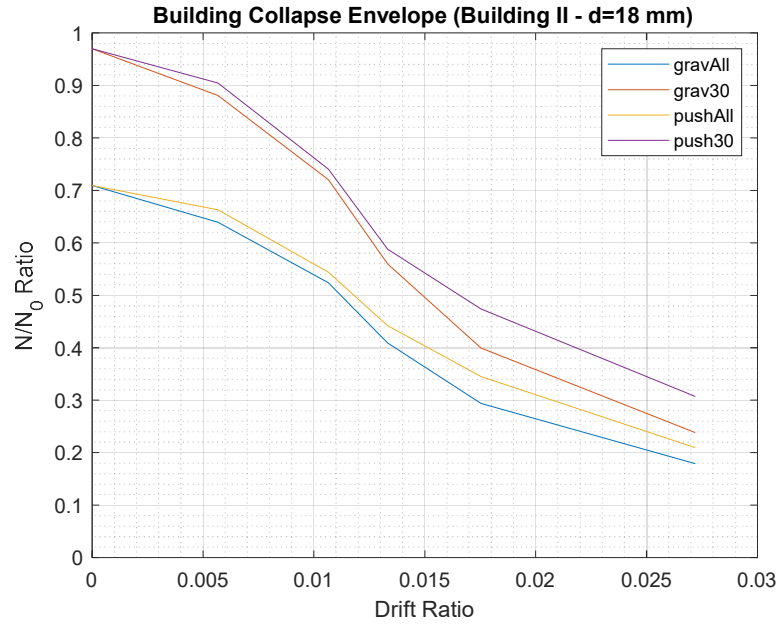

Figure 3.64 Building collapse envelope for the modified model of Building II with d=18 mm for longitudinal reinforcing steel bars

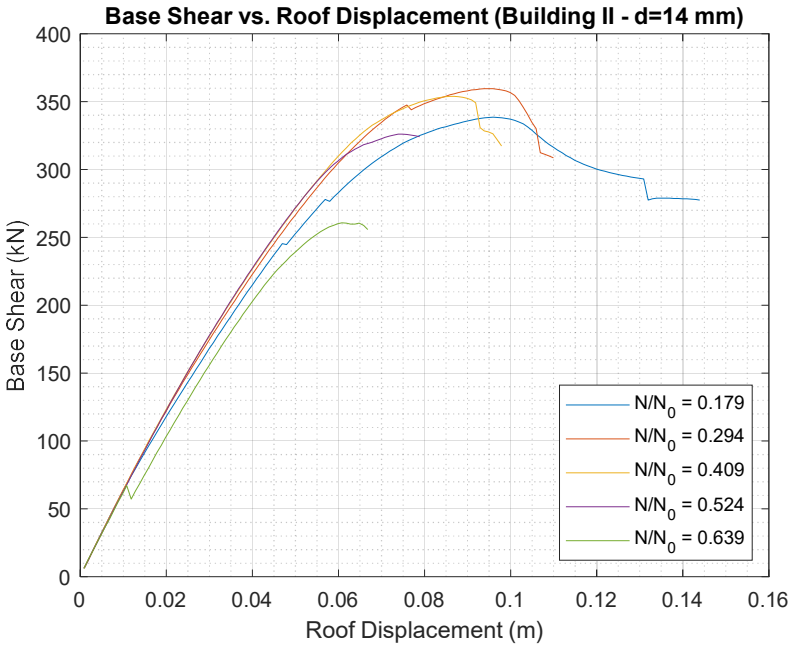

Figure 3.65 Pushover curves for the modified model of Building II with d=14 mm for data points used in corresponding envelope

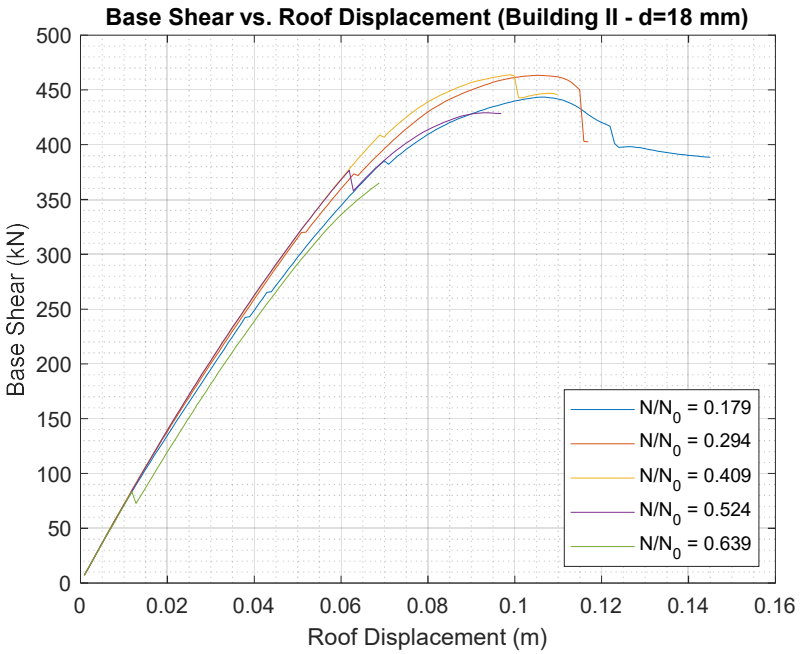

Figure 3.66 Pushover curves for the modified model of Building II with d=18 mm for data points used in corresponding envelope

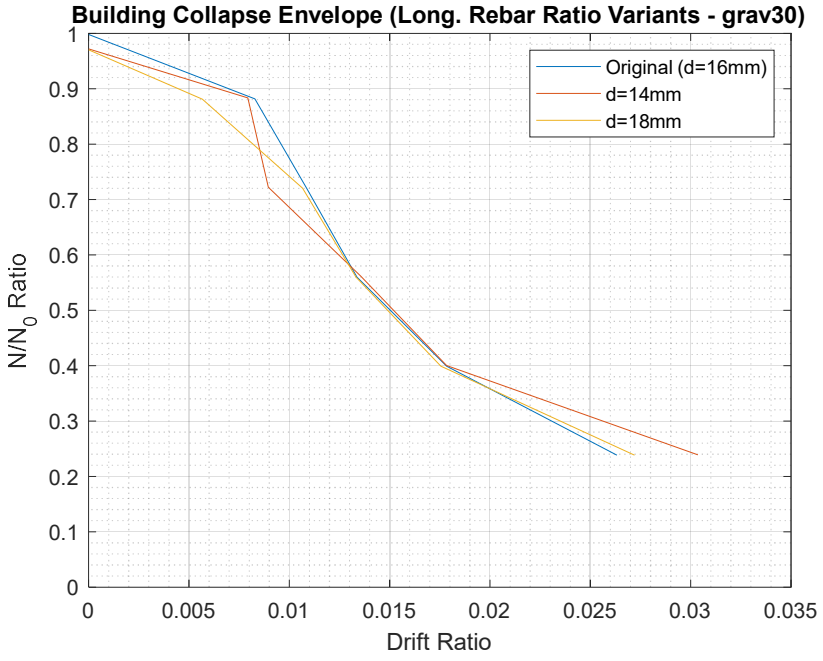

Figure 3.67 Building collapse envelopes of the longitudinal rebar ratio variants of Building II for the average of DCR values of 30% of first-floor columns with highest DCR values under the application of gravity loads only

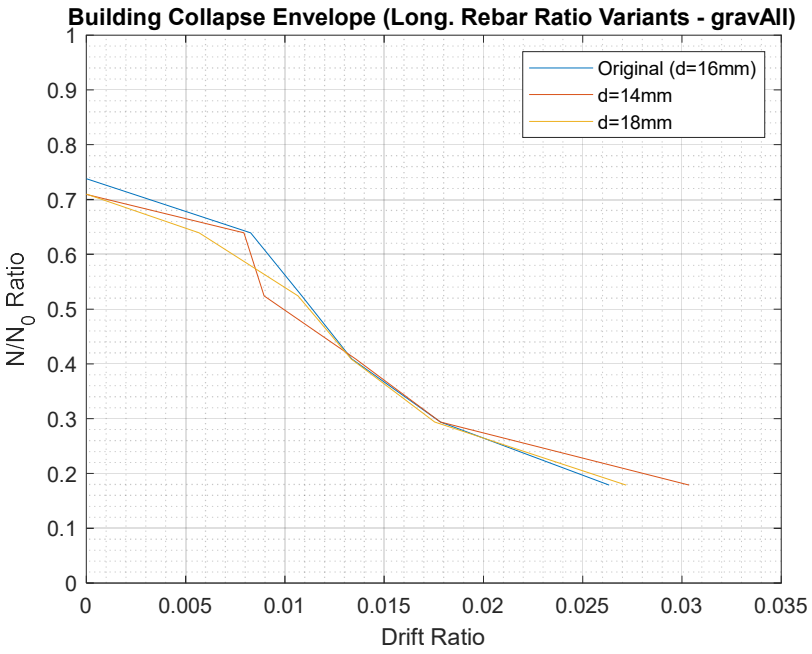

Figure 3.68 Building collapse envelopes of the longitudinal rebar ratio variants of Building II for the average of DCR values of all first-floor columns recorded under the application of gravity loads only

Figures 3.63, 3.64, 3.67 and 3.68 pinpoint that, compared to the envelope of the original model with a longitudinal reinforcing steel diameter of 16 mm (average steel ratio ≈ 1.5%), envelopes of buildings with columns having larger longitudinal steel diameters record smaller drift ratio values; yet, N/N_0 values corresponding to these ultimate drift ratio values do not change. This observation is supported by the building structural responses represented in the pushover curves in Figures 3.65 and 3.66, and by the discussion of the analyses presented in the same model parameter group for Building I. N/N_0 values for particular drift ratio values are mostly reduced with increasing longitudinal steel ratios (or diameters), indicating that increased capacities in first-floor columns result in capacity use levels less than the original case.

3.4.2.2.4 Envelopes for Stirrup Spacing Variants

Envelopes for the variants of the original model of Building II with stirrup spacing values of s=100 mm and s=200 mm are presented in Figures 3.69 and 3.70, respectively, and corresponding pushover curves at their data points are given in Figures 3.71 and 3.72.

Comparative plots for building collapse envelopes for the stirrup spacing variants of Building II for the DCR averaging cases according to gravity analysis results are given in Figures 3.73 and 3.74.

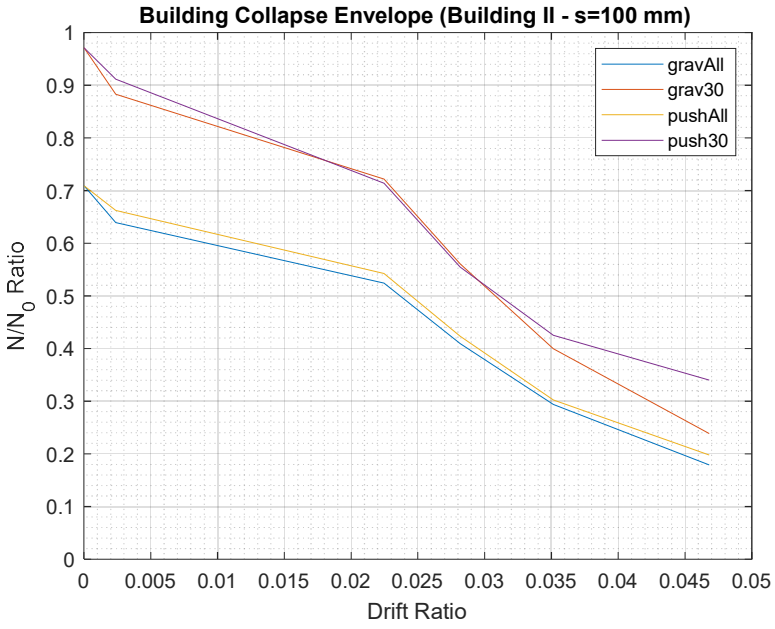

Figure 3.69 Building collapse envelope for the modified model of Building II with s=100 mm

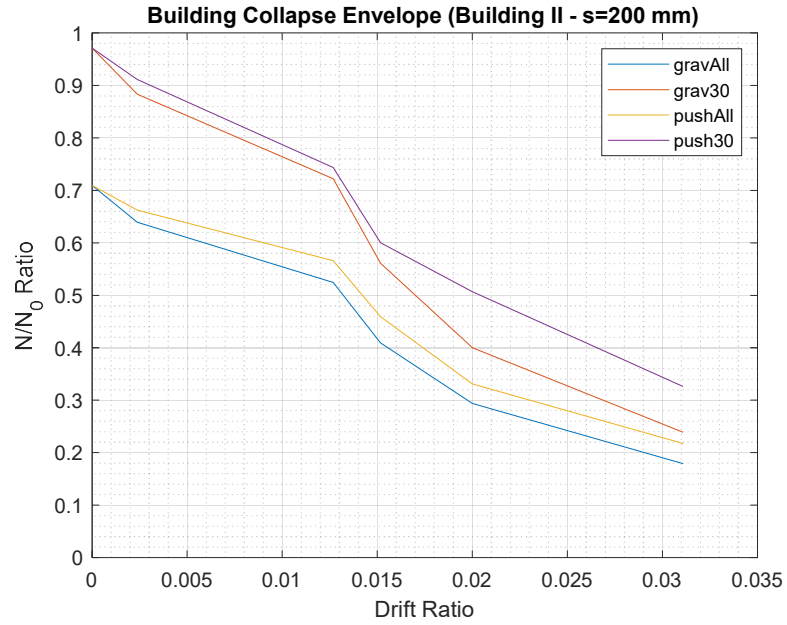

Figure 3.70 Building collapse envelope for the modified model of Building II with s=200 mm

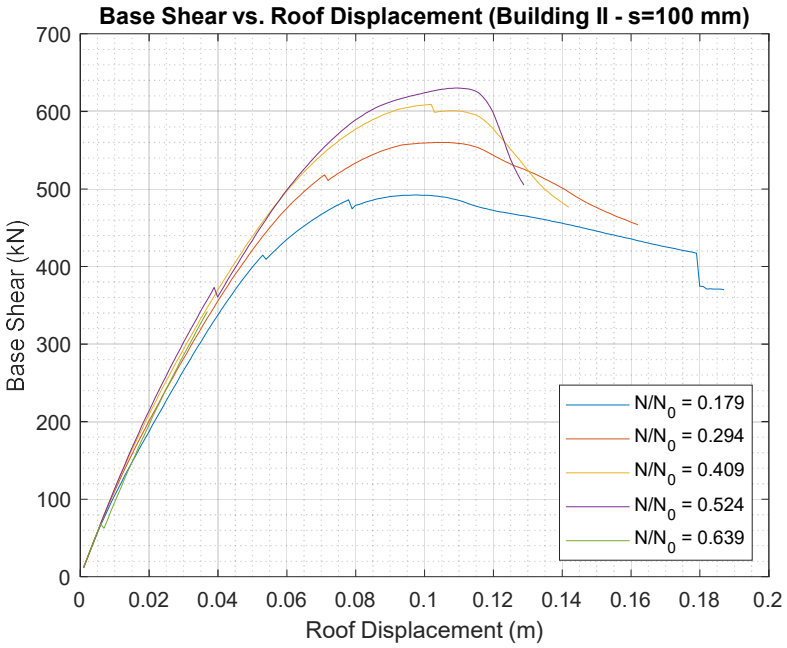

Figure 3.71 Pushover curves for the modified model of Building II with s=100 mm for data points used in corresponding envelope

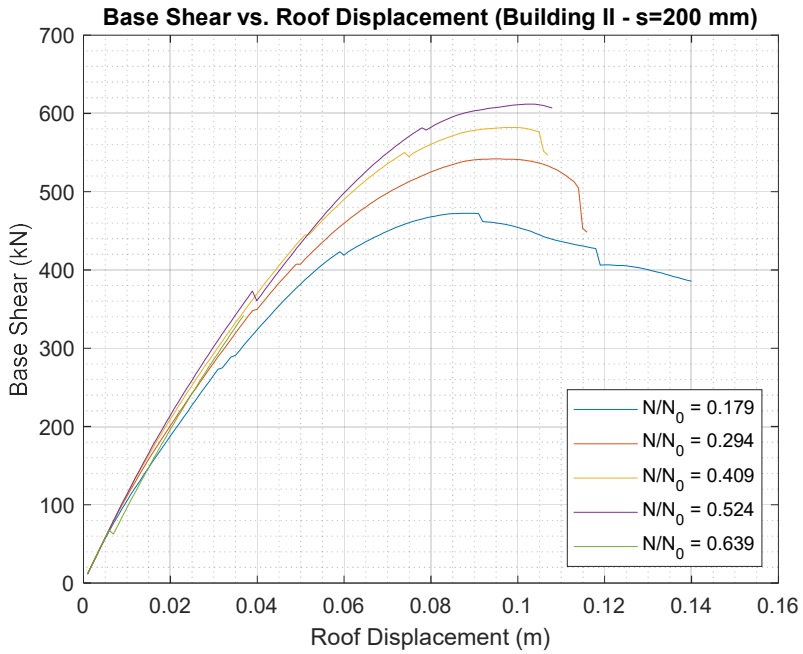

Figure 3.72 Pushover curves for the modified model of Building II with s=200 mm for data points used in corresponding envelope

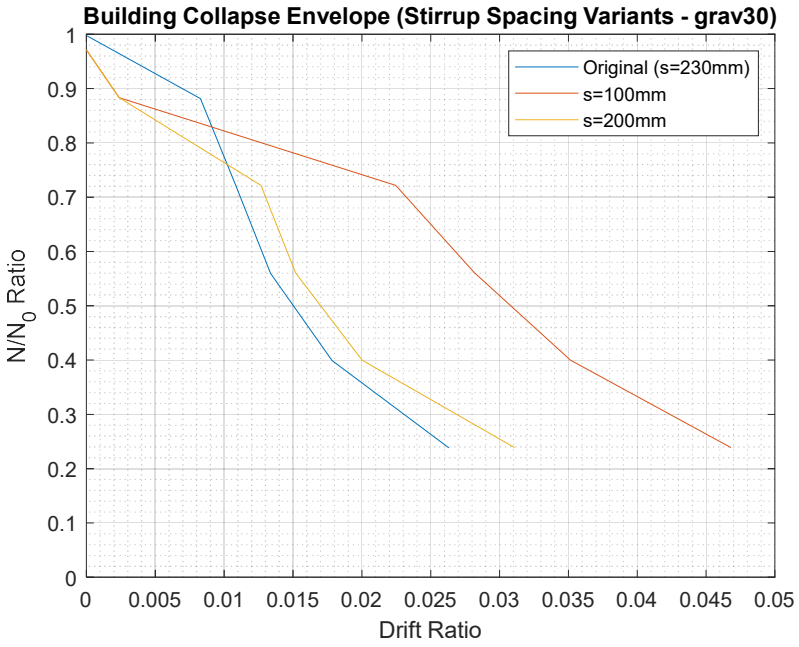

Figure 3.73 Building collapse envelopes of the stirrup spacing variants of Building II for the average of DCR values of 30% of first-floor columns with highest DCR values under the application of gravity loads only

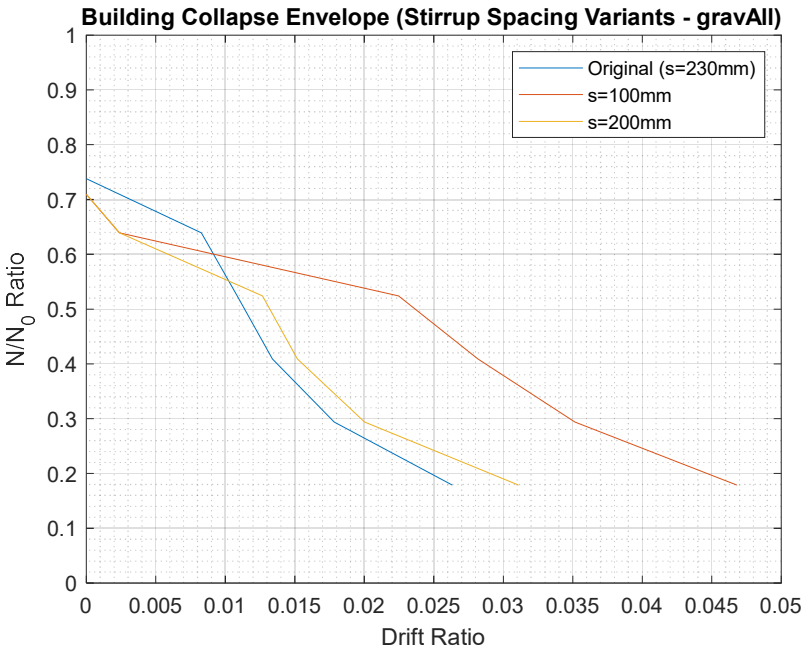

Figure 3.74 Building collapse envelopes of the stirrup spacing variants of Building II for the average of DCR values of all first-floor columns recorded under the application of gravity loads only

Figures 3.69 and 3.70 indicate that denser stirrup configurations result in larger drift ratios in corresponding envelopes, with no changes in N/N_0 values, demonstrating agreement with the conclusions drawn in the same case for Building I. Smaller stirrup spacing values also resulted in slightly smaller N/N_0 values for some drift ratio value, but this observation is, as was the case for the counterpart of this parameter group for Building I, not decisive. Pushover curves given in Figures 3.71 and 3.72 exhibit that ultimate roof displacement values are improved with decreased stirrup spacing values, supporting the first observation stated above.

CHAPTER 4

DISCUSSIONS AND CONCLUSIONS

This final chapter of the study is reserved for a general discussion of the results, in addition to drawing conclusions for the study and exploring possible venues of research to further improve the contribution of the study to the relevant literature.

4.1 Discussion of Results

Results obtained by the analysis and comparison of building collapse envelopes lead to the following observations related to the influence of reinforced concrete column details on these envelopes:

- Increasing concrete compressive strength value for a given building results in improved column load-carrying capacities, which, in turn, brings about smaller N/N_0 values on the corresponding building collapse envelope for a given drift ratio value, and a smaller maximum drift ratio for the first-floor columns. Therefore, the fraction of column capacities that could not be utilized becomes greater, and this state is reflected by the collapse envelope encompassing a smaller area representing non-failure zone for the given building.
- Increasing the number of floors introduces additional loads, causing amplified P-Delta effects and bringing the structure of interest to its failure point on the collapse envelope at smaller N/N_0 values and with a smaller maximum drift ratio for the first-floor columns. Resultant collapse envelope in the presence of such change is one encapsulating a smaller non-failure zone for the scrutinized building.

- Greater longitudinal reinforcing steel ratio values correspond to smaller maximum drift ratios for the first-floor columns and smaller N/N_0 values for any given drift ratio value, once again resulting in a narrower non-failure zone represented by the collapse envelope.
- Decreasing the stirrup spacing values was observed to create greater N/N_0 values for any given drift ratio value for the first-floor columns, but this observation requires further evidence. Ultimate drift ratio values provided on the collapse envelopes were observed to be increasing. Overall, selecting smaller values for this parameter expands the non-failure zone remaining below the collapse envelope.

Some minor discussions are also required for better interpreting the results, and these discussions are as follows:

- Greater DCR values normally point out to greater moment capacities, which in turn result in greater shear capacities. Yet, these changes are not reflected on building collapse envelopes, possibly due to the fact that different DCR averaging methods are employed or that P-Delta effects in columns are taken into consideration.
- Building collapse envelopes for any given case investigated in this study might not be covering the whole drift ratio domain due to the utilized data point selection method; therefore, their coverage of overall structural response might be limited by the amount of data involved in constructing these envelopes.
- It is expected to observe greater ductility in the buildings with increased concrete strength or increased longitudinal rebar ratio, but the envelopes constructed in this study depict cases opposing this expectation. Nevertheless, different load multipliers are used for obtaining each data point comprising the envelopes, and this methodological consideration might have an influence on ductility greater than the influence imposed on the envelopes by changes in concrete strength values.

- Most of the building collapse envelopes follow a horizontal path before going beyond similar drift ratio thresholds, and this trend could possibly be explained by the fact that the rotation-based column removal criterion used in our study might be exceeded very quickly in all analyses. Another possible explanation for this observation could be that P-Delta effects have considerable impact on structural response for high load multiplier values.

4.2 Conclusions

Construction of building collapse envelopes investigated in this study was carried out by creating data points according to a predetermined procedure. Preparing larger data sets for each parameter case and employing probabilistic methods or machine learning algorithms are thought to have promise for yielding more reliable and widely applicable results.

Number of variants created for each parameter case was limited to two, thus affecting the generalizability of the results in relevant fields of research. Nevertheless, the cases examined within the scope of this study are reckoned to have collectively set a sound point of departure for future research endeavors related to the topics included in this body of work.

4.3 Future Directions

Some future research possibilities could be listed as follows:

- The intended purpose of this study could be improved by future studies involving the analyses of a greater number of cases to be assessed for the influences of reinforced concrete column parameters on building collapse envelopes.
- Effects of non-structural members, such as infill walls, on building collapse envelopes might be explored.

- Research could be extended to different types of buildings with a variety of purposes of use, thus providing a general framework for evaluating design and assessment efforts in the presence of progressive collapse risk by means of building collapse envelopes.
- Machine learning algorithms could be used for working with larger data sets to obtain widely applicable building collapse envelope construction and utilization methods.
- Building collapse envelopes could be synchronized with earthquake response data to create a multi-faceted structural design and assessment approach for specific types of structures.

REFERENCES

Adam, J. M., Parisi, F., Sagaseta, J., & Lu, X. (2018). Research and practice on progressive collapse and robustness of building structures in the 21st century. *Engineering Structures*, *173*(June), 122–149. https://doi.org/10.1016/j.engstruct.2018.06.082

Arup Group Ltd. (2011). Review of international research on structural robustness and disproportionate collapse. Department for Communities and Local Government.

American Society of Civil Engineers. (2017, June). Minimum design loads and associated criteria for buildings and other structures. American Society of Civil Engineers.

Bayrak, O. (1998). *Seismic performance of rectilinearly confined high strength concrete columns* (Doctoral dissertation).

Bažant, Z. P., & Verdure, M. (2007). Mechanics of Progressive Collapse: Learning from World Trade Center and Building Demolitions. *Journal of Engineering Mechanics*, *133*(3), 308–319. https://doi.org/10.1061/(asce)0733-9399(2007)133:3(308)

Byfield, M., & Paramasivam, S. (2007). Catenary action in steel-framed buildings. *Proceedings of the Institution of Civil Engineers-Structures and Buildings*, *160*(5), 247-257.

Byfield, M., Mudalige, W., Morison, C., & Stoddart, E. (2014). A review of progressive collapse research and regulations. *Proceedings of the Institution of Civil Engineers-Structures and Buildings*, *167*(8), 447-456.

Cormie, D., Mays, G., & Smith, P. (Eds.). (2009). *Blast effects on buildings*. Thomas Telford Publishing.

de Normalisation, C. C. E. (2006). EN 1991-1-7: eurocode 1–actions on structures–part 1–7: general actions–accidental actions. *Brussels (Belgium): CEN*.

Ellingwood, B. R., Smilowitz, R., Dusenberry, D. O., Duthinh, D., Lew, H. S., & Carino, N. J. (2007). Best practices for reducing the potential for progressive collapse in buildings. *U.S. National Institute of Standards and Technology (NIST).*, 216.

Ellingwood, B. R. (2006). Mitigating Risk from Abnormal Loads and Progressive Collapse. *Journal of Performance of Constructed Facilities*, *20*(4), 315–323. https://doi.org/10.1061/(asce)0887-3828(2006)20:4(315)

Elwood, K. J., Matamoros, A. B., Wallace, J. W., Lehman, D. E., Heintz, J. A., Mitchell, A. D., ... & Moehle, J. P. (2007). Update to ASCE/SEI 41 concrete provisions. *Earthquake Spectra*, *23*(3), 493-523.

Ferretti, D., & Bažant, Z. P. (2006). Stability of ancient masonry towers: Moisture diffusion, carbonation and size effect. *Cement and Concrete Research*, *36*(7), 1379–1388. https://doi.org/10.1016/j.cemconres.2006.03.013

Ghannoum, W. M., & Matamoros, A. B. (2014). Nonlinear modeling parameters and acceptance criteria for concrete columns. *ACI Special Publication*, *297*(1), 1-24.

GSA. (2013). General Services Administration Alternate Path Analysis & Design Guidelines for Progressive Collapse Resistance. *General Services Administration*, 143.

Gurley, C. (2008). Progressive Collapse and Earthquake Resistance. *Practice Periodical on Structural Design and Construction*, *13*(1), 19–23. https://doi.org/10.1061/(asce)1084-0680(2008)13:1(19)

International Building Code (IBC). (2009). https://doi.org/10.5040/9781501365171.2089

Izzuddin, B. A., & Elghazouli, A. Y. (2004). Failure of Lightly Reinforced Concrete Members under Fire. I: Analytical Modeling. *Journal of Structural Engineering*, *130*(January 2004), 3–17. https://doi.org/10.1061/(ASCE)0733-9445(2004)130

Karsan, I. D., & Jirsa, J. O. (1969). Behavior of concrete under compressive loadings. *Journal of the Structural Division*, *95*(12), 2543-2564.

Kent, D. C., & Park, R. (1971). Flexural members with confined concrete. *Journal of the structural division*, *97*(7), 1969-1990.

Khandelwal, K., & El-Tawil, S. (2011). Pushdown resistance as a measure of robustness in progressive collapse analysis. *Engineering Structures*, *33*(9), 2653–2661. https://doi.org/10.1016/j.engstruct.2011.05.013

Kiakojouri, F., De Biagi, V., Chiaia, B., & Sheidaii, M. R. (2020). Progressive collapse of framed building structures: Current knowledge and future prospects. *Engineering Structures*, *206*(January), 110061. https://doi.org/10.1016/j.engstruct.2019.110061

Kim, T., Kim, J., & Park, J. (2009). Investigation of Progressive Collapse-Resisting Capability of Steel Moment Frames Using Push-Down Analysis. *Journal of Performance of Constructed Facilities*, *23*(5), 327–335. https://doi.org/10.1061/(asce)0887-3828(2009)23:5(327)

Kunnath, S. K., Bao, Y., & El-Tawil, S. (2018). Advances in Computational Simulation of Gravity-Induced Disproportionate Collapse of RC Frame Buildings. *Journal of Structural Engineering*, *144*(2), 03117003. https://doi.org/10.1061/(asce)st.1943-541x.0001938

Li, Y., Lu, X., Guan, H., & Ye, L. (2011). An improved tie force method for progressive collapse resistance design of reinforced concrete frame structures. *Engineering Structures*, *33*(10), 2931–2942. https://doi.org/10.1016/j.engstruct.2011.06.017

Liu, M. (2015). Pulldown Analysis for Progressive Collapse Assessment. *Journal of Performance of Constructed Facilities*, *29*(1), 04014027. https://doi.org/10.1061/(asce)cf.1943-5509.0000459

Mazzoni, S., McKenna, F., Scott, M. H., & Fenves, G. L. (2006). OpenSees command language manual. *Pacific Earthquake Engineering Research (PEER) Center*, *264*, 137-158.

McKay, A., Marchand, K., & Diaz, M. (2012). Alternate path method in progressive collapse analysis: Variation of dynamic and nonlinear load increase factors. *Practice Periodical on Structural Design and Construction*, *17*(4), 152-160.

Mlakar, Sr., P. F., Corley, W. G., Sozen, M. A., & Thornton, C. H. (1998). The Oklahoma City Bombing: Analysis of Blast Damage to the Murrah Building. *Journal of Performance of Constructed Facilities*, *12*(3), 113–119. https://doi.org/10.1061/(asce)0887-3828(1998)12:3(113)

NIST. (2005). Final Report on the Collapse of the World Trade Center Towers. In *NIST NCSTAR 1. WTC Investigation* (Vol. 32, Issue 9).

Paulay, T., & Priestley, M. N. (1992). Seismic design of reinforced concrete and masonry buildings.

Pearson, C., & Delatte, N. (2005). Ronan Point Apartment Tower Collapse and its Effect on Building Codes. *Journal of Performance of Constructed Facilities*, *19*(2), 172–177. https://doi.org/10.1061/(asce)0887-3828(2005)19:2(172)

Qian, K., Li, B., & Ma, J.-X. (2015). Load-Carrying Mechanism to Resist Progressive Collapse of RC Buildings. *Journal of Structural Engineering*, *141*(2), 04014107. https://doi.org/10.1061/(asce)st.1943-541x.0001046

Qiao, H., Yang, Y., & Zhang, J. (2018). Progressive Collapse Analysis of Multistory Moment Frames with Varying Mechanisms. *Journal of Performance of Constructed Facilities*, *32*(4), 04018043. https://doi.org/10.1061/(asce)cf.1943-5509.0001192

Russell, J. M., Sagaseta, J., Cormie, D., & Jones, A. E. K. (2019). Historical review of prescriptive design rules for robustness after the collapse of Ronan Point. *Structures*, *20*(May), 365–373. https://doi.org/10.1016/j.istruc.2019.04.011

RYTEIE. (2013). The Principles for the Identification of Risky Structures [in Turkish]. Retrieved from https://webdosya.csb.gov.tr/db/altyapi/icerikler/ek-2-ryteie-20190705155915.pdf

Scott, M. H., & Fenves, G. L. (2006). Plastic hinge integration methods for force-based beam–column elements. *Journal of Structural Engineering*, *132*(2), 244-252.

Starossek, U. (2007). Typology of progressive collapse. *Engineering Structures*, *29*(9), 2302–2307. https://doi.org/10.1016/j.engstruct.2006.11.025

TBEC. (2018). Turkish Seismic Earthquake Code. Retrieved from https://www.resmigazete.gov.tr/eskiler/2018/03/20180318M1-2-1.pdf

UFC. (2016). UFC 4-023-03. Design of Buildings To Resist Progressive Collapse. *Design of Buildings To Resist Progressive Collapse*, *November*, 34–37.